



Institut national  
de la recherche  
scientifique



Université du Québec  
Institut National de la Recherche  
Scientifique  
Centre Énergie Matériaux  
Télécommunications

Munich University of Applied Sciences  
Department of Applied Sciences and  
Mechatronics

# Numerical investigation of water impurity effects on CO<sub>2</sub> Plasma conversion yield

Par  
Felix Bandle

Thèse présentée pour l'obtention du grade de  
*Maître es Sciences* (M.Sc.)  
en sciences de l'énergie et des matériaux

25.02.2025

## Jury d'évaluation

<b>Research Director</b>	Prof. Dr. Émile Carbone
<b>Research Co-Director</b>	Prof. Dr. Matthias Gramich
<b>Internal Reviewer, Jury President</b>	Prof. François Vidal
<b>External Reviewer</b>	Dr. Nicolaas den Harder



# Résumé

L'émission de dioxyde de carbone représente un défi environnemental important, principalement en raison de son impact sur le climat par le biais de l'effet de serre. Il est donc essentiel de mettre au point des procédés à haut rendement énergétique pour la conversion de CO<sub>2</sub> afin de produire des combustibles à partir de sources d'énergie renouvelables. La production de CO à partir de CO<sub>2</sub> peut être réalisée avec une grande efficacité grâce à l'utilisation de réacteurs à plasma micro-ondes. La présence d'impuretés dans le gaz de traitement a un impact significatif sur l'efficacité du processus de conversion.

Ce rapport présente les résultats préliminaires du développement d'un modèle complet de dissociation thermique du CO<sub>2</sub> avec les impuretés de l'eau. Un modèle de dissociation cinétique pour CO<sub>2</sub> a été développé qui s'aligne étroitement sur l'équilibre chimique calculé thermodynamiquement. Le modèle a été amélioré pour être utilisé dans une gamme de températures plus large grâce à l'extension aux réactions du carbone atomique. La précision de plusieurs modèles pour la dissociation de H<sub>2</sub>O a été évaluée par rapport à l'équilibre chimique. Cependant, aucun modèle approprié n'a pu être identifié pour être intégré au modèle de dissociation de CO<sub>2</sub>.

Les résultats représentent une étape importante dans le développement d'un modèle complet permettant d'étudier l'impact des impuretés de l'eau sur l'efficacité de la conversion de CO<sub>2</sub> en CO.

## Mots-clés :

Conversion du CO<sub>2</sub> par plasma, dissociation du CO<sub>2</sub>, étude numérique, effets des impuretés de l'eau, dissociation du H<sub>2</sub>O.



# Abstract

Carbon dioxide emissions represent a significant environmental challenge, largely due to their impact on the climate via the greenhouse effect. It is therefore essential to develop highly energy-efficient processes for the conversion of CO<sub>2</sub> to produce combustible fuels from renewable energy sources. CO is an intermediate product in the conversion to combustible fuels. Production of CO from CO<sub>2</sub> can be achieved with great efficiency through the utilization of microwave plasma reactors. The presence of impurities in the process gas, however, has a significant impact on the efficiency of the conversion process.

This work presents preliminary results in the development of a comprehensive thermal CO<sub>2</sub> dissociation model with water impurities. A kinetic dissociation model for CO<sub>2</sub> was developed which closely aligns with the thermodynamically calculated chemical equilibrium. The model was further improved for use in a broader temperature range through extension with atomic carbon reactions. Validation of the enhanced model is possible with thermodynamic calculations for pressures ranging from 1 Pa to 1 MPa, at temperatures between 1000 K and 7000 K. In addition, verification of the CO<sub>2</sub> dissociation models is possible with published experiments. The accuracy of multiple models for H<sub>2</sub>O dissociation was benchmarked against chemical equilibrium. However, no suitable model could be identified for integration with the CO<sub>2</sub> dissociation model.

The results of this work indicate that more work is necessary on water dissociation models. CO<sub>2</sub> dissociation models were verified, which represents an important step in the development of a comprehensive model for investigating the impact of water impurities on the conversion efficiency of CO<sub>2</sub> to CO.

## Keywords:

Plasma-based CO<sub>2</sub> conversion, CO<sub>2</sub> dissociation, numerical investigation, water impurity effects, H<sub>2</sub>O dissociation



# Contents

<b>1. Introduction</b>	<b>1</b>
<b>2. Fundamentals</b>	<b>3</b>
2.1. Plasma . . . . .	3
2.1.1. Microwave plasma . . . . .	5
2.1.2. Quenching . . . . .	6
2.2. Thermodynamic calculations . . . . .	7
2.2.1. Chemical Equilibrium . . . . .	7
2.2.2. CEARUN . . . . .	8
2.3. Kinetic model . . . . .	9
2.3.1. Density . . . . .	11
2.3.2. Pressure . . . . .	12
2.4. Code validation . . . . .	13
2.5. Benchmarking of different models . . . . .	14
<b>3. CO<sub>2</sub> dissociation</b>	<b>15</b>
3.1. NASA CEA . . . . .	15
3.2. Code validation . . . . .	16
3.3. Benchmarking . . . . .	19
3.4. Addition of carbon atom kinetics . . . . .	22
3.4.1. Validation with shock tube experiment . . . . .	24
3.4.2. Model validation with thermodynamic results . . . . .	24
3.5. Quenching . . . . .	26
<b>4. H<sub>2</sub>O dissociation</b>	<b>31</b>
4.1. NASA CEA . . . . .	31
4.2. Kinetic model . . . . .	32
4.2.1. Srinivasan model . . . . .	32
4.2.2. Lédé model . . . . .	34
4.2.3. Avtaeva model . . . . .	35
4.2.4. Medodovic model . . . . .	36
4.2.5. Liu model . . . . .	38
<b>5. Summary and Outlook</b>	<b>41</b>

<b>Sommaire récapitulatif en français: Étude numérique des effets des impuretés de l'eau sur le rendement de conversion du CO<sub>2</sub> par plasma</b>	<b>45</b>
<b>List of Figures</b>	<b>69</b>
<b>List of Tables</b>	<b>73</b>
<b>Bibliography</b>	<b>75</b>
<b>A. CEARUN files for CO<sub>2</sub></b>	<b>81</b>
A.1. 1000 - 3000 K . . . . .	81
A.2. 3100 - 5100 K . . . . .	87
A.3. 5200 - 6100 K . . . . .	94
<b>B. CO<sub>2</sub> Dissociation Models</b>	<b>99</b>
B.1. den Harder Model . . . . .	99
B.2. Koelman Model . . . . .	100
B.3. Combined den Harder/Beuthe Model . . . . .	101
<b>C. CEARUN files for H<sub>2</sub>O</b>	<b>103</b>
C.1. 1000 - 3000 K . . . . .	103
C.2. 3100 - 5100 K . . . . .	108
C.3. 5200 - 6100 K . . . . .	113
<b>D. H<sub>2</sub>O Dissociation Models</b>	<b>119</b>
D.1. Srinivasan Model . . . . .	119
D.2. Lede Model . . . . .	120
D.3. Avtaeva Model . . . . .	121
D.4. Mededovic Model . . . . .	122
D.5. Liu Model . . . . .	124

# 1. Introduction

Rapid economical growth and industrialization increases the human demand for energy. Currently the main energy source is fossil fuels. This consumption of fossil fuels has lead to a massive increase in CO<sub>2</sub> emissions [1–3]. Emissions of carbon dioxide are currently one of the main environmental challenges due to their direct impact on climate via the greenhouse effect. Reduction of carbon emissions is of crucial importance in the effort to combat climate change [4].

CO<sub>2</sub> emissions into the atmosphere could be decreased by conversion of CO<sub>2</sub> into fuels and other high-value chemical products, therefore establishing a ‘carbon cycle’ which consists of carbon capture, production and consumption. Furthermore, this process should also address issues that are a consequence of the decline in the availability of fossil resources [5]. In recent years, plasma based chemistry has attracted a lot of attention because of the opportunity to use renewable energy sources for the direct conversion of stable molecules such as CO<sub>2</sub> into CO and O<sub>2</sub> without the need for a catalyst [6].

Microwave plasma conversion of CO<sub>2</sub> is one of the most energy-efficient processes currently available. For the production of CO<sub>2</sub> neutral fuels, microwave plasma reactors are powered by renewable electrical energies such as hydroelectric power, wind or solar energy. To achieve energy-efficient and CO<sub>2</sub> neutral fuel production, a high CO<sub>2</sub> to CO conversion yield is required. To achieve high efficiency, the gas is rapidly cooled by quenching. A crucial factor in this process is the proportion of CO lost during cooling. This factor indicates how much CO is unintentionally converted back into other species, reducing the overall efficiency.

Captured CO<sub>2</sub> can be fed into a microwave plasma reactor, where it is then converted by pyrolysis into CO, O and O<sub>2</sub>. At temperatures above 5000 K, further pyrolysis of CO into C and O is possible. The heated gas mixture is then rapidly cooled down by quenching to sustain the chemical composition to the greatest possible extent. The CO produced is captured and can be further used for basic chemicals or fuel synthesis. Together with hydrogen, CO forms syngas, which is already a combustible fuel and can be further liquified into gasoline. CO<sub>2</sub> neutral fuel production is only possible if all the electrical energy which is required in production and storage originates from renewable energy sources.

Promising CO<sub>2</sub> conversion results have been obtained using low pressure, high temperature plasma sources which are best suited for industrial applications. However, the impact of impurities in the gas feed can be detrimental to the plasma process. This work aims to investigate the impact of an ever-present impurity in CO<sub>2</sub> sources, i.e. water vapour, on the CO<sub>2</sub> conversion yield. Water molecules as an additive are still highly debated regarding their potential benefits or actual negative effects on CO<sub>2</sub> conversion by plasma. Recently, Kiefer et al. [7] provided an extensive dataset indicating a strongly decreasing CO<sub>2</sub> conversion rate with the introduction of ambient air in the reactor compared to dry air. The group claims one possible explanation is the presence of moisture in the air introduced into the reactor. In contrast, Ong et al. [8] propose that water may be beneficial to the CO<sub>2</sub> dissociation process, given that it has a higher thermodynamic potential, which facilitates a more efficient dissociation pathway [8].

Preliminary work for the further theoretical investigation of this statement is done in this work through the development of CO<sub>2</sub> and H<sub>2</sub>O 0D-kinetic dissociation models, which are each benchmarked regarding their accuracy against the chemical equilibrium calculated with NASA's CEA solver. These two parts are necessary for the theoretical investigation of the claims from Kiefer et al. [7], where the models should be combined for a comprehensive CO<sub>2</sub>–H<sub>2</sub>O 0D-kinetic dissociation model. Further reactions must be considered for the components of CO<sub>2</sub> and H<sub>2</sub>O.

## 2. Fundamentals

The aim of this work is to numerically investigate the influence of water vapour on the CO<sub>2</sub> conversion yield in a plasma reactor. In this chapter, the basics of plasma are explained, as well as the different approaches to calculating the equilibrium composition.

### 2.1. Plasma

Plasma is also known as the ‘fourth state of matter’ alongside solids, liquids and gases [8, 9]. Over 99 % of the visible universe consists of plasma [10]. In solid bodies particles are arranged and packed closely, their mobility is restricted. In liquids, they can move but only with limited freedom. In gases, the molecules and atoms can move freely [9]. In a plasma, electrons are freed from the atoms or molecules, forming charged ions. Molecules become more energetic with rising temperatures and matter is transformed in a sequence from solid, to liquid, to gas and finally gradually to a plasma [10]. As the transition occurs gradually with increasing temperature, it is not a phase transition (see table 2.1) in the thermodynamical sense, even though it is usually labeled as a phase transition [11].

Table 2.1. Possible phase transitions. To transition to the plasma state of matter, the species must be gaseous. There is no possible way for a direct phase transition from a solid or liquid directly into a plasma as its a continuous process from the gas phase [11]. The transition to plasma is not considered a phase transition in the thermodynamical sense, but usually labeled as such.

From \ To	Solid	Liquid	Gas	Plasma
Solid		Melting	Sublimation	
Liquid	Freezing		Vaporization	
Gas	Deposition	Condensation		Ionization
Plasma			Recombination	

Plasma is defined as an highly energized (ionized) gas with an overall neutral electrical charge. The macroscopically quasi-neutral substance consists of molecules, free electrons, ions and radicals as displayed in figure 2.1 [11]. A plasma is formed from a neutral gas when the gas is subject to sufficiently high energy. This energy is specific for each gas and is necessary for ionization of the gas molecule. The electrons are then removed from the neutral gas molecule and a charged gas molecule is formed. This charged gas becomes highly conductive, so that electric and magnetic fields can influence its behaviour and

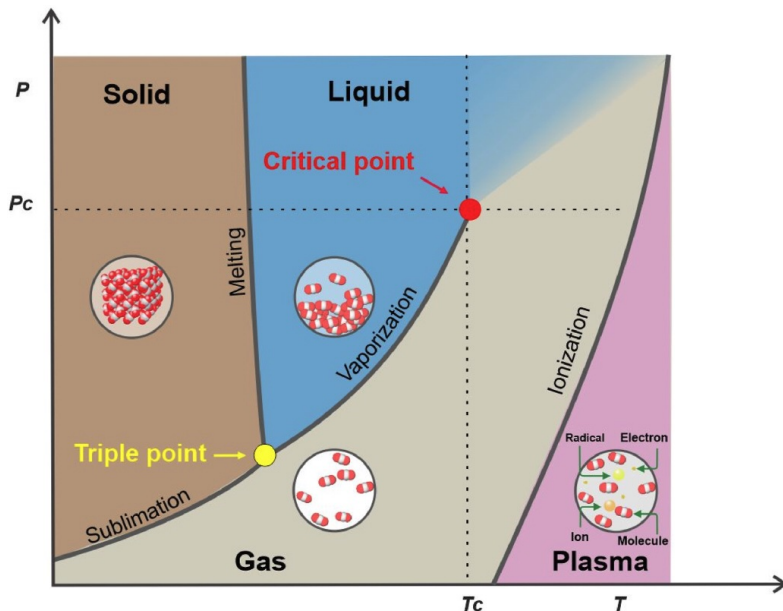


Figure 2.1. The phase diagram shows the states of matter in dependence of temperature (x axis) and pressure (y axis). On the intersections between the different phases, the name of the respective phase transition is given. The critical point is at a substance specific critical temperature and critical pressure, where all three phases coexist. Above this point it is not possible to distinguish between a liquid and a gas. The arrangement of the molecules is displayed in each state as a schematic. From this diagram it is clear that plasma only occurs at high temperatures, even at low pressures. (Cf. [8, Figure 2]).

change the shape of a plasma. It follows a collective behaviour due to Debye shielding, where the charged particles influence other close particles within their shielding length (Debye length) by Coulomb interactions.

The main difference from a gas is that the atoms and molecules are ionized in the plasma and that the particles interact with electromagnetic (EM) fields, whilst particles in a gas are neutral and individually interact with EM fields. Key characteristics of plasma are:

- Macroscopic quasi-neutrality
- Debye shielding
- Ionization

At the edge of a plasma, a boundary layer is formed. The plasma sheath is formed due to the higher mobility of electrons compared to ions, leading to charge separation and the creation of an electric field which repels electrons and attracts ions, resulting in a thin ion-rich sheath near the adjacent material. This charge separation creates a potential difference across the sheath, with the plasma side being at a higher potential than the surface of the adjacent material. There are various types of plasma reactors. The

most common ones are dielectric-barrier-discharge (DBD) reactors, where the plasma is generated between two electrodes with a dielectric material in-between. For this plasma breakdown, high electric fields are required. For CO<sub>2</sub> dissociation, microwave plasma reactors are most commonly used. Therefore these will be explained in more detail in the following section.

### 2.1.1. Microwave plasma

Microwave plasma refers to a plasma which is generated and sustained by the utilization of microwave electromagnetic radiation, typically with a frequency of 915 MHz or 2.45 GHz [12–15]. For CO<sub>2</sub> dissociation, microwave plasma torches are most common due to their higher energy efficiency and their high CO<sub>2</sub> conversion values [7]. The schematic setup of such a plasma reactor is displayed in figure 2.2.

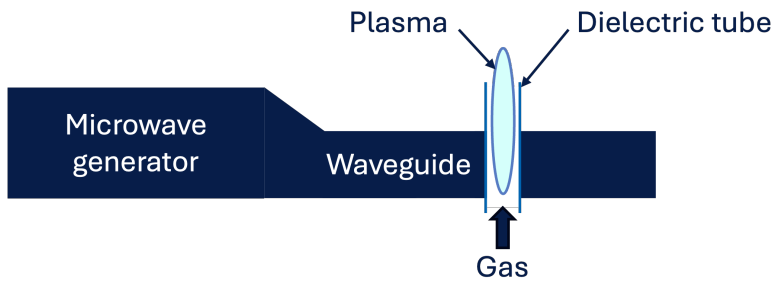


Figure 2.2. A schematic overview of a typical microwave plasma torch setup. The microwaves are generated and then coupled into the waveguide, which guides the microwaves to the dielectric tube where the gas absorbs the microwaves and the energy is high enough to ionize the gas. To sustain the plasma, a gas is continuously fed into the dielectric tube. The waveguide is designed in such a way that a maximum of the EM wave is at the intersection of the dielectric tube and the waveguide.

The key components of a microwave plasma system are:

- Microwave Source: Production of high-frequency electromagnetic waves.
- Waveguide: Guides the microwaves from the source to the discharge chamber.
- Plasma discharge chamber: The dielectric tube in which the gas is ionized and a plasma is formed.

The microwaves are generated at the source and then guided into a stub tuner which is used for impedance matching and to minimize the microwave power reflected from the plasma [7]. From here, the waves are guided through the waveguide to the dielectric tube which is placed in the center of the resonator, located at the maximum of the EM wave. Microwave plasmas can be used for thin film deposition [16], etching [17] or for environmental applications such as CO<sub>2</sub> dissociation [18].

In this thesis, the microwave plasma generator is assumed to be a variable heat source with adjustable temperatures.

In figure 2.2 a schematic of a commonly used microwave plasma torch is presented. The gas is continuously fed into the dielectric tube, where it is ionized by the high energy of the EM waves, resulting in the formation of a plasma. Convective mass transport is of great importance in the context of a microwave plasma torch, as it is essential for the gas mixing and therefore defining the time that the gas is exposed to the plasma. As the ionized gas expands and is forced through the dielectric tube as a plasma jet, this convective flow is also crucial for the transport of the ionized gas out of the plasma region, where it then cools and recombines. The gas flow rate has no influence on the residence time of the gas in the plasma [6]. To prevent recombination of CO to CO<sub>2</sub> during the cooling of a plasma, quenching is introduced in the following section.

Insufficient gas flow rates can result in plasma extinction, due to a lack of sufficient gas particles for ionization, leading to a evaporation of the reaction chamber. However, in a well-designed plasma torch, the plasma can be sustained for extended periods without considerable issues. To achieve this, the gas is injected so that a vortex flow is created.

### 2.1.2. Quenching

In the field of plasma physics, quenching refers to the rapid cooling of ionized gases, which suppresses the conversion of CO back to CO<sub>2</sub> (known as the 'recombination process'). This process allows for the sustained maintenance of the gas composition from plasma temperatures (several thousand Kelvin) [7]. Quenching is a non-equilibrium effect as the temperature is constantly and rapidly changed before the steady state is reached. Fast quenching is important as the recombination and thermal dissociation is no longer important at room temperatures (300 K) and the reaction products are 'frozen' [19]. It also plays another important role as it withdraws excess energy from the formed products [20]. As the quenching is not instantaneous and the reactants and products remain in the gas phase afterwards, there are still back reactions on the way from the high plasma temperatures, back to room temperature [13]. Quenching is used in almost all CO<sub>2</sub> dissociation reactions as it always leads to higher conversion rates [19]. Kinetic models have shown that cooling rates are best at 10<sup>6</sup> or 10<sup>7</sup> K s<sup>-1</sup> [22], other models recommend even higher cooling rates for high CO<sub>2</sub> conversion rates [13]. A schematic overview of quenching methods with typical rates of 10<sup>6</sup> K s<sup>-1</sup> is shown in figure 2.3. To reach quenching rates of up to 10<sup>6</sup> K s<sup>-1</sup>, the gas mixing method can be used, where a cold gas is rapidly fed into the outflow of the reaction chamber [23]. An additional enhancement to the cooling performance can be achieved by allowing the cold gas to swirl around the ionized gas, which is done by default in high power plasma reactors.

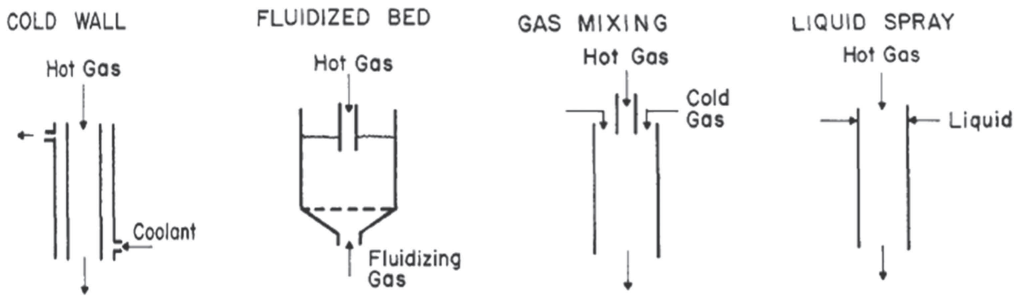


Figure 2.3. Overview of quenching methods. The ionized gas from the plasma is always described as hot gas in the figure. In these processes, the cooling fluid is typically the process gas, which prevents further contamination of the reaction. The only exception is the cold wall method, where any fluid can be used as it should not come in contact with the ionized gas. With these methods, quenching rates of up to  $10^6 \text{ K s}^{-1}$  are commonly realized. (Cf. [21, Figure 4])

## 2.2. Thermodynamic calculations

Thermodynamic calculations are performed with the NASA Chemical Equilibrium and Application (NASA CEA) solver, which is a program to calculate the chemical equilibrium compositions and properties of complex mixtures by minimization of the Gibbs free energy. It represents the latest in a number of programs developed by NASA at the Glenn Research Center since the 1950s [24]. The applications include assigned thermodynamic states, theoretical rocket performance or shock-tube parameter calculations. It is widely used in the aerodynamics and thermodynamics communities. A huge advantage of this approach is that no set of reactions has to be specified *a priori* [25]. The main disadvantage is the inability to investigate the time-resolved evolution of a system in order to understand how it reaches chemical equilibrium.

### 2.2.1. Chemical Equilibrium

In chemical equilibrium, the concentration of reactants and products remains constant over time, assuming the system is closed and is at a constant temperature and pressure. The main principle of the CEA Solver to reach chemical equilibrium is the minimization of the Gibbs free energy ( $G$ ) for specified temperature and pressure with the given reactants [13]. Other ways to calculate chemical equilibrium are the minimization of the Helmholtz energy or the maximization of entropy. The Gibbs free energy, the Helmholtz energy, and the entropy are state functions that maintain different variables at constant values. For the purposes of this thesis, the most suitable approach is the minimization of the Gibbs free energy, as temperature and pressure are its natural variables [25]. The Gibbs free energy is a thermodynamic potential that measures the maximum reversible work which a system can provide with constant temperature and pressure. The Gibbs free energy is

defined as

$$G = H - T \cdot S, \quad (2.1)$$

where  $H$  is the enthalpy,  $T$  is the temperature and  $S$  is the entropy of the system. The enthalpy is defined as,

$$H = U + p \cdot V, \quad (2.2)$$

with the internal energy  $U$ , pressure  $p$  and volume  $V$  of the system. The Gibbs energy  $G$  with intensive variables is,

$$G = \sum n_i \mu_i, \quad (2.3)$$

with the sum of the number of particles  $n_i$  and the chemical potential  $\mu_i$ . This expression is only applicable in cases where temperature and pressure remain constant.

With  $T$ ,  $p$  and the number of particles of a species  $n_i$  as control parameters, the change in the free Gibbs energy can be expressed as

$$dG = Vdp - SdT + \sum_i \mu_i dn_i \quad (2.4)$$

The minimization of the Gibbs free energy can be specified as

$$dG = \sum_i \left( \frac{\partial G}{\partial n_i} \right)_{T,p,n_j \neq n_i} = 0 \quad (2.5)$$

where  $i$  is the number of species and  $n_i$  is the number of particles of a species  $i$ . The advancement of a chemical reaction  $\xi$  in time is described as

$$\frac{d\xi}{dt} = \frac{d(n_i(t) - n_i(t=0))}{\nu_i dt} \quad (2.6)$$

with the stoichiometric number  $\nu_i$  of the species  $i$  [26, 27]. The equilibrium of a chemical reaction is therefore:

$$dG = \left( \frac{\partial G}{\partial \xi} \right)_{T,p,d\xi} = 0 \quad (2.7)$$

The minimization of Gibbs free energy is solved in CEA using the iterative Newton-Raphson method [25].

### 2.2.2. CEARUN

In the displayed work, the web-based implementation CEARUN of the CEA solver is used to calculate the chemical equilibrium of the models used [28]. This version is easier accessible compared to the FORTRAN implementation of the CEA solver.

First the type of problem has to be selected from the various applications of the solver. The list of problem types is shown in table 2.2. Each problem type has its own input mask which generates the input file for the CEA solver. In this work, the ‘Assigned

Table 2.2. Problem types in the CEARUN program which can be selected to use the web-based implementation of the NASA CEA solver. Only one problem type can be selected per program run [29]. The selection of any problem type leads to an input mask, specific to the selected problem.

Type Code	Description
rocket	Rocket
hp	Assigned Enthalpy & Pressure
tp	Assigned Temperature & Pressure
det	Chapman-Jouguet Detonation
shock	Shock Tube
tv	Assigned Temperature & Density
uv	Combustion at Assigned Density
sp	Assigned Entropy & Pressure
sv	Assigned Entropy & Density

Temperature and Pressure Problem' is used. For this, an input of up to 24 different temperatures and up to 24 different pressures is possible. For more temperature steps or pressures, another run of CEARUN is necessary. The reactants of the reactions have to be selected, as well as the ratio of fuels and oxidizers. All mixtures in these calculations are assumed to be pure.

It is furthermore possible to include transport properties. The output can be displayed in mass-fractions or mole-fractions. The output of the program is given in a text file, where the equilibrium composition of the reaction is displayed at any given input pressure and temperature.

## 2.3. Kinetic model

To understand the temporal development of CO<sub>2</sub> or H<sub>2</sub>O dissociation, a 0D-time dependent kinetic model is developed in Python. This model provides a simplified approach for examining chemical reactions and plasma processes in systems where spatial variations are negligible, focusing purely on temporal evolution. This leads to a homogeneous system without gradients. This model was chosen over more complex 1D, 2D or 3D Models due to its simplicity as thermodynamic state functions are independent of space and time. The temporal calculation is important for the simulation of quenching where the temperature is changed in time. The plasma is assumed to be an ideal thermalized bath with an external set temperature, other control parameters in the model are the initial densities or pressures.

The kinetic model is calculated for a defined timespan, with the objective of reaching a steady state at the end of the timespan. A steady state is defined as a point in time where the concentration of the species in the given system is no longer changing. This is of crucial importance for the benchmarking against the chemical equilibrium from the thermodynamic calculations. In contrast, for the simulation of the quenching, the reac-

tion does not have to be in the steady state, as quenching is a non-equilibrium effect.

Table 2.3. Exemplary list of reactions. With the species A, B, C, D and E

Index $j$	Reaction
1	$A + B \rightarrow C + D + E$
2	$C + D + E \rightarrow A + B$

Each reaction yields a specific rate coefficients, which form the temperature dependent rate coefficients  $k_j(T)$ . They are calculated using an Arrhenius equation, with dependence of a pre-exponential factor  $A_j$  and the activation energy of the reaction  $E_a$ .

$$k_j(T) = A_j \cdot \exp\left(-\frac{E_{a,j}}{k_B T}\right), \quad (2.8)$$

where  $k_B$  is the Boltzmann constant and  $T$  is the temperature. The reaction rates are then calculated with the temperature dependent rate coefficients as input parameter. An example set of reactions is given in table 2.3. For the bimolecular (two-body) reaction 1 the reaction rate of species C over time is

$$\frac{dn_{C,1}}{dt} = k_1(T) \cdot n_A \cdot n_B \quad (2.9)$$

with  $k_1(T)$  the temperature dependent rate coefficient of reaction 1,  $n_A$  the density of the species A and  $n_B$  the density of the species B. In the considered bimolecular reaction rate for species C, the reactants A and B are destructed and the products C, D and E are produced. All production terms have to be considered with a positive sign in the total reaction rate, whilst destruction rates are considered with a negative sign. The reaction rate of the trimolecular (three-body) reaction 2 for species C over time is therefore

$$\frac{dn_{C,2}}{dt} = -k_2(T) \cdot n_C \cdot n_D \cdot n_E \quad (2.10)$$

with  $k_2(T)$  the temperature dependent rate coefficient of reaction 1,  $n_C$  the density of the species C,  $n_D$  the density of the species D and  $n_E$  the density of the species E. To respect the conservation of mass, forward and backward reactions are given in table 2.3, so that, the reactions 1 and 2 are in equilibrium. The total reaction rates for each species are calculated as a sum of all the production and destruction terms [13]. Therefore, the total reaction rate for species C over time is

$$\frac{dn_C}{dt} = k_1(T) \cdot n_A \cdot n_B - k_2(T) \cdot n_C \cdot n_D \cdot n_E \quad (2.11)$$

The temporal behaviour is then calculated by numerically integrating the system of dif-

ferential equations over a given time. After this timespan, the system should be at a steady state, which should be equal to the chemical equilibrium.

The chemical reaction constants were implemented as a list. For every species in the reaction there is a separate ordinary differential equation (ODE). With this method, a system of coupled ODEs is created. After solving the system of ODEs, the evolution of the chemical composition can be plotted over time.

For comparison between the CEA solver (see section 2.2) and the 0D kinetic model, the model is solved for a given set of temperatures. Every temperature step needs its own calculation. The final concentrations are then taken after a sufficiently long time and saved in a list, a similar plot to the CEA results can be created from the final concentrations. Coupling the two different approaches of calculating the equilibrium and using the CEA as a verification for the equilibrium composition, a comprehensive analysis of both transient and steady-state behaviours in plasma systems can be performed.

However, these calculations differ from a real setup, as the time can be specified as an indefinite period. Whilst in an actual plasma torch the gas is only at these high temperatures for a few milliseconds before it cools down, this time span is called residence time. It is defined by the convective mass flow.

To simulate the cooling behaviour, quenching is introduced in section 2.1.2. This step is necessary to calculate the chemical composition after cooling. The composition at high temperatures can be sustained by the introduction of high quenching rates, and therefore halting the recombination processes.

### 2.3.1. Density

In the density based calculation, the volume of the system is constant at all temperatures. The initial density must be calculated in every single temperature step, as the total number density increases. The initial pressure has to be converted into an initial density. For this, the starting point is the ideal gas law,

$$p = nk_B T, \quad (2.12)$$

with the pressure  $p$ , the volume  $V$ , the number of particles of the gas  $N$ , the Boltzmann constant  $k_B$  and the gas temperature  $T$ . To calculate the number of particles per volume (number density), the ideal gas law from equation 2.12 has to be divided by volume, Boltzmann constant and temperature, as follows

$$\frac{p}{k_B T} = \frac{N}{V} \quad (2.13)$$

From equation 2.13 it is clear that for a constant number of particles the volume only can change if pressure or temperature change, as  $k_B$  is a constant.

The number of particles divided by the volume can then be expressed by  $n_i$  for each species  $i$ .

$$n_i = \frac{N_i}{V} \quad (2.14)$$

The number density for a species  $i$  has two adjustable parameters: first is the partial pressure of every species  $p_i$  and the second is the gas temperature.

$$n_i = \frac{p_i}{k_B \cdot T} \quad (2.15)$$

The pressure of the system is the sum of all the partial pressures of the different species.

$$p = \sum_i p_i \quad (2.16)$$

With this, the total number density for all species can be calculated as,

$$n = \frac{p}{k_B \cdot T} \quad (2.17)$$

With every calculation where the temperature changes also the number density changes, as the initial pressure is fixed. During the calculation of the kinetic model, the temperature, pressure and number of particles are considered constant, therefore the only parameter which can influence the number density is the volume. In a realistic setup the pressure and temperature are constant, therefore the volume must change. This is realized with the pressure based calculations.

### 2.3.2. Pressure

To keep a constant pressure in the plasma system at high temperatures, the volume must change during the calculations, therefore pressure based calculation are introduced. The fictional pressure of the system before relaxation is calculated in each time step as the sum of all species in the reaction

$$p_{system} = \sum p_i(t) \quad (2.18)$$

with the pressure  $p_i(t)$  dependent on each species  $i$ . In the ODEs the densities are converted into partial pressures.

Hence, equation 2.9 for the pressure based model without correction terms is  $\frac{dp_{C,1}}{dt}$  the evolution of the pressure of species C over time for the bimolecular reaction 1 from table 2.3

$$\frac{dp_{C,1}}{dt} = k_1(T) \cdot \frac{p_A}{p_{system}} \cdot \frac{p_B}{p_{system}} \quad (2.19)$$

with the partial pressures of the species  $p_A$  and  $p_B$  and the pressure in the system at each discrete time step  $p_{system}$ . With all necessary correction terms applied to equation 2.19

the full term is for reaction rate of the two-body reaction 1 from table 2.3 is

$$\frac{dp_{C,1}}{dt} = k_1(T) \cdot \frac{p_A}{p_{system}} \cdot \frac{p_B}{p_{system}} \cdot corr_2 \cdot p_{corr} \quad (2.20)$$

with a unit correction term  $corr_2$  for bimolecular reactions and the pressure correction term  $p_{corr}$ . The unit correction term is necessary as the literature values for rate constants are commonly in density based units. As the units change for two-body and three-body reactions, the pressure term has to change too. This correction term was introduced by den Harder et al. [13]. It is a unit correction factor for the density based pre-exponential factor in the temperature dependent rate coefficient. For two-body reactions the correction term is

$$corr_2 = \frac{p_{init}^2}{k_B \cdot T} \quad (2.21)$$

with the pressure of a real system  $p_{init}$ , the Boltzmann constant  $k_B$  and the Temperature  $T$ .  $p_{init}$  is the pressure at which the reactions are calculated. For the 3-body reactions, the correction term is

$$corr_3 = \frac{p_{init}^3}{(k_B \cdot T)^2} \quad (2.22)$$

As the volume of the system is kept constant, the pressure rises during the splitting of a molecule into its parts. Due to the non-equilibrium nature of this system, the rise in pressure has to be compensated for in the calculations

$$p_{corr} = \frac{p_{init}}{p_{system}} \quad (2.23)$$

with the correction term  $p_{corr}$ , the initial pressure in the system  $p_{init}$  and the pressure at each time step  $p_{system}$ .

The full term for reaction rate 1 with correction terms applied is

$$\frac{dp_{C,1}}{dt} = k_1(T) \cdot \frac{p_A}{p_{system}} \cdot \frac{p_B}{p_{system}} \cdot \frac{p_{init}^2}{k_B \cdot T} \cdot \frac{p_{init}}{p_{system}} \quad (2.24)$$

The pressure based rate of the trimolecular reaction 2 from table 2.3 would be

$$\frac{dp_{C,2}}{dt} = -k_2(T) \cdot \frac{p_C}{p_{system}} \cdot \frac{p_D}{p_{system}} \cdot \frac{p_E}{p_{system}} \cdot \frac{p_{init}^3}{(k_B \cdot T)^2} \cdot \frac{p_{init}}{p_{system}} \quad (2.25)$$

For a better legibility and comprehensibility, the correction terms are included in the rate constants  $k_j(T)$  in the Python implementation of the model.

## 2.4. Code validation

The code of the newly implemented 0D-kinetic python model for the thermal dissociation of CO<sub>2</sub> was validated by comparing its output to the output of the python implementation

by den Harder et al. [13]. Furthermore an initial Mathematica implementation of the CO<sub>2</sub> model based on table B.1 done by Prof. Carbone (INRS) is used for the validation of the model. These comparisons with the absolute deviations are presented in section 3.2. Validation of the CO<sub>2</sub> and the H<sub>2</sub>O models is further possible with the results from shock tube experiments. In a shock tube experiments the reaction rates are experimentally determined. The benchmarked CO<sub>2</sub> model is then further validated with shock tube results from Brabbs et al. [30] which is carried out at pressures of 11 bar to 20 bar.

## 2.5. Benchmarking of different models

In order to select an appropriate model for the CO<sub>2</sub> and H<sub>2</sub>O dissociation combination, it is necessary to choose a comprehensive model from the available literature. Multiple different models are implemented and their output is afterwards benchmarked against the results from NASA's CEA solver. All models from literature are implemented in Python and their output is then benchmarked against the CEARUN output. A small deviation of the output to the CEARUN results is expected.

This deviation can be explained by the different physics employed in the calculation of the chemical composition. NASA's CEA solver employs a minimization of the Gibbs free energy to calculate chemical equilibrium, which is an effective and precise method for determining a system's chemical equilibrium state. In any case, thermodynamics do not allow any investigation of reaction development over time. The kinetic models calculate the chemical composition over time until the steady state is reached, allowing for investigation of the chemical composition at any discrete time step. To conduct quenching simulations, the kinetic calculations are necessary, as similar results cannot be obtained with the CEA solver.

The benchmarking is done with respect to the most correct chemical composition at every temperature step. The following section presents the results of the recently implemented CO<sub>2</sub> dissociation model, employing the aforementioned methods.

## 3. CO<sub>2</sub> dissociation

In this chapter, the results of the CO<sub>2</sub> calculations will be presented and discussed. The results of the NASA CEA solver will be compared to the output from the developed models. A few different models are taken into account to find the best fitting result for the thermodynamic calculations. Furthermore, issues with the initial implementation of the model will be discussed in section 3.2.

### 3.1. NASA CEA

The CEARUN program is used with the assigned temperature and pressure program. To cover the entire temperature range from 1000 K to 6100 K in steps of 100 K, multiple runs of CEARUN are performed. The pressure is kept at a constant 100 mbar. The temperature range is chosen to cover all models selected for comparison [13, 31, 32]. The full input and output files are given in Appendix A. CO<sub>2</sub> is used as fuel and as oxidizer. It must be selected from the periodic table as it is not a standard mixture. No other fuels or oxidizers are chosen, therefore the initial gas mixture is 100 % CO<sub>2</sub>. The output of the calculations is then given in mole-fractions. The plot of the output is presented in figure 3.1. CO<sub>2</sub> dissociation starts at 1500 K and CO<sub>2</sub> is fully dissociated at 4000 K. Starting at 5000 K, CO is dissociated into C and O.

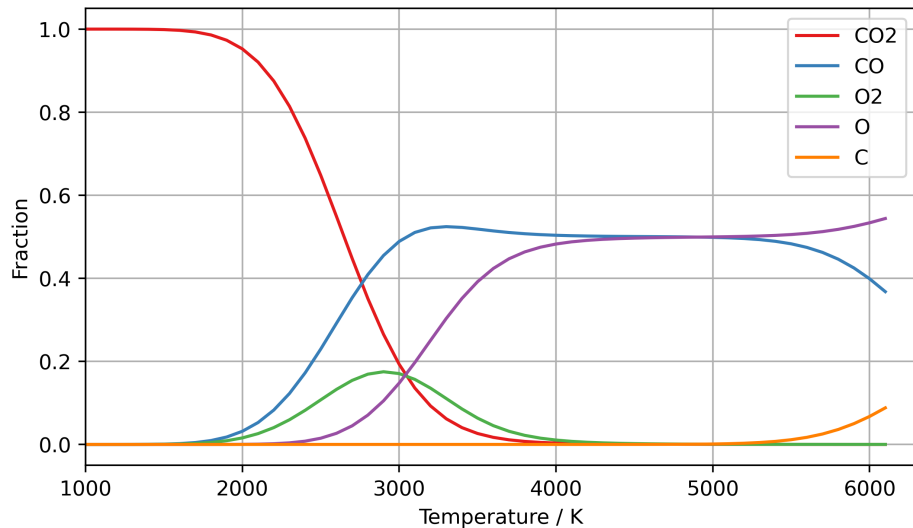


Figure 3.1. Output from CEARUN for a temperature range from 1000 K to 6100 K. The pressure is fixed at 100 mbar.

## 3.2. Code validation

In this section, the output of the Python model is verified with the result from the implementation of den Harder et al. [13] and a Mathematica model by Prof. Carbone (INRS). Rate constants for the python model were calculated with the values from den Harder et al. [13, Table 1]. A comparison of these results is presented in figure 3.2. The newly implemented is density based and is calculated in a temperature range from 1000 K to 6100 K, the mixtures initial composition is 100 %  $\text{CO}_2$  with a calculated density at a pressure of 100 mbar. A time span of 2.5 s is considered for the code validation with the Mathematica model. The full reaction set is given in table B.1.

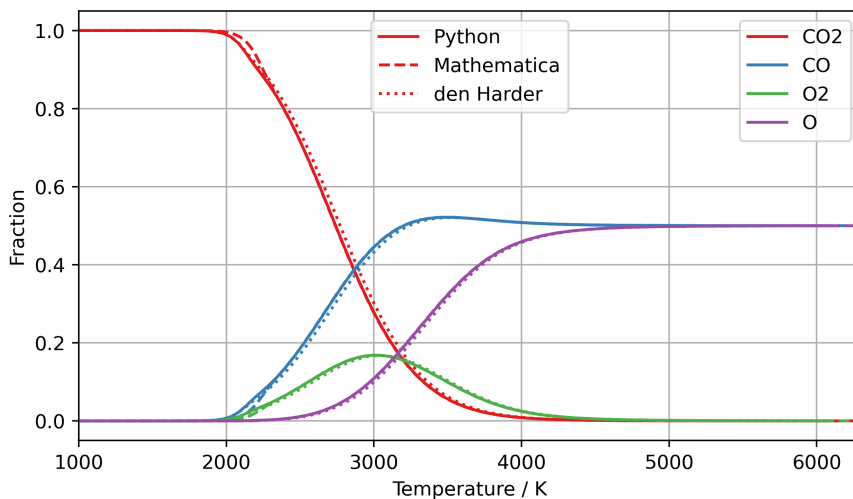


Figure 3.2. Comparison of the newly implemented Python model with den Harder's implementation and the Mathematica model. The Mathematica implementation clearly deviates in the range from 2000 K to 2300 K. The deviation of the other models is noticeable in the range of 2300 K to 4000 K.

In figure 3.2, a deviation is seen for all the plots. The clear deviation in the range from 2000 K to 2300 K is the Mathematica model, which deviates from the other implementations. This is due to the usage of a different solving algorithm, as the model is later congruent with the python implementation.

However, this does not explain the small but noticeable deviation from den Harder's original model to the new implementation. To understand this deviation, the paper from which den Harder's implementation is based on has to be considered. This is a paper from Butylkin et al. [32]. After converting the activation energy necessary to calculate the rate constants from kcal/mole from Butylkin et al. [32] to eV, a deviation for the reactions 9, 10 and 11 is found. The exact numbers are given in table 3.1.

This deviation could only be found after tracing the calculations in the original Python implementation of den Harder et al. [13], where the numbers published and used in the code deviate. After correcting the values of the activation energy, the implementation

Table 3.1. Comparison of the values published in den Harder’s paper and in Butylkin’s paper. The implementation of den Harder directly used the converted values from the original paper.

Index	den Harder in eV [13]	Butylkin in eV [32]	Butylkin in kcal/mole [32]
9	0.13	0.188 33	4.340
10	0.13	0.188 33	4.340
11	0.13	-0.160 55	-3.700

showed the same results as den Harder’, with only a minor deviation, due to numerical inaccuracies. This inaccuracies are probably from the usage of two different solvers in Python. While den Harder’s model uses the `odeint` function, which is the Python implementation of lsoda from FORTRAN’s library `odepack`, the new Python implementation uses the `solve_ivp` function, which is a faster and more modern implementation, with more options regarding the accuracy and usage of different solving methods [33]. In figure 3.3, the corrected implementation is shown with the original implementation. In order to reach the steady state, the time span is extended to 10 000 s.

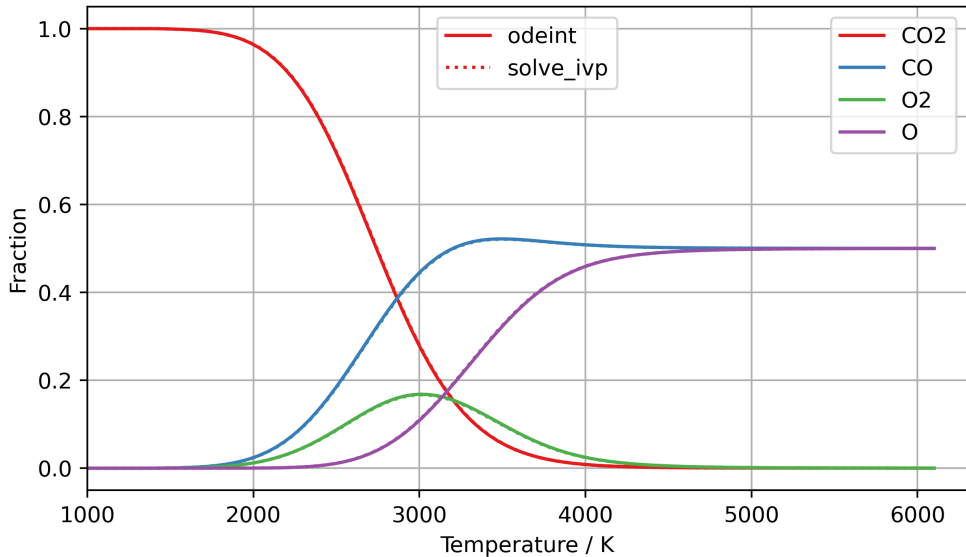
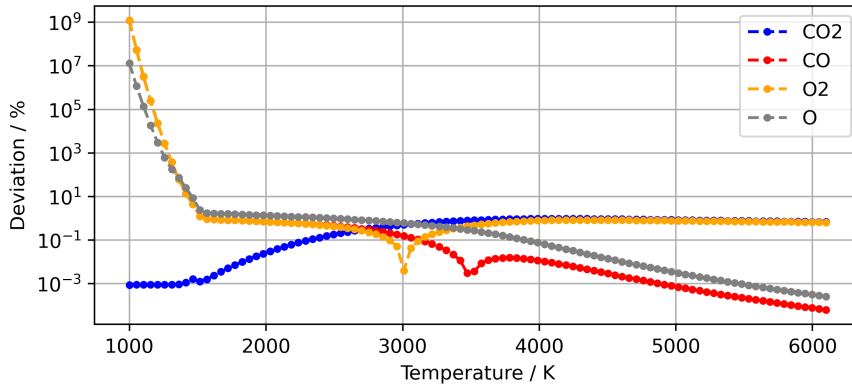


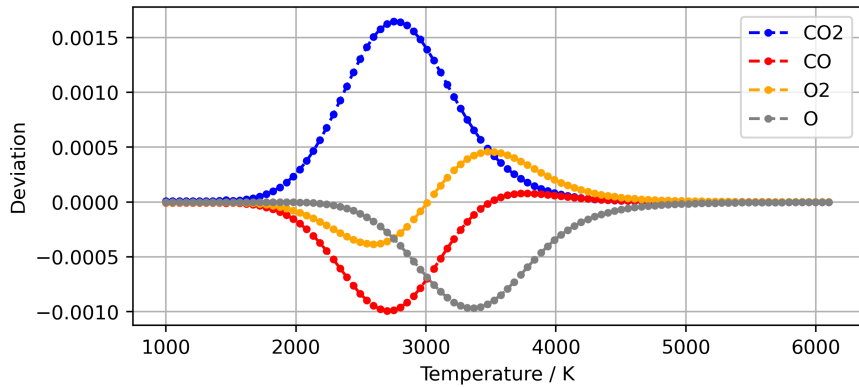
Figure 3.3. Comparison of the Python implementation with `odeint` from den Harder and the new Python implementation with `solve_ivp`. It is not possible to see a difference on this scale.

As it is impossible to see a deviation from figure 3.3, the relative deviation of both implementations is presented in Figure 3.4a. A huge deviation up to  $1 \times 10^9$  % is seen at 1000 K for the oxygen. The deviation descends until it reaches below 1 % at 1500 K. At this temperature no dissociation of  $\text{CO}_2$  can be observed in figure 3.3. This is also a probable reason for the deviation. At 1000 K the amount of  $\text{O}_2$  is at  $1 \times 10^{-6}$  for

den Harder's implementation. At the same temperature, the amount of O<sub>2</sub> in the new implementation is at  $1 \times 10^{-13}$ . For O, the same behaviour can be observed. This high deviation of the concentrations can only be explained with the usage of different solving algorithms. The relative deviation of CO<sub>2</sub>, where there is a high concentration in the beginning, is in the range of  $1 \times 10^{-3} \%$ .



(a) Relative deviation of Python implementations



(b) Absolute deviation of Python implementations

Figure 3.4. Relative and absolute deviation for den Harder's model with `odeint` and the new Python implementation with `solve_ivp`. The given deviation is always the between den Harder's original implementation and the new Python implementation.

The absolute deviation is given in Figure 3.4b, where it is obvious that the very high relative deviation for temperatures below 1500 K is negligibly low. CO<sub>2</sub> has the highest absolute deviation at 2750 K with  $1.6 \times 10^{-3}$  which translates to a relative deviation of 0.3 %. This is in the range of numerical inaccuracies for the two implementations. The new implementation which uses Python's `solve_ivp` function is therefore validated within solver accuracy. The following section will present the benchmarking of various

models with the results of the CEARUN solver, with a focus on the accuracy in chemical equilibrium.

### 3.3. Benchmarking

After the validation of the Python implementation, the model was benchmarked regarding the accuracy with the result of the CEA solver. The previously validated implementation, based on the model from den Harder et al. [13], which uses Python's `solve_ivp` function is from here on labeled as den Harder model. Further considered models are similarly designated. All models are considered in a temperature range from 1000 K to 6100 K, the initial CO<sub>2</sub> density is calculated for a mixture of 100 % CO<sub>2</sub> at 100 mbar, with a considered time span of 10000 s.

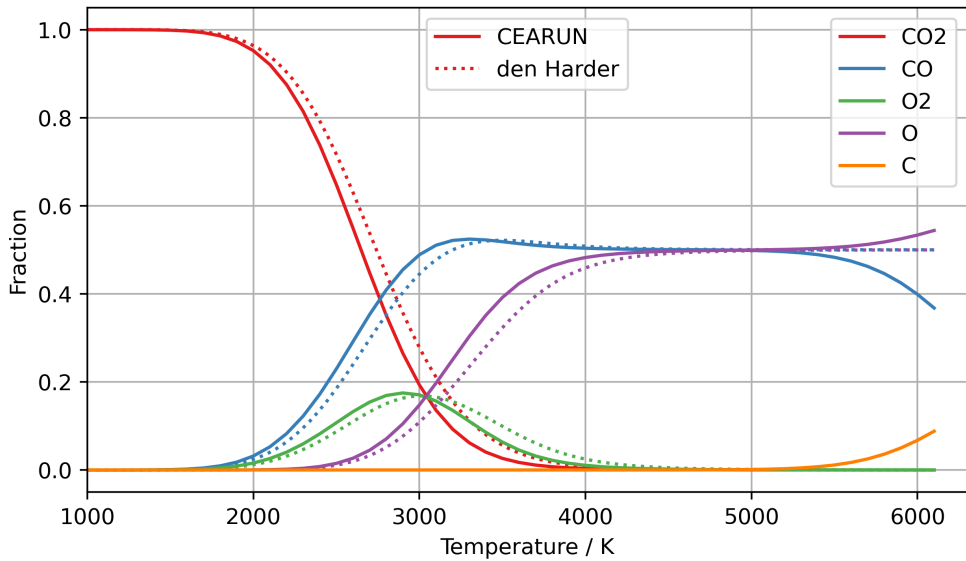


Figure 3.5. Comparison of the CEARUN result and den Harder's model. There is a deviation in the range from 2000 K to 4500 K. Above 5000 K there is again a deviation which is a result of thermal CO dissociation into C and O which is not covered by this model.

There is an obvious deviation from the CEARUN result in figure 3.5. Especially in the temperature range above 5000 K, where the further thermal dissociation of CO is present in the result from CEARUN. This dissociation is not shown in the kinetic model, as carbon is not present in den Harder's model. To get a better result, carbon can be added to the model or another more comprehensive model including carbon can be used. Another comprehensive model is found in the literature from Koelman et al. [31]. The advantage of Koelman's model is that it also features carbon. A implementation of Koelman's model is presented in figure 3.6, together with the result of the CEA solver and the result from den Harder's model. The full set of reactions for Koelman's model is given in table B.2. From figure 3.6, it is clear that the model from Koelman et al. [31] is further away from

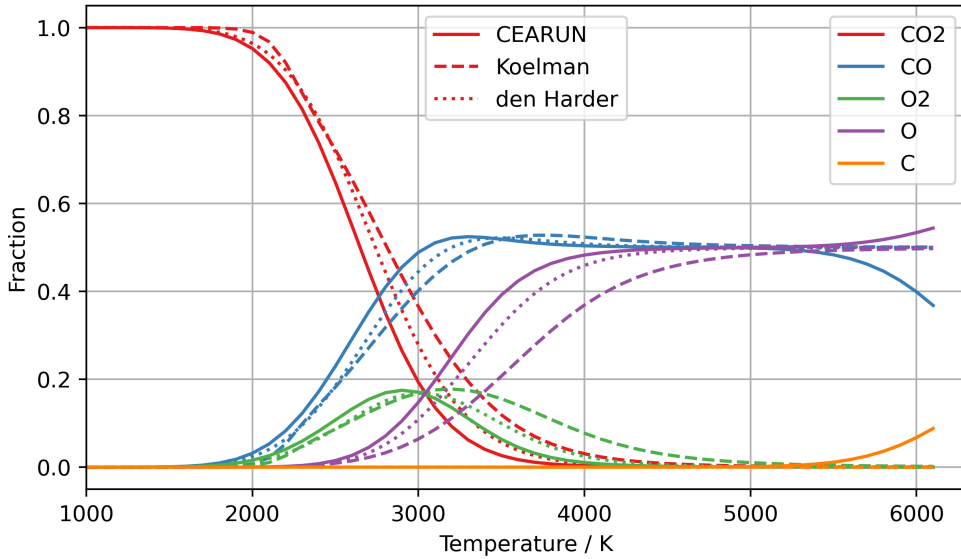


Figure 3.6. Comparison of the CEARUN result, with the den Harder model and the Koelman model. The den Harder model fits far better to the result from CEARUN than the Koelman model.

chemical equilibrium than the model from den Harder et al. [13]. The Koelman model should be more comprehensive than the den Harder model as it adds C,  $\text{O}_3$  and  $\text{C}_2\text{O}$ . Following further analysis, it was identified that the results are not better as no production term for C is present in Koelman's model. This means that the further thermal CO dissociation cannot be considered with this model. The  $\text{O}_3$  and  $\text{C}_2\text{O}$  also does not show in the results to any meaningful degree. As they are under 20 ppm (parts per million) for every temperature in the CEARUN results, they are therefore not further considered. For all subsequent calculations, the model developed by den Harder et al. [13] is considered, as its final concentrations are more closely aligned with the chemical equilibrium data from CEARUN and no improvement could be found with the model from Koelman et al. [31]. The model from den Harder et al. [13] is improved in the following section 3.4 to also feature carbon.

Beforehand, this model is converted to pressure based calculations. This should bring the model closer to the CEARUN results. The pressure based calculations should be more accurate as the volume of the system changes with density based calculations. With the pressure based calculations, the volume is kept constant, so the pressure can rise within the system. This is especially important when atomic C is added to the den Harder's Model in section 3.4.

The pressure based model is presented in figure 3.7, together with the results of the CEA solver and the previously implemented density based model. A significant improvement

### 3.3. BENCHMARKING

---

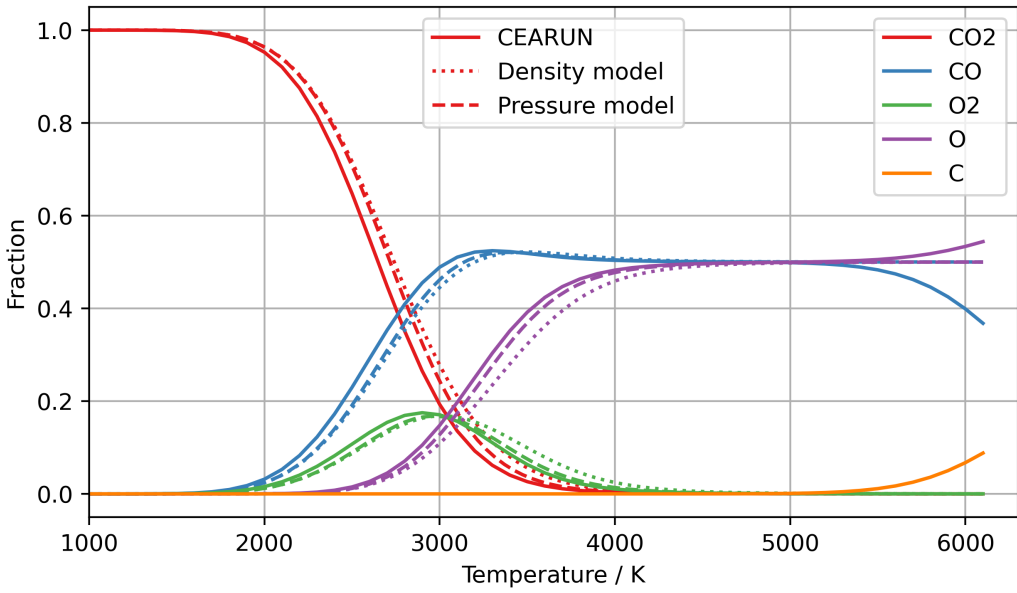


Figure 3.7. In this plot, the result from the CEARUN program is compared to the result from the density based and the pressure based den Harder model.

of the model is noticed by the change to a pressure based model. The absolute deviation of each model against the CEA result is presented in figure 3.8. The change improves the accuracy of the results by notable margin. The greatest improvement is visible in the range from 2000 K to 4000 K with CO and O. These results reinforce confidence in the model to a significant extent. Also, the deviation for O<sub>2</sub> is significantly improved in the range from 3000 K to 4000 K.

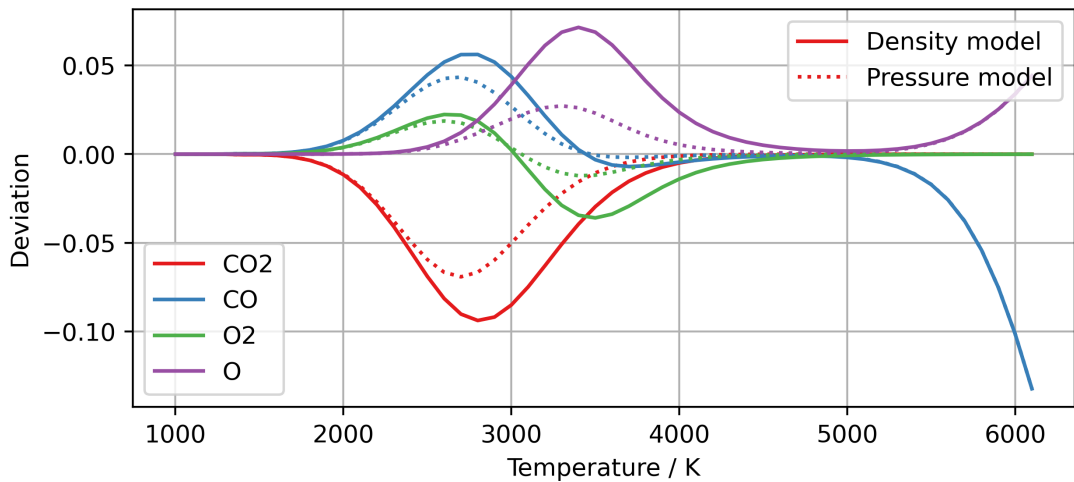


Figure 3.8. The absolute deviation of the density and pressure model against the CEA result is presented.

The greatest absolute deviation from the CEARUN results are at temperatures above 5000 K, this is expected. At these temperatures, the thermal dissociation of CO into C and O becomes a more significant process. This result cannot be reproduced with the current implementation of the kinetic model, as C is not part of it. The following section addresses this issue.

### 3.4. Addition of carbon atom kinetics

Until now the model does not consider carbon, which is an important species for temperatures above 5000 K. This was not addressed in den Harder's Model before, as temperatures above 5000 K were not considered [13,32]. The calculations in this section are carried out in a temperature range from 1000 K to 6100 K with an initial pressure of 100 mbar. The initial mixture contains 100 %  $\text{CO}_2$ . The considered time span is 10 000 s.

To consider carbon in the model, a suitable implementation of the thermal CO dissociation must be found. In the publication of Butylkin et al. [32] a carbon production term was found for temperatures below 5000 K. This term is based on a shock tube experiment for CO diluted in argon, published by Fairbairn [34]. This term is implemented but yields no change in the reaction. A more promising set of reactions is found published

Table 3.2. Reactions from Beuthe et al. [35] involving C. These reactions are implemented into the pressure based model. With argon as M (see text for more details). The unit of the reaction rate constants is  $\frac{\text{cm}^3}{\text{s}}$  for two-body reactions and in  $\frac{\text{cm}^6}{\text{s}}$  for three-body reactions.  $T_g$  is the temperature of the gas

Index	Reaction	Reaction rate constants
C1	$\text{CO} + \text{M} \rightarrow \text{C} + \text{O} + \text{M}$	$1.46 \times 10^6 \cdot T_g^{-3.52} \exp(-128700/T_g)$
C2	$\text{CO}_2 + \text{C} \rightarrow \text{CO} + \text{CO}$	$1.0 \times 10^{-15}$
C3	$\text{C} + \text{O} + \text{M} \rightarrow \text{CO} + \text{M}$	$9.1 \times 10^{-22} \cdot T_g^{-3.08} \exp(2114/T_g)$

from Beuthe et al. [35]. The relevant neutral reactions are given in table 3.2. This model consists of production and destruction terms of the carbon atom. Argon was used as a bath gas in this model. As an implementation of argon would add unnecessary complexity to the model it is circumvented by replacing it with  $\text{CO}_2$  as a first step. This is only possible as  $\text{CO}_2$  has a similar molecular mass (44 u) compared with argon (40 u). The results from these calculations are displayed in figure 3.9 and yielded an improvement over the den Harder model without atomic carbon. Pyrolysis of CO started in this implementation at too high temperatures, therefore more rate constants for the production terms were investigated.

In the kinetic reaction database of the US American National Institute of Standards and Technology (NIST) 3 more reaction rate constants are found [36]. These rate constants are originally published by Mick et al. [37], Hanson [38] and Appleton et al. [39]. Mick's reaction rate constant leads to lower C production and the pyrolysis started at even

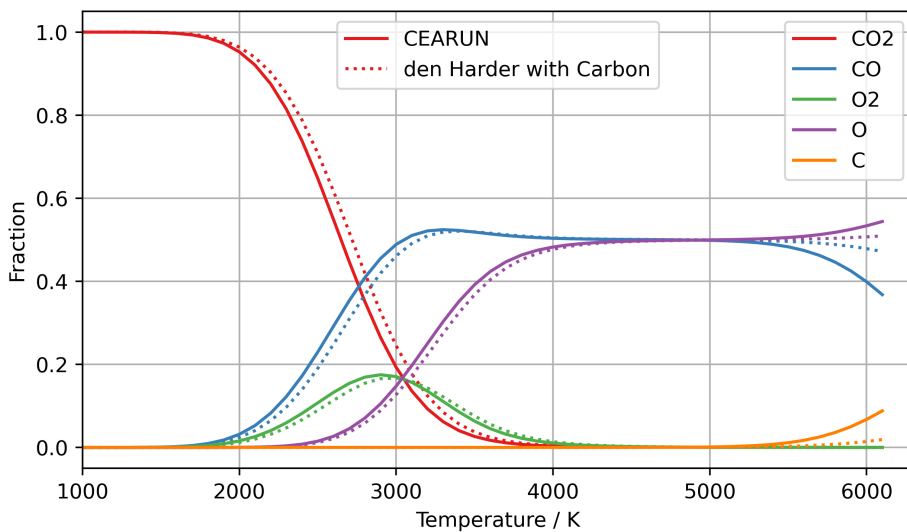


Figure 3.9. The CEARUN result is presented with the pressure based den Harder model with carbon from Beuthe's Model added to it.  $\text{CO}_2$  is used as bath gas instead of argon. The deviation from the CEA result for temperatures above 5000 K is smaller. The additional consideration of carbon enhances the model.

higher temperatures. Hanson's model presents production of atomic carbon already at temperatures of 4500 K and overestimates the carbon concentration at 6000 K. With Appleton's model CO is dissociated at too high temperatures. The best fitting result yields Beuthe's implementation.

To improve the model, the mass of Ar which was previously replaced by  $\text{CO}_2$  is considered. The reactions involving C are corrected for the mass. As the  $\text{CO}_2$  concentration approaches zero at higher temperatures, the sum of all mass corrected species in the reaction is used as a replacement for argon. So as a result the whole gas is used as process gas instead. After the extension of the model by carbon, the present species are  $\text{CO}_2$ , CO, O,  $\text{O}_2$  and C. To correct for the mass of the missing argon the following term was multiplied by the reaction rate constants

$$Corr_{Mass} = \frac{\sum \frac{m_i}{m_{Ar}} \cdot p_i}{p_{system}} \quad (3.1)$$

where  $m_i$  is the atomic mass of the species i and  $p_i$  is the pressure of species i, the atomic mass of argon is  $m_{Ar}$ . This correction term is used for the reactions C1 and C3 from table 3.2 as both feature argon in the Beuthe's original model. The improved model is presented together with the CEARUN result in figure 3.10. The chemical equilibrium is improved, especially for temperatures above 5000 K, where the difference between the solving methods is below 0.01 mole fractions. This now comprehensive model for

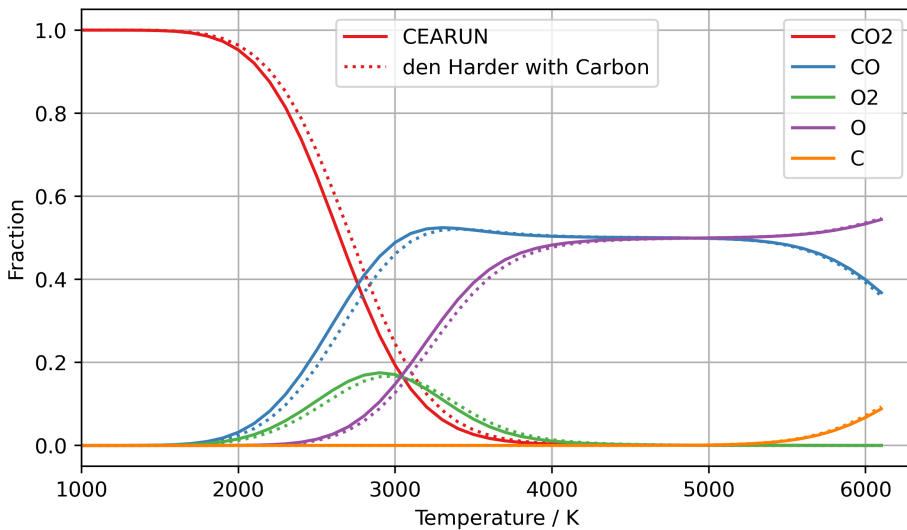


Figure 3.10. The CEARUN result is presented with the improved pressure based den Harder model with carbon from Beuthe's Model added to it. In the range above 5000 K, the deviation from the CEA result is minimal. The additional mass correction noticeably enhances the model.

temperatures between 1000 K and 6100 K is used in the following section for quenching simulations. The performance of the model at lower temperatures cannot be improved by the addition of carbon, as carbon production does not take place at these lower temperatures. The combined model is given in table B.4.

### 3.4.1. Validation with shock tube experiment

The implemented pressure based Python model based on den Harder's model with added atomic carbon reactions from Beuthe et al. [35] is verified in this section with results from shock tube experiments published by Brabbs et al. [30]. The model is validated at a temperature of 2665 K, the shock tube used a pressure of 20.68 atm (20.95 bar). The CO<sub>2</sub> partial pressure was 7.02 %. The publication yields a CO concentration of 7.6 kPa after 600  $\mu$ s. The Python implementation is displayed in figure 3.11 and yields a CO concentration of 7.5 kPa after 600  $\mu$ s. This deviation is within the range of acceptable reading accuracy. The implemented model is therefore validated.

### 3.4.2. Model validation with thermodynamic results

The enhanced model with carbon is further validated with thermodynamic results from the CEA Solver. The model is valid from pressures of 1 Pa up to up to 1 MPa in a temperature range from 1000 K to 7000 K. Validation with CEARUN at 1 Pa is displayed in figure 3.12 and the validation at 1 MPa in figure 3.13.

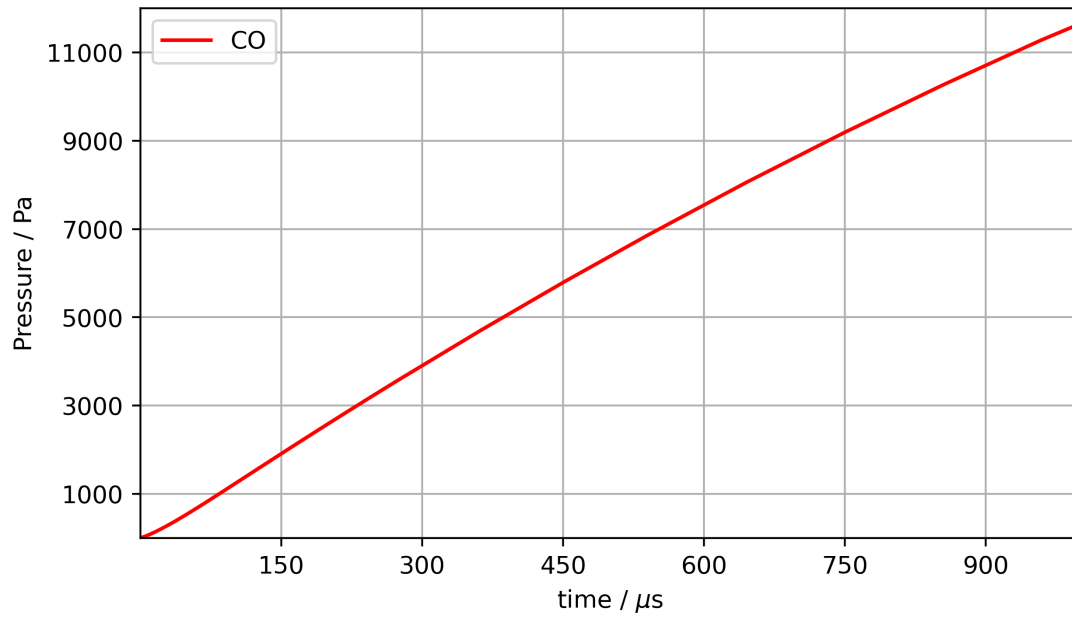


Figure 3.11. The development of CO at 2665 K is shown. The initial  $\text{CO}_2$  concentration is 7.02 % of 20.95 bar.

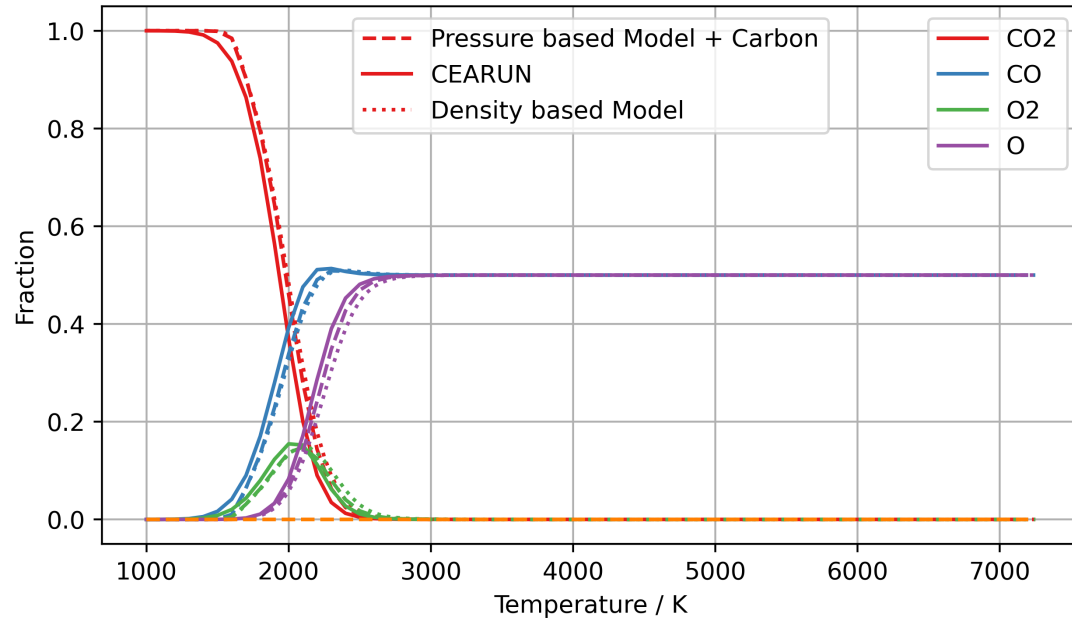


Figure 3.12. Validation of the pressure based model extended with carbon at a pressure of 1 Pa. CEARUN result and density based model are given as references.

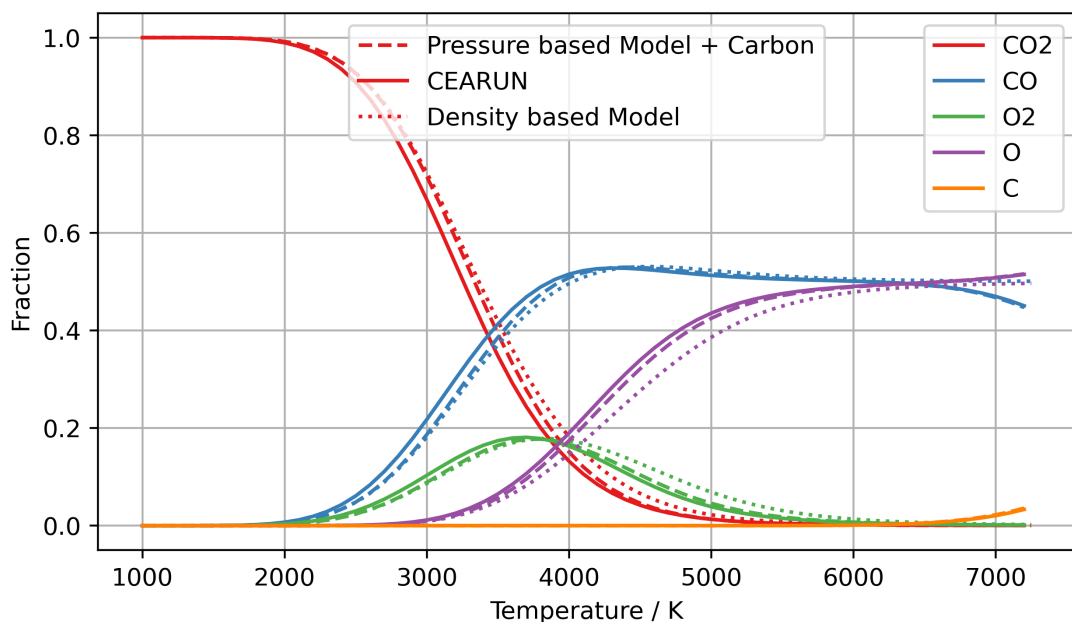


Figure 3.13. Validation of the pressure based model extended with carbon at a pressure of 1 MPa. CEARUN result and density based model are given as references.

## 3.5. Quenching

In this section, the now enhanced pressure based den Harder model is used to simulate the process of a microwave plasma reactor. The timescale can also be interpreted as a progression scale in the plasma system. In the first few milliseconds, the gas is still at room temperatures and no dissociation of CO<sub>2</sub> can occur. Then the gas is instantaneously heated up to a given temperature where CO<sub>2</sub> dissociation takes place. The gas is kept at this high temperature for a few hundred milliseconds. From this high temperature regime, the now ionized gas enters the cooling area, where the gas is then cooled by quenching. In this process, usually a cold gas swirls around the hot plasma gas to quickly dissipate the heat of the plasma.

In industry and in laboratories, quenching rates of up to  $1 \times 10^7$  K/s are commonly used. At these quenching rates, the gas can be cooled to room temperature (300 K) from the plasma temperature of 5000 K in less than 0.5 ms. For lower cooling rates, this process can take up to half a second.

In figure 3.14 a simulated quenching experiment is displayed. The gas is heated to 3000 K after 100 ms at room temperature. After 600 ms, the quenching starts until the gas is at room temperature. The recombination of CO<sub>2</sub> is clearly visible in this plot, where the fraction of CO<sub>2</sub> in the gas rises up to 80 % from below 40 % when the reaction reaches equilibrium. It is also very clear that CO, O<sub>2</sub> and O react back to form CO<sub>2</sub>. The reverse reactions during quenching lead to the destruction of CO. At room temperature,

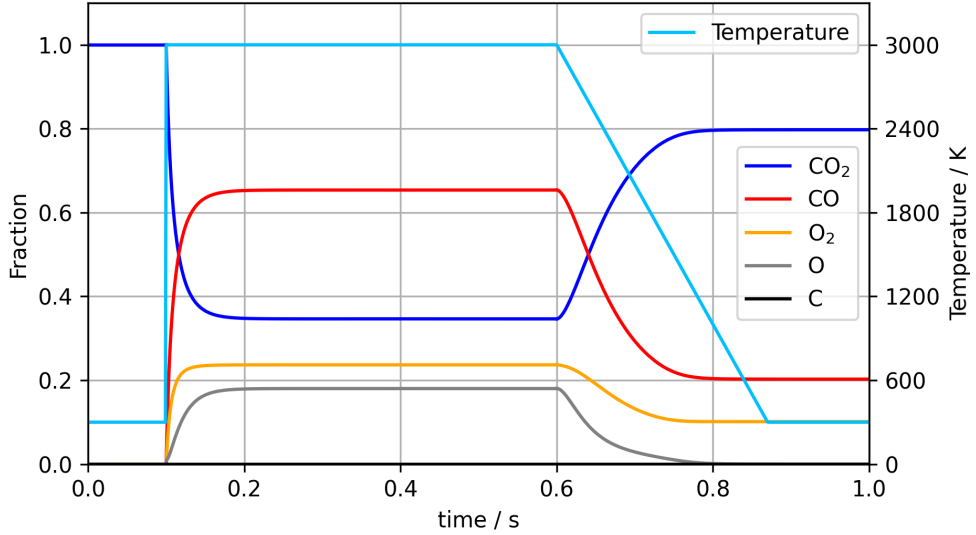


Figure 3.14. The temporal development of the mixture composition is presented. The gas is at room temperature for 100 ms, afterwards it is instantaneously heated to 3000 K where it stays for 500 ms. During this time the  $\text{CO}_2$  is dissociated and the other species are produced. After this constant heating period, the gas is quenched and rapidly cooled. In the plot, the cooling rate is  $1 \times 10^4 \text{ K/s}$ , hence the room temperature is reached after 270 ms. This cooling rate is chosen to better visualize the quenching.

these reactions are suppressed and further reactions are almost halted as the rates are reduced by up to 80 orders of magnitude. This explains the need for fast quenching rates. The model focusses on species which are relevant at high temperatures, therefore species which play a role at low temperatures, such as ozone, are not included [13]. The CO loss is calculated as the percentile loss of the difference between the CO fraction at equilibrium and after quenching.

$$CO_{LOSS} = \frac{\Delta CO}{CO_{Eq}} \quad (3.2)$$

It is highly dependent on the plasma temperature as this determines the composition of the mixture being quenched. The CO loss fraction is presented in figure 3.15.

Most interesting is the evolution of CO losses at a plasma temperature of 6000 K, where the CO loss fraction turns negative at a cooling rate of  $4 \times 10^5 \text{ K/s}$  due to the CO pyrolysis where CO is dissociated into C and O. The concentration of CO decreases. At the moment prior to cooling, the concentration of CO is lower than after quenching, as the reaction between C and O to form CO occurs during the cooling process.

At cooling rates below  $1 \times 10^1 \text{ K/s}$  almost all produced CO is lost. For cooling rates between  $1 \times 10^1 \text{ K/s}$  and  $1 \times 10^5 \text{ K/s}$  the CO losses are highly dependent on the initial

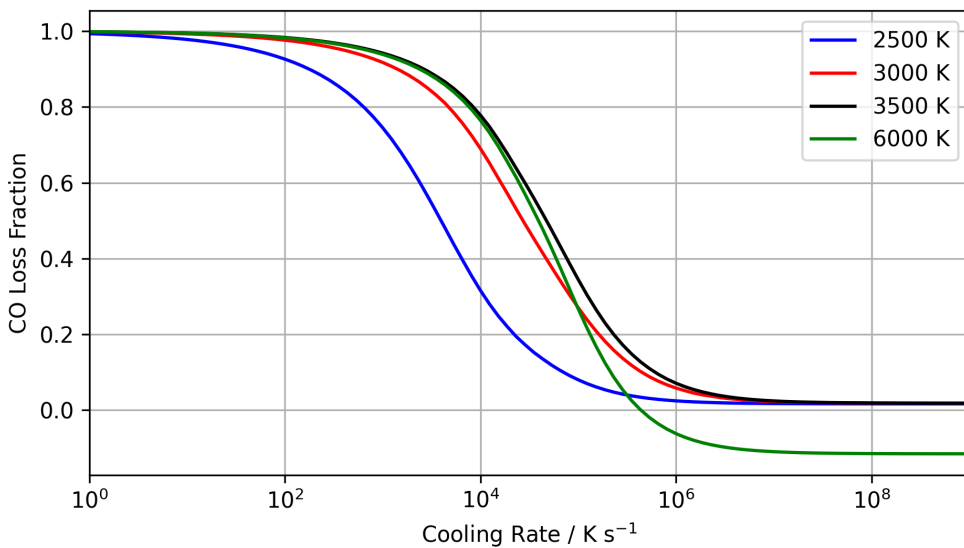


Figure 3.15. The evolution of the CO loss fraction is presented in dependence of the cooling rate. The lowest losses are reached for lower temperatures or at cooling rates above  $1 \times 10^7$  K/s. A commonly used temperature for quenching is 3000 K as the energy efficiency for the conversion from  $\text{CO}_2$  into CO is excellent at this temperature. The temperatures in the legend are the temperatures in the plasma region.

temperature. Towards higher cooling rates, the CO losses saturate at a CO loss fraction of 2 % for all initial temperatures except 6000 K. The point of minimum CO loss is reached earlier for a lower starting temperature, as the room temperature is reached more rapidly. From looking at the temperatures except 6000 K, one conclusion may be that the temperature used may be just a small factor at higher cooling rates. To understand this better in the following the absolute production of CO is taken into account. In figure 3.16 a double logarithmic plot of the production of CO is presented with the cooling rates. The initial  $\text{CO}_2$  pressure for all of these temperatures is 10 000 Pa (0.1 mbar). Cooling rates below  $1 \times 10^3$  K/s do not result in distinguishable differences in CO production, despite the notable reduction in relative CO losses at lower temperatures. Already at cooling rates of  $1 \times 10^4$  K/s, the production of CO is noticeably higher for higher temperatures. The production of CO also saturates, like the CO losses. The most significant deviation in CO production is in the saturation region. The highest production efficiency is reached at high temperatures and high cooling rates. In this plot the difference between 3500 K and 6000 K is barely noticeable. Due to mass conservation no higher CO production is possible even with negative relative losses. At a cooling rate of  $1 \times 10^9$  the absolute difference in produced CO is 656 Pa. This is a negligible increase in CO. For reference, the difference between the produced CO at a plasma temperature of 2500 K and the produced CO at 3500 K is 7090 Pa. It can be concluded that the effort

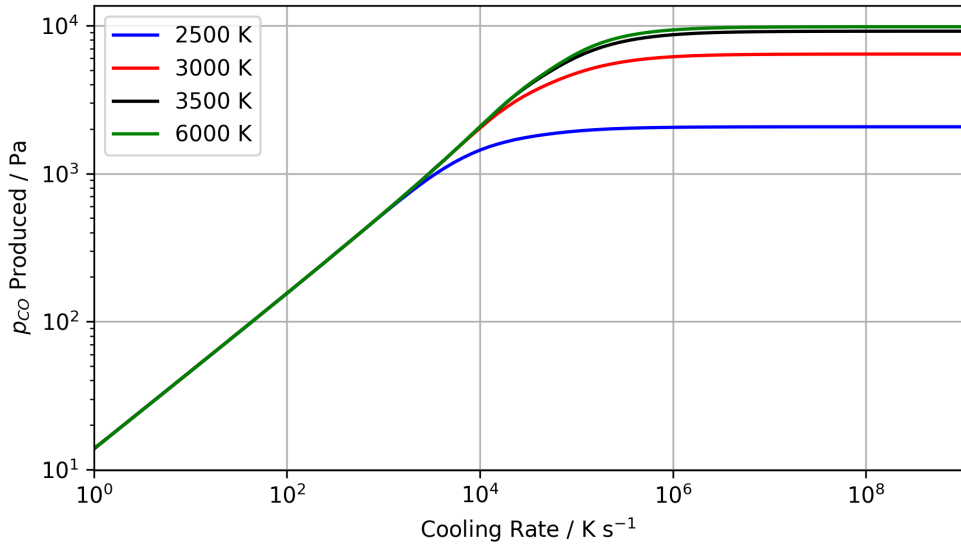


Figure 3.16. Double logarithmic plot of the evolution of the absolute CO production in dependance from the cooling rate. The temperatures in the legend are the temperatures in the plasma region.

to reach temperatures of 6000 K is not a valuable use of resources, given the relatively minor increase in CO production that would result.

Towards lower cooling rates the conversion efficiency rapidly decrease. Therefore it is necessary to produce CO at intermediate plasma temperatures in the range of 3500 K to get the best conversion efficiency for the used resources. Much higher plasma temperatures are also not desirable as the minor increase in CO production cannot outweigh the massively increased resource usage.

In conclusion, the most effective CO production is achieved at 3500 K, with quenching rates at or above  $1 \times 10^6$  K/s. At lower temperatures, too little CO is produced and at higher temperatures the increase of resource usage does not justify the minor increase in CO production. At lower cooling rates, the recombination of CO is too high and therefore the production and energy efficiency decrease rapidly.



## 4. H<sub>2</sub>O dissociation

In this chapter, all results from the water (H<sub>2</sub>O) dissociation calculations are discussed. The NASA CEA solver is employed to calculate the composition at chemical equilibrium. The output from implemented models are then compared to the output from CEARUN. Several models are compared to find the most suitable result. Issues with models will be discussed throughout the chapter.

### 4.1. NASA CEA

The CEARUN solver is used with the assigned temperature and pressure module. For water, the same temperature range from 1000 K to 6300 K in steps of 100 K is chosen. To cover the entire range, multiple runs of the program are performed. The pressure is kept at a constant value of 1 bar. This temperature range covers and even exceeds all the selected models [40–44]. The full input and output files are given in Appendix C. A mixture of 100 % gaseous H<sub>2</sub>O is used as fuel and oxidizer. As this is not a standard mixture, it is selected from the periodic table. No other species are initially present. The output is given in mole-fractions. The output is presented in figure 4.1. The CEARUN result is always displayed as solid line.

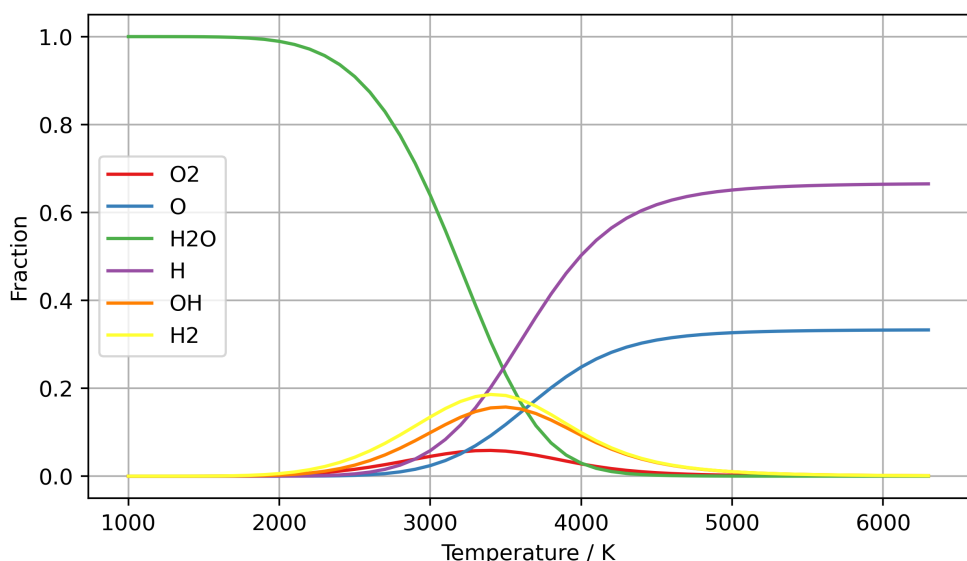


Figure 4.1. Output from CEARUN for a temperature range from 1000 K to 6300 K. The pressure is fixed at 1 bar.

## 4.2. Kinetic model

The kinetic models are benchmarked with respect to the accuracy against the results from the CEARUN presented in figure 4.1.

### 4.2.1. Srinivasan model

The first model is a shock tube experiment, from Srinivasan et. al. [40]. Beforehand, this model is validated with the published temporal OH absorption plot. In the publication, the model is fitted to the measured values. The values are recorded at a temperature of 2712 K, a pressure of 5.95 Torr (790 Pa), with a initial  $H_2O$  concentration of  $4.253 \times 10^{15}$  molecules  $cm^{-3}$ , the overall density of molecules in the shock tube region is  $1.431 \times 10^{-18}$  molecules  $cm^{-3}$  [40, Figure 2]. The full model is presented in table D.1. A side-by-side comparison is presented in figure 4.2; in 4.2a the OH absorption is presented as published by Srinivasan et al. [40].

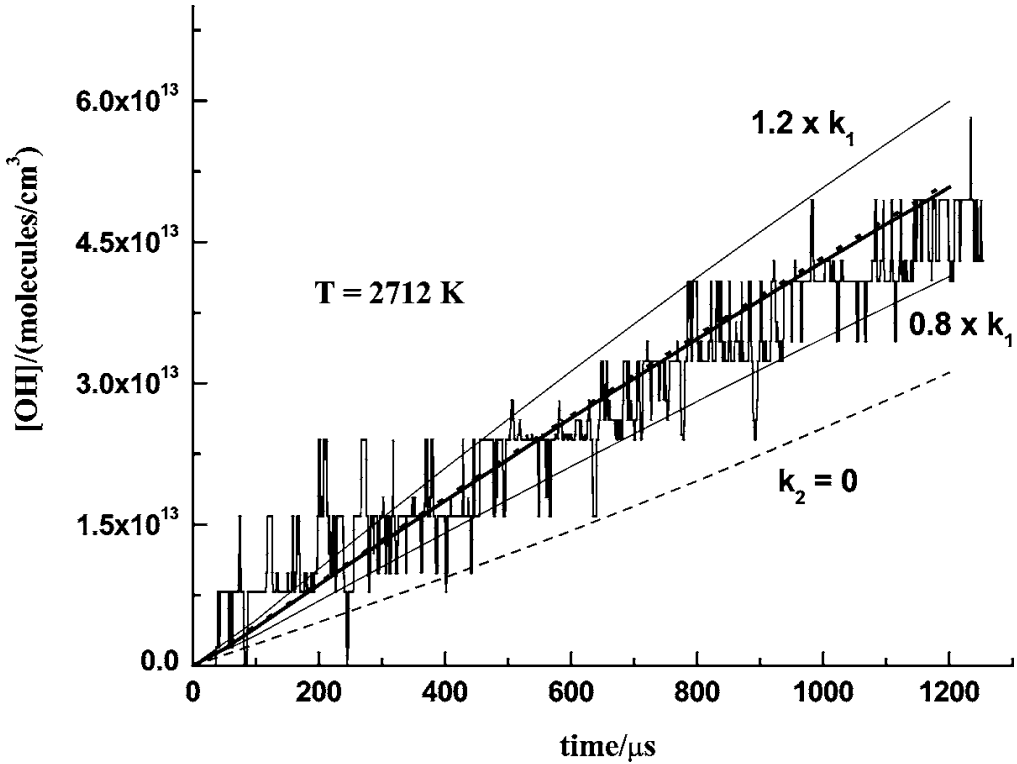
The gradient of the OH profile is the same in figures 4.2a and 4.2b. It is not possible to compare the exact numbers as they were not published by Srinivasan et al. [40]. The implementation is successfully validated with this comparison.

The Srinivasan model is benchmarked against the CEARUN result. To reach the steady state, the Srinivasan model is calculated for 10 000 s, for the comparison with CEARUN the initial  $H_2O$  density is calculated at a pressure of 1 bar. The comparison is presented in figure 4.3.

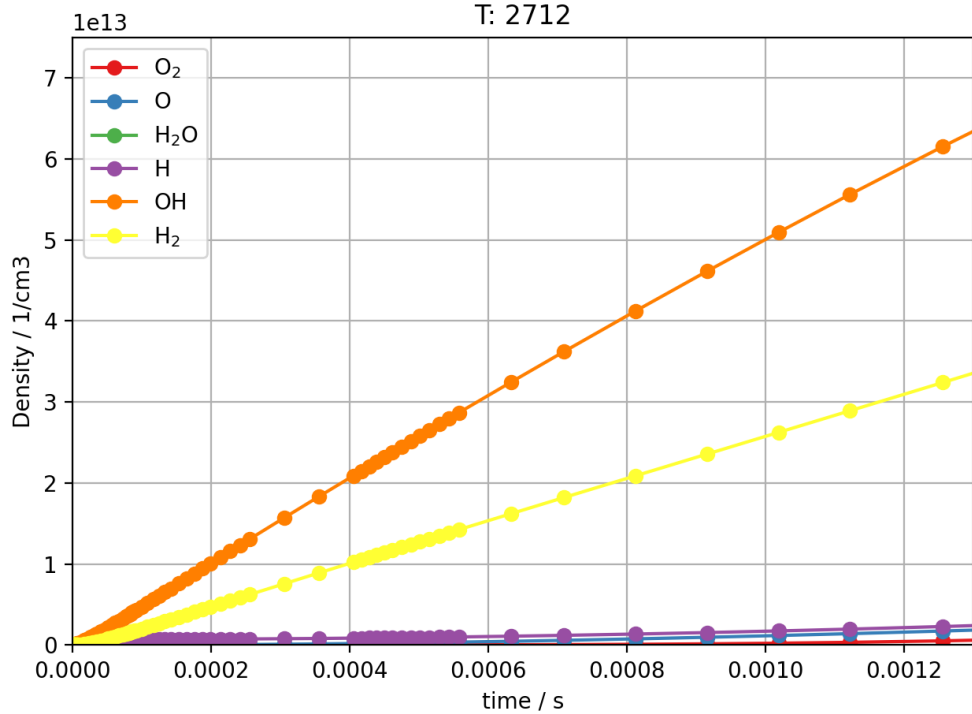
There is a very clear deviation between the kinetic steady state calculations and the chemical equilibrium. The dissociation of  $H_2O$  occurs at temperatures that are considerably lower than in the CEA result. From this result, it is clear that the values published by Srinivasan et. al. [40] are not measured at the steady state of the reaction. Therefore the fitted parameters lead to wrong results in simulations with higher simulation times. A result closer to chemical equilibrium is desirable. In order to obtain a useful result the calculation time is changed to 1.3 ms. Which is the end time of the OH measurement in figure 4.2a. This should lead to  $H_2O$  dissociation temperatures closer to the results from CEARUN. The results of these calculations are presented in figure 4.4.

The calculations still lead to  $H_2O$  dissociation at excessively low temperatures. The calculation times would have to be even shorter to get close to the chemical equilibrium. For temperatures above 5000 K the steady state of the model and the chemical equilibrium seem to come closer. Therefore the model would be good for high temperatures, but is unsuitable for temperatures between 1000 and 5000 K. Srinivasan's model is not converted to pressure based calculations, as it is not sufficiently close to chemical equilibrium to justify for such a conversion. Furthermore, quenching simulations are not conducted, as the calculations lead to an incorrect composition in the interesting range around 3000 K.

#### 4.2. KINETIC MODEL



(a) Figure 2 from Srinivasan et al. [40] publication, the thick solid line is the model fitted to the OH profile



(b) Result from the implemented model, the orange OH line has the same gradient as the published plot.

Figure 4.2. Comparison of the OH profile from Srinivasan et al. [40] and the implemented model based on their publication. Both figures yield the same gradient for the OH profile.

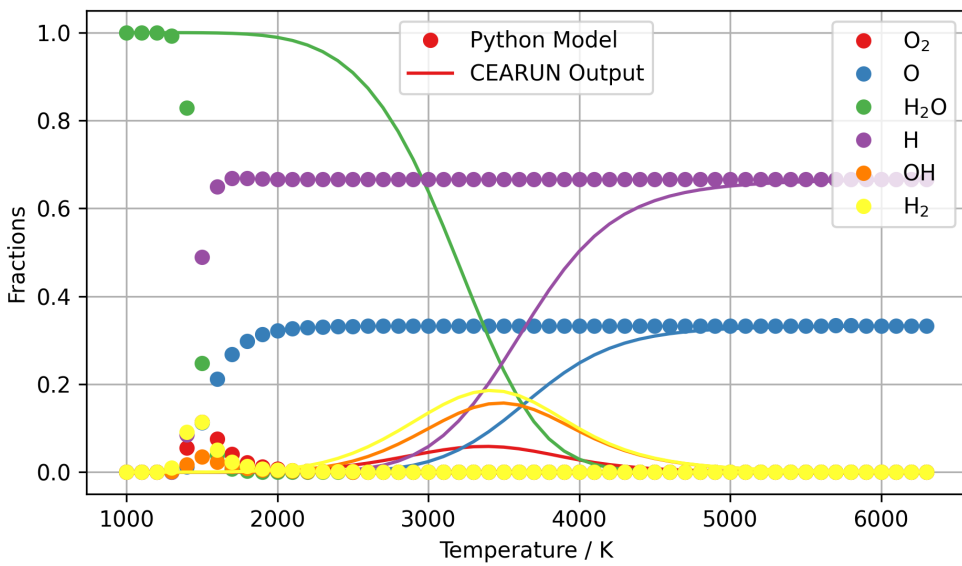


Figure 4.3. Comparison of the Python implementation from Srinivasan et al. [40] with the CEARUN result. The initial  $H_2O$  density is calculated at 1 bar. The datapoints for this plot are taken after 10 000 s.

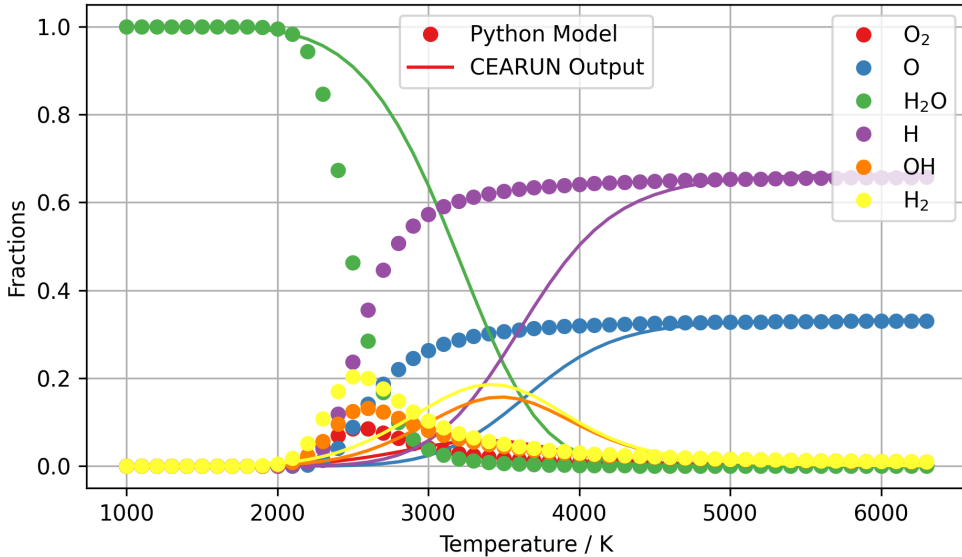


Figure 4.4. Comparison of the Python implementation from Srinivasan et al. [40] with the CEARUN result. The calculation time is 1.3 ms, the pressure is kept at 1 bar.

#### 4.2.2. Lédé model

Another model is published by Lédé et al. [41]. With this model, it is not possible to calculate the steady state as it has massive convergence issues due to numerical inaccuracy.

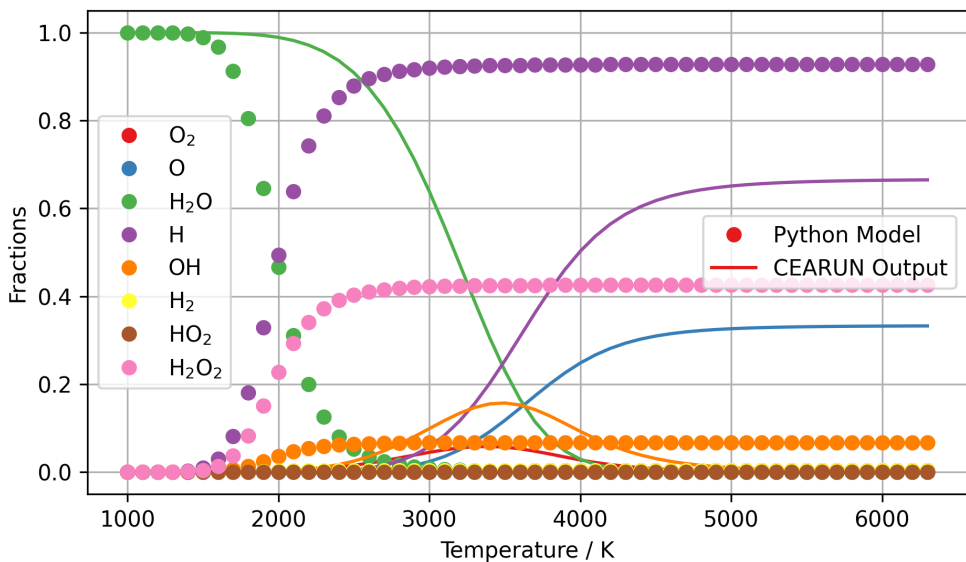


Figure 4.5. Comparison of the Python implementation from Avtaeva et al. [42] with the CEARUN result. The calculation time is 10 000 s; the pressure is kept at 1 bar.

racies. The model should be fairly simple as it is the detailed balance of 4 reactions. In the publication only very short times are considered for the steady state calculations. Therefore a similar result as with Srinivasan’s model would be expected.

#### 4.2.3. Avtaeva model

The next model is published by Avtaeva et al. [42]. This model is more complex as it includes 19 reactions. It also includes  $HO_2$  and  $H_2O_2$  which are not included in the previously implemented models. The full set of reactions is given in table D.4. One probable issue can be identified upfront as most of the reactions have no temperature dependence and therefore do not change in the temperature range from 1000 K to 6300 K. This is very unlikely as the species behave very differently over the temperature range.

The results from Avtaeva’s model are presented in figure 4.5. In this model the same behaviour can be found as with Srinivasan’s model; the  $H_2O$  dissociates at too low temperatures. The longest timescale found in the publication is  $1 \times 10^{-4}$  s, therefore it can be concluded that the model was not investigated at steady state. Another limitation of this model is that it does not approach the chemical equilibrium composition as closely as Srinivasan et al. [40] at higher temperatures. In fact, the model is off by orders of magnitude from the chemical equilibrium. This can be especially seen for the  $H_2O_2$  concentration, a species which is not present in the CEA result.  $H_2O_2$  is absent in the

CEA result as its concentration of it is below  $5 \times 10^{-6}$  mole fractions at all temperatures. Therefore, it should have never appeared as such a prominent species.

Another issue with the model is that some of the reactions are not possible in the way they are described in the model. This is especially the case for reactions 7 and 19. The

Table 4.1. Reactions of Avtaeva model. According to the NIST kinetic reactions database, these reactions should be 3-body reactions [36].

No.	Reaction
7	$OH + OH \rightarrow H_2O_2$
19	$H + O_2 \rightarrow HO_2$

reactions are given in table 4.1. These reactions should be 3-body reactions according to the kinetic reaction database from NIST [36]. The reactions can be found as 3-body reactions, mostly with  $N_2$  as third reaction partner.

Most rate coefficients from this model are given at 300 K, also most of the reaction rates are not valid at higher temperatures according to the NIST database [36]. Therefore this model is also not suitable for the desired use case.

#### 4.2.4. Medodovic model

Medodovic et al. [43] published two separate models, one for lower temperatures (300 K - 2000 K) and one for high temperatures (2000 K - 5000 K). At first only the model for high temperatures is considered. During the implementation the first issues occurred as some of the reactions are only valid for temperatures up to 2500 K or 3000 K, which is too low for the desired use case of the model of 2000 K to 5000 K. Furthermore, some reactions do not depend on the current temperature. The high-temperature model is presented in figure 4.6. In this model, the same issues are present as with other models:  $H_2O$  is dissociated at too low temperatures. A disadvantage of this model compared to Srinivasan's model is that the steady-state composition never gets close to the chemical equilibrium from CEARUN. Another noticeable difference of this high temperature range model and the CEARUN result is that the fraction of  $H_2O$  rises again at around 4000 K. In the CEARUN result, the  $H_2O$  is almost fully dissociated at these temperatures and does not rise again.

As the low temperature model is only valid for a small portion of the desired temperature range from 1000 K up to 6000 K, both models are combined to arrive at a more comprehensive model. In this process, 4 reactions are found which are present in the low and high temperature model. For these reactions, the rate constants with the broader temperature range are selected. The second reaction of the low temperature model is  $O + OH \rightarrow H_2O$ . This reaction is not possible as two oxygen atoms and one hydrogen atom cannot form two hydrogen atoms and one oxygen atom. The reaction is therefore

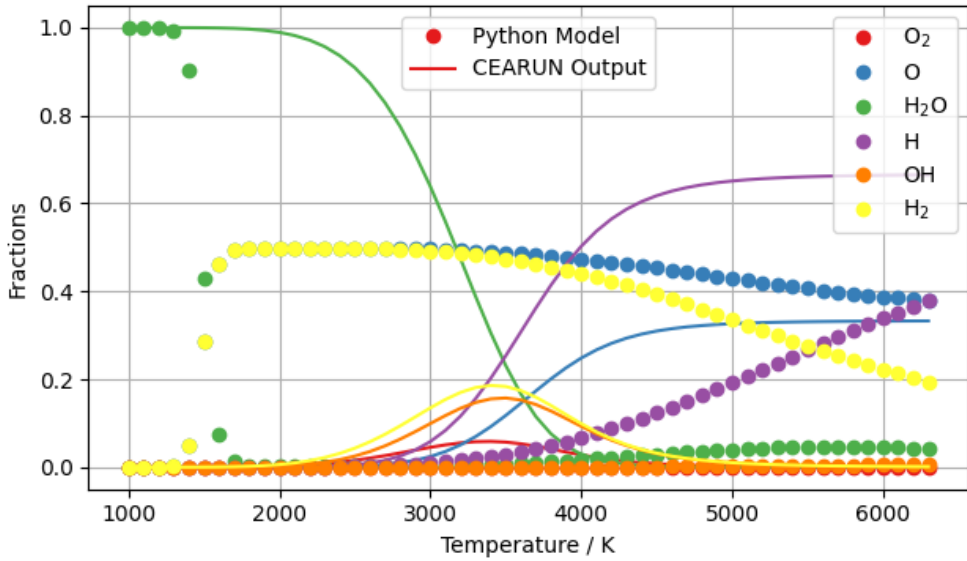


Figure 4.6. Comparison of the high temperature model from Medodovic et al. [43] with the CEARUN result. The calculation time is 10 000 s, the pressure is kept at 1 bar.

corrected to  $O + OH \rightarrow HO_2$ . The combined model with the high and low temperature range reactions is given in table D.6 and presented in figure 4.7. In this model the opposite of what previously happened occurs as  $H_2O$  is dissociated at too high temperatures. This behaviour usually only occurs for very short calculation times. The steady state is

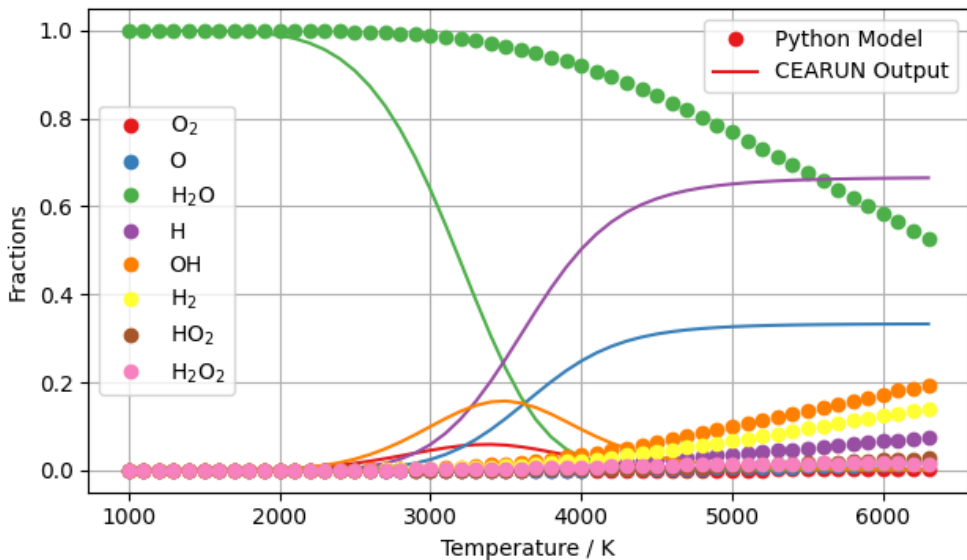


Figure 4.7. Comparison of the combined Medodovic model with the CEARUN result. The calculation time is 10 000 s, the pressure is kept at 1 bar.

reached, so increasing the calculation time will not improve the outcome of the model. The temporal evolution of the concentration is presented in figure 4.8. From this semi-logarithmic plot at 5000 K, it is evident that the steady state is reached in less than 1  $\mu$ s. To improve the model, other rate constants with broader temperature ranges must be tested.

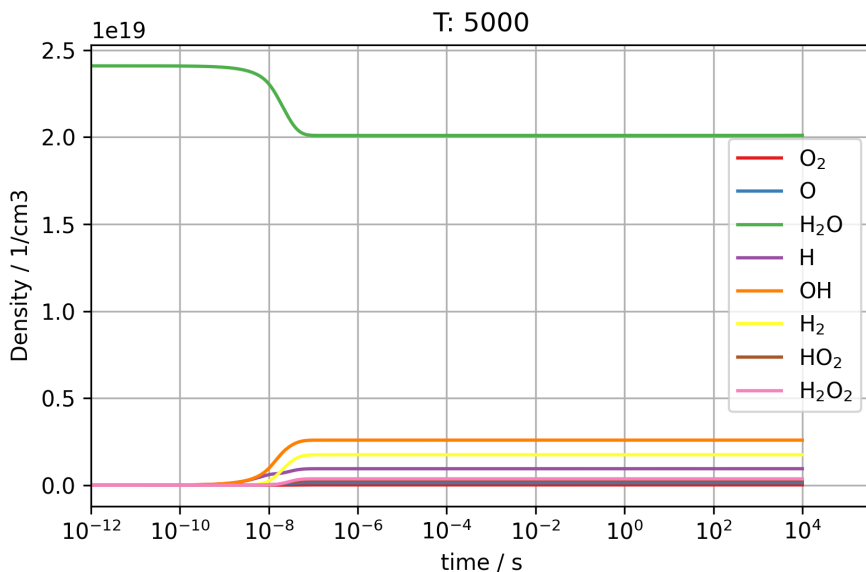


Figure 4.8. Result of the temporal calculations of the combined model at 5000 K. From this plot it is very obvious that the steady state was reached in under 1  $\mu$ s.

#### 4.2.5. Liu model

This model was originally published by Liu et al. [44]. It comprises 45 neutral reactions, making it the most complex model considered in this work. The species which are present in this model are  $O_2$ ,  $O$ ,  $H_2O$ ,  $H$ ,  $OH$ ,  $H_2$ ,  $HO_2$  and  $H_2O_2$ . The full set of reactions is given in table D.7. The output of the model is presented in figure 4.9.

This model yields a similar result to the combined model of Medodovic et al. [43]. The  $H_2O$  is dissociated at temperatures which are too high. A extension of the calculated timespan, would not improve the result as the steady state was reached in a shorter time period. The model is investigated closer at a temperature of 5000 K to gain insight into the temporal evolution of the mixture. This semi-logarithmic plot is presented in figure 4.10. The steady state is reached at this temperature in under 20  $\mu$ s. This model can only be improved by replacing some of the rate coefficients, with coefficients which yield lower temperatures. Although this model does not reach the chemical equilibrium at steady state, it is still more suitable for quenching simulations than the model from Srinivasan et al. [40]. For a quenching simulation, the mixture is cooled after a given time. For this kind of experiment, the steady state should be reached very quick as

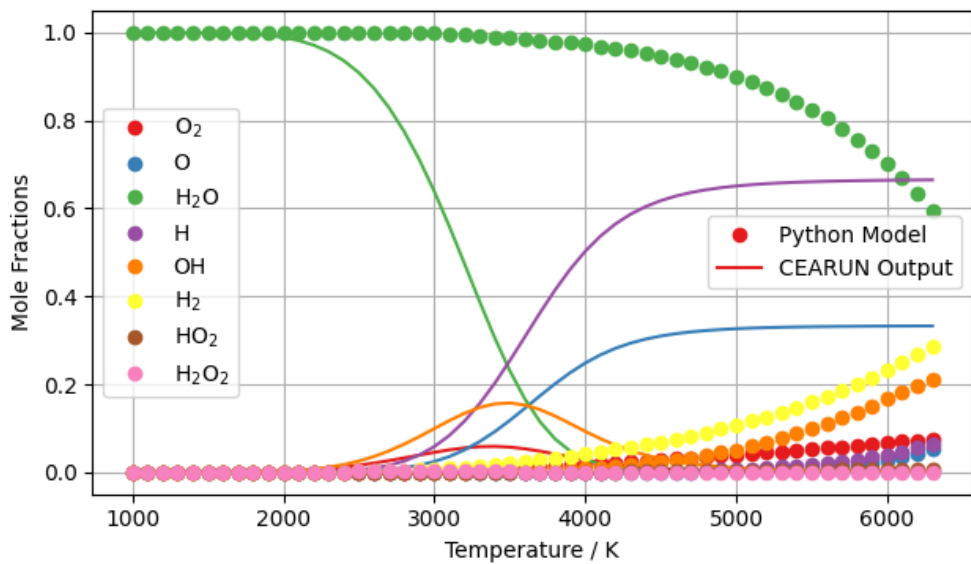


Figure 4.9. Comparison of Liu's model with the CEARUN result. The calculation time is 10 000 s, the pressure is kept at 1 bar.

during cooling only back reactions should occur. This is not the case with all models except Liu et al. [44] and the combined Medodovic model.

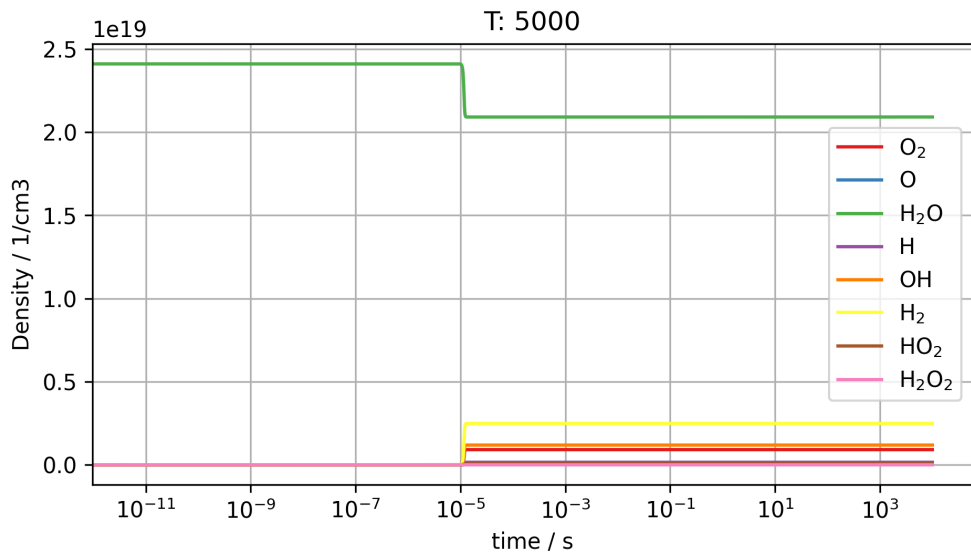


Figure 4.10. Result of the temporal evolution of Liu's model at 5000 K. From this it is clear that the steady state was reached in under 20  $\mu$ s.



## 5. Summary and Outlook

The goal of the work was to find suitable CO<sub>2</sub> and H<sub>2</sub>O dissociation models for a combination to investigate the effect of water impurities on the yield of CO<sub>2</sub> to CO conversion. Models for CO<sub>2</sub> and H<sub>2</sub>O dissociation are presented and benchmarked regarding their accuracy in steady state with the chemical equilibrium. The chemical equilibrium is calculated using the web based implementation of NASA's CEA solver.

For the CO<sub>2</sub> dissociation, a suitable model was successfully found. The successfully validated model is the pressure based CO<sub>2</sub> dissociation model published by den Harder. This model could also be validated with independently performed shock tube experiments from literature. It is extended by atomic carbon reactions in the scope of this work. Another considered model for CO<sub>2</sub> dissociation, published by Koelman, already includes atomic carbon reactions. Koelman's model is not considered further as den Harder's model yields a lower deviation from the CEA results.

The deviation is then further reduced by a conversion from density based calculations to pressure based calculations. With this step, the reaction volume of the model does not change during the calculations, so the pressure in the system can rise, which is the more realistic simulation approach. The deviation is further successfully reduced by the introduction of atomic carbon reactions. The atomic carbon reactions were taken from a published Ar-CO<sub>2</sub>-dissociation model by Beuthe. Further rate constants were taken into account for these reactions from NIST's kinetic database. The best fitting results are the ones published by Beuthe. With this extension of the model by including atomic carbon kinetics, there is no visible deviation from the CEA model in the temperature range from 5000 K to 6100 K. Validation of this enhanced model with the CEA Model was conducted in a pressure range from 1 Pa up to 1 MPa at temperatures of 1000 K to 7000 K.

This extended den Harder model is also used for simulated quenching experiments, where the gas is at plasma temperatures for several milliseconds before it is cooled down to room temperature. These experiments are important as there are recombination processes during the cooling of the process gas. From this experiment, the amount of CO produced can be determined. The quenching experiments are simulated at 2500, 3000, 3500 and 6000 K. The highest CO production is archived with 6000 K and cooling rates higher than  $1 \times 10^6$  K/s. The relative CO loss fraction saturates for cooling rates above  $1 \times 10^7$  K/s, for all temperatures at 2 %, except for 6000 K where the relative loss fraction

turns negative at a cooling rate of  $4 \times 10^5$  K/s. This phenomena is only possible due to thermal pyrolysis of CO into C and O. Therefore, the concentration of CO is greater following the cooling process than it was during the steady state at plasma temperatures.

The combined pressure based den Harder/Beuthe model should be used for the combination with a H<sub>2</sub>O dissociation model. It should then be extended for the direct reactions of H<sub>2</sub>O with OH, H, C, CO and CO<sub>2</sub>.

Here a suitable H<sub>2</sub>O dissociation model still is to be found, as all of the compared models are far off the chemical equilibrium when considered in steady state. The model by Srinivasan is a fairly simple model which is verified by the published shock tube experiment. It has a very good fit at steady state for temperatures above 5000 K. For temperatures in the range from 1000 K to 5000 K, the steady state composition is very distant from chemical equilibrium. H<sub>2</sub>O is dissociated at far too low temperatures. An improvement can be found if the model is considered after only a few milliseconds, although H<sub>2</sub>O is still dissociated at too low temperatures. Quenching experiments are not possible with this model due to the excessively low dissociation temperature of H<sub>2</sub>O, which would lead to a distortion of the results. Another simple model was found by Lédé, but the calculations always lead to convergence issues, resulting in the model not yielding any meaningful results.

A slightly more complex set of reactions is introduced with the model of Avtaeva. It also includes HO<sub>2</sub> and H<sub>2</sub>O<sub>2</sub>, which were not considered previously. Most of the rate constants in this model are given at a fixed temperature of 300 K and have no temperature dependent parameter. This leads, much like Srinivasans model, to H<sub>2</sub>O dissociation at temperatures which are too low. Therefore, this model is also unsuitable for the desired use case.

Medodovic et al. provided two models, one model for lower temperatures of 300 K to 2000 K and one model for high temperatures between 2000 K and 5000 K. The high temperature model dissociates H<sub>2</sub>O at too low temperatures in its steady state. In this model, H<sub>2</sub>O is produced again at temperatures above 4000 K, which is not the case with the CEA result. To improve the high temperature model and expand it towards lower temperatures, the two available models are combined. With this combined model, the H<sub>2</sub>O is dissociated at temperatures higher than the CEA predicts. The steady state is reached at 5000 K in under 1  $\mu$ s so an extension of the calculation times will not improve the accuracy.

The last investigated model is published by Liu. This model is the most complex considered model. H<sub>2</sub>O is dissociated at too high temperatures in this model. The steady state at 5000 K is reached in less than 20  $\mu$ s, therefore an extension of the calculation times would not improve the outcome.

---

The combination of both models is not possible within the scope of this work. Further work must be performed with H<sub>2</sub>O dissociation models. A model which closer fits the chemical equilibrium at its steady state must be found. Then it is possible to combine the models for CO<sub>2</sub> dissociation and for H<sub>2</sub>O dissociation, to investigate the water impurity influence on CO<sub>2</sub> conversion yield.



# **Sommaire récapitulatif en français : Étude numérique des effets des impuretés de l'eau sur le rendement de conversion du CO<sub>2</sub> par plasma**

## **Introduction**

La croissance économique et l'industrialisation rapides augmentent la demande d'énergie de l'humanité. Actuellement, la principale source d'énergie est constituée par les combustibles fossiles. Cette consommation de combustibles fossiles a entraîné une augmentation massive des émissions de CO<sub>2</sub> [1–3]. Les émissions de dioxyde de carbone constituent actuellement l'un des principaux défis environnementaux en raison de leur impact direct sur le climat par le biais de l'effet de serre. La réduction des émissions de carbone est d'une importance cruciale dans la lutte contre le changement climatique [4].

Les émissions de CO<sub>2</sub> dans l'atmosphère pourraient être réduites par la conversion de CO<sub>2</sub> en carburants et autres produits chimiques de grande valeur, établissant ainsi un «cycle du carbone» qui consiste en la capture, la production et la consommation de carbone. En outre, ce processus devrait également permettre de résoudre les problèmes liés à la diminution de la disponibilité des ressources fossiles [5]. Ces dernières années, la chimie du plasma a suscité beaucoup d'intérêt en raison de la possibilité d'utiliser des sources d'énergie renouvelables pour la conversion directe de molécules stables telles que CO<sub>2</sub> en CO et O<sub>2</sub> sans avoir recours à un catalyseur [6].

La production de carburants neutres en CO<sub>2</sub> est une étape importante vers la décarbonisation de notre atmosphère. Pour y parvenir, il est nécessaire de disposer d'un processus de conversion énergétiquement efficace pour le CO<sub>2</sub>. La conversion de CO<sub>2</sub> par plasma micro-ondes est l'un des processus les plus efficaces sur le plan énergétique actuellement disponibles. Pour la production de combustibles neutres à base de CO<sub>2</sub>, les réacteurs à plasma micro-ondes sont alimentés par des énergies électriques renouvelables telles que l'énergie hydroélectrique, l'énergie éolienne ou l'énergie solaire. Pour obtenir une production de combustibles neutres efficaces sur le plan énergétique et efficaces sur le plan du CO<sub>2</sub>, il faut un rendement élevé de conversion du CO<sub>2</sub> en CO. Ce rendement élevé

est obtenu au moyen de la trempe, la fraction de perte de CO représentant une mesure importante dans ce contexte, car elle indique les pertes relatives de CO dues à la recombinaison. Le CO<sub>2</sub> capturé peut être introduit dans un réacteur à plasma micro-ondes, où il est ensuite converti par pyrolyse en CO, O et O<sub>2</sub>. À des températures supérieures à 5000 K, une pyrolyse supplémentaire de CO en C et O est possible. Le mélange gazeux chauffé est ensuite rapidement refroidi par trempe afin de maintenir la composition chimique dans toute la mesure du possible. Le CO produit est capturé et peut être utilisé pour la synthèse de produits chimiques ou de carburants. Avec l'hydrogène, le CO forme le gaz de synthèse, qui est déjà un combustible et peut être liquéfié en essence. La production de carburant neutre en CO<sub>2</sub> n'est possible que si toute l'énergie électrique nécessaire à la production et au stockage provient de sources d'énergie renouvelables.

Des résultats prometteurs en matière de conversion du CO<sub>2</sub> ont été obtenus en utilisant des sources de plasma à basse pression et à haute température, qui sont les mieux adaptées aux applications industrielles. Cependant, l'impact des impuretés dans l'alimentation en gaz peut être préjudiciable au processus de plasma. Ce travail vise à étudier l'impact d'une impureté toujours présente dans les sources de CO<sub>2</sub>, à savoir la vapeur d'eau, sur le rendement de conversion du CO<sub>2</sub>. Les molécules d'eau en tant qu'additif sont encore très discutées en ce qui concerne leurs avantages potentiels ou leurs effets négatifs réels sur la conversion du CO<sub>2</sub> par le plasma. Récemment, Kiefer et al. [7] ont fourni un vaste ensemble de données indiquant une forte diminution du taux de conversion du CO<sub>2</sub> avec l'introduction de l'air ambiant dans le réacteur par rapport à l'air sec. Le groupe affirme que l'une des explications possibles est la présence d'humidité dans l'air introduit dans le réacteur.

Les travaux préliminaires en vue d'une étude théorique plus approfondie sur cette question sont effectués dans le présent travail par le biais du développement de modèles cinétiques 0D de la dissociation thermique du CO<sub>2</sub> et de H<sub>2</sub>O, dont la précision est comparée à celle de l'équilibre chimique calculé à l'aide du solveur CEA de la NASA. Ces deux parties sont nécessaires pour l'étude théorique des affirmations de Kiefer et al. [7], où les modèles devraient être combinés pour un modèle complet de dissociation thermique CO<sub>2</sub>–H<sub>2</sub>O. D'autres réactions doivent être envisagées pour les composants de CO<sub>2</sub> et H<sub>2</sub>O.

## Fondamentaux

Le but de ce travail est d'étudier numériquement l'influence de la vapeur d'eau sur le rendement de conversion du CO<sub>2</sub> dans un réacteur à plasma. Les bases du plasma sont expliquées ainsi que les différentes approches pour calculer la composition d'une réaction.

---

Les réacteurs à plasma micro-ondes sont couramment utilisés pour la dissociation thermique du CO<sub>2</sub> en ses composants. Pour éviter la recombinaison des composants pendant le refroidissement lent à partir des températures élevées du plasma, la trempe est utilisée pour atteindre des taux de refroidissement élevés et maintenir ainsi la composition du plasma.

Le CO<sub>2</sub>, en tant que gaz de traitement, contient toujours des impuretés, les principales étant les composants de l'air tels que l'azote, l'oxygène et l'argon. L'influence de ces éléments sur la conversion du CO<sub>2</sub> a déjà été étudiée par Kiefer et al. [7]. Il a été constaté que la vapeur d'eau peut avoir une forte influence sur le rendement de conversion du plasma dans la décomposition du CO<sub>2</sub> [7].

## Plasma

Le plasma est également connu comme le « quatrième état de la matière », à côté des solides, des liquides et des gaz [8, 9]. Plus de 99 % de l'univers visible est constitué de plasma [10]. Dans les corps solides, les particules sont disposées et emballées étroitement, leur mobilité est restreinte. Dans les liquides, elles peuvent se déplacer, mais avec une liberté limitée. Dans les gaz, les molécules et les atomes peuvent se déplacer librement [9]. Dans un plasma, les électrons sont libérés des atomes ou des molécules et forment des ions. Les molécules deviennent plus énergétiques avec l'augmentation de la température et la matière se transforme successivement en solide, en liquide, en gaz et enfin progressivement en plasma [10]. Comme la transition se produit progressivement avec l'augmentation de la température, il ne s'agit pas d'une transition de phase (voir table 2.1) au sens thermodynamique, même si elle est généralement étiquetée comme une transition de phase [11].

Le plasma est défini comme un gaz hautement énergisé (ionisé) dont la charge électrique est globalement neutre. La substance macroscopiquement neutre se compose de molécules, d'électrons libres, d'ions et de radicaux, comme le montre figure 5.1 [11]. Un plasma se forme à partir d'un gaz neutre lorsque celui-ci est soumis à une énergie suffisamment élevée. Cette énergie est spécifique à chaque gaz et est nécessaire pour que les électrons orbitaux se détachent de la molécule de gaz. Les électrons sont alors retirés de la molécule de gaz neutre et une molécule de gaz chargée est formée. Ce gaz chargé devient hautement conducteur, de sorte que les champs électriques et magnétiques peuvent influencer son comportement et modifier la forme d'un plasma. Il suit un comportement collectif dû au blindage de Debye, où les particules chargées influencent d'autres particules proches dans leur longueur de blindage (longueur de Debye) par des interactions de Coulomb.

La principale différence avec un gaz est que les atomes et les molécules sont ionisés dans le plasma et que les particules interagissent avec les champs électromagnétiques (EM), alors que les particules dans un gaz sont neutres et interagissent individuellement avec les champs EM. Les principales caractéristiques du plasma sont les suivantes

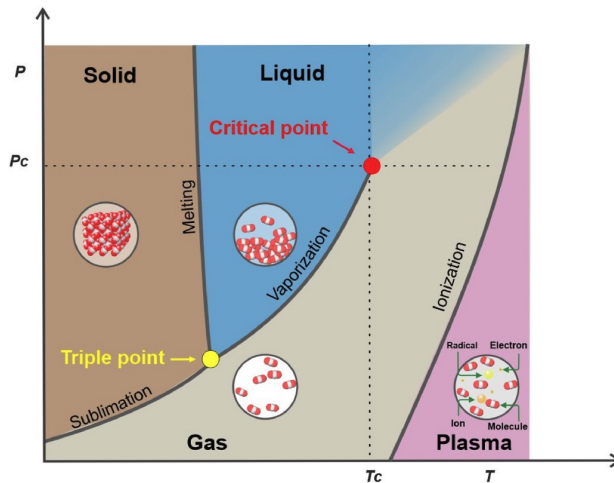


FIGURE 5.1. Le diagramme de phase montre les états de la matière en fonction de la température (axe x) et de la pression (axe y). Aux intersections entre les différentes phases, le nom de la transition de phase correspondante est indiqué. Le point critique se situe à une température critique et à une pression critique spécifiques à la substance. Au-dessus de ce point, il n'est pas possible de faire la distinction entre un liquide et un gaz. La disposition des molécules est représentée schématiquement dans chaque état. Ce diagramme montre clairement que le plasma ne se produit qu'à des températures élevées, même à des pressions faibles. (Cf. [8, Figure 2]).

- La quasi-neutralité macroscopique
- Le blindage de Debye
- Ionisation

Au bord d'un plasma, une couche limite se forme. La gaine de plasma se forme en raison de la différence de potentiel électrique entre le plasma et le matériau adjacent. Il existe différents types de réacteurs à plasma. Les plus courants sont les réacteurs à décharge à barrière diélectrique (DBD), dans lesquels le plasma est généré entre deux électrodes séparées par un matériau diélectrique. Pour cette décomposition du plasma, des champs électriques élevés sont nécessaires. Pour la dissociation du CO<sub>2</sub>, les réacteurs à plasma micro-ondes sont les plus couramment utilisés.

### Plasma micro-ondes

Le plasma micro-ondes se réfère à un plasma qui est généré et maintenu par l'utilisation d'un rayonnement électromagnétique micro-ondes, généralement à une fréquence de 915 MHz ou 2,45 GHz [12–15]. Pour la dissociation du CO<sub>2</sub>, les torches à plasma micro-ondes sont les plus courantes en raison de leur efficacité énergétique supérieure et de leurs valeurs élevées de conversion du CO<sub>2</sub> [7]. La configuration schématique d'un tel réacteur à plasma est présentée dans la figure 5.2.

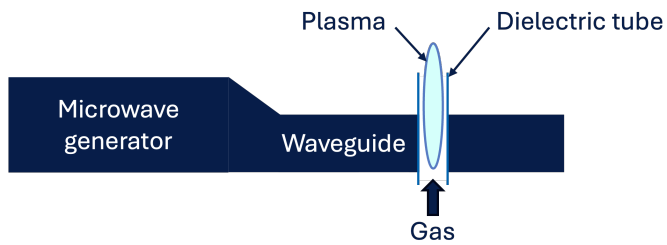


FIGURE 5.2. Une vue d'ensemble schématique d'une installation typique de torche à plasma micro-ondes. Les micro-ondes sont générées puis couplées au guide d'ondes, qui guide les micro-ondes vers le tube diélectrique où le gaz absorbe les micro-ondes et où l'énergie est suffisamment élevée pour ioniser le gaz. Pour entretenir le plasma, le tube diélectrique est continuellement alimenté en gaz. Le guide d'ondes est conçu de manière à ce que le maximum de l'onde électromagnétique se trouve à l'intersection du tube diélectrique et du guide d'ondes.

Les principaux composants d'un système plasma micro-ondes sont les suivants :

- Source de micro-ondes : Production d'ondes électromagnétiques à haute fréquence.
- Guide d'ondes : Guide les micro-ondes de la source vers la chambre de décharge.
- Chambre de décharge du plasma : Tube diélectrique dans lequel le gaz est ionisé et un plasma se forme.

Les micro-ondes sont générées à la source, puis guidées vers un syntoniseur à stub qui est utilisé pour l'adaptation d'impédance et pour minimiser la puissance des micro-ondes réfléchie par le plasma [7]. De là, les ondes sont guidées à travers le guide d'ondes vers le tube diélectrique qui est placé dans le résonateur, situé au niveau des maxima de l'onde EM. Les plasmas micro-ondes peuvent être utilisés pour le dépôt de couches minces [16], la gravure [17] ou pour des applications environnementales telles que la dissociation du CO<sub>2</sub> [18]. Dans cette thèse, le générateur de plasma micro-ondes est supposé être une source de chaleur variable avec des températures réglables.

Dans la figure 5.2, un schéma d'une torche à plasma à micro-ondes couramment utilisée est présenté. Le gaz est introduit en continu dans le tube diélectrique, où il est ionisé par l'énergie élevée des ondes électromagnétiques, ce qui entraîne la formation d'un plasma. Le transport de masse convectif est très important dans le contexte d'une torche à plasma micro-ondes, car il est essentiel pour le mélange des gaz et définit donc le temps pendant lequel le gaz est exposé au plasma. Lorsque le gaz ionisé se dilate et est forcé à travers le tube diélectrique sous la forme d'un jet de plasma, ce flux convectif est également crucial pour le transport du gaz ionisé hors de la région du plasma, où il se refroidit et se recombine. Le débit de gaz n'a aucune influence sur le temps de séjour du gaz dans le plasma [6]. Pour empêcher la recombinaison pendant le refroidissement d'un plasma, la

trempe est présentée dans la section 2.1.2.

Des débits de gaz insuffisants peuvent entraîner l'extinction du plasma, faute de particules suffisantes pour l'ionisation, ce qui conduit à une réduction de la densité du plasma. Toutefois, dans une torche à plasma bien conçue, le plasma peut être maintenu pendant de longues périodes sans problème majeur.

## Quenching

En physique des plasmas, la trempe fait référence au refroidissement rapide du gaz ionisé, conduisant à la suppression des processus de recombinaison et donc au maintien de la composition du gaz à des températures de plasma (plusieurs milliers de kelvins) [7]. La trempe est un effet de non-équilibre car la température est constamment et rapidement modifiée avant que l'état d'équilibre ne soit atteint. La trempe rapide est importante car la recombinaison et la dissociation thermique ne sont plus importantes à température ambiante (300 K) et les produits de la réaction sont «gelés» [19]. Elle joue également un autre rôle important en retirant l'énergie excédentaire des nouvelles espèces qui ont été formées [20]. Comme la trempe n'est pas instantanée et que les réactifs et les produits restent ensuite en phase gazeuse, il y a toujours des réactions en retour sur le chemin des hautes températures du plasma vers la température ambiante [13]. La trempe est utilisée dans presque toutes les réactions de dissociation du CO<sub>2</sub> car elle conduit toujours à des taux de conversion plus élevés [19]. Les modèles cinétiques ont montré que les taux de refroidissement sont meilleurs à 10<sup>6</sup> ou 10<sup>7</sup> K s<sup>-1</sup> [22], d'autres modèles recommandent des taux de refroidissement encore plus élevés pour des taux de conversion CO<sub>2</sub> élevés [13]. Un aperçu schématique des méthodes de trempe avec des taux typiques de 10<sup>6</sup> K s<sup>-1</sup> est présenté dans la figure 5.3. Pour atteindre des taux de trempe allant jusqu'à 10<sup>6</sup> K s<sup>-1</sup>, il est possible d'utiliser la méthode de mélange de gaz, dans laquelle un gaz froid est rapidement introduit dans le flux de sortie de la chambre de réaction [23]. Il est possible d'améliorer encore les performances de refroidissement en permettant au gaz froid de tourbillonner autour du gaz ionisé.

## Calculs thermodynamiques

Les calculs thermodynamiques sont effectués à l'aide du solveur NASA Chemical Equilibrium and Application (NASA CEA), qui est un programme permettant de calculer les compositions et les propriétés d'équilibre chimique de mélanges complexes par minimisation de l'énergie libre de Gibbs. L'un des grands avantages de cette approche est qu'il n'est pas nécessaire de spécifier a priori un ensemble de réactions [25]. L'inconvénient est que le solveur suppose toujours qu'un système atteint l'équilibre chimique, ce qui n'est pas toujours le cas, en particulier lorsque les conditions changent. En outre, il n'est pas possible d'étudier l'évolution temporelle d'un système afin de comprendre comment il atteint l'équilibre chimique.

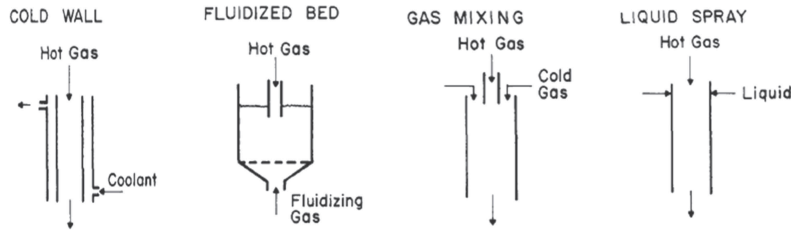


FIGURE 5.3. Aperçu des méthodes de trempe. Le gaz ionisé provenant du plasma est toujours décrit comme un gaz chaud dans la figure. Dans ces procédés, le fluide de refroidissement est généralement le gaz de traitement, ce qui permet d'éviter toute contamination supplémentaire de la réaction. La seule exception est la méthode de la paroi froide, où n'importe quel fluide peut être utilisé, à condition qu'il n'entre pas en contact avec le gaz ionisé. Avec ces méthodes, des taux d'extinction allant jusqu'à  $10^6 \text{ K s}^{-1}$  sont couramment réalisés. (Cf. [21, Figure 4])

### Equilibre chimique

Dans l'équilibre chimique, la concentration des réactifs et des produits reste constante dans le temps, en supposant que le système est fermé et se trouve à une température et une pression constantes. Le principe de base du CEA Solver pour atteindre l'équilibre chimique est la minimisation de l'énergie libre de Gibbs ( $G$ ) pour une température et une pression spécifiées avec les réactifs donnés [13]. La minimisation de l'énergie de Helmholtz ou la maximisation de l'entropie sont d'autres façons de calculer l'équilibre chimique. L'énergie libre de Gibbs, l'énergie de Helmholtz et l'entropie sont des fonctions d'état qui maintiennent différentes variables à des valeurs constantes. Dans le cadre de cette thèse, l'approche la plus appropriée est la minimisation de l'énergie libre de Gibbs, car la température et la pression sont ses variables naturelles [25]. L'énergie libre de Gibbs est un potentiel thermodynamique qui mesure le travail réversible maximal qu'un système peut fournir à température et pression constantes. L'énergie libre de Gibbs est définie comme suit

$$G = H - T \cdot S, \quad (5.1)$$

où  $H$  est l'enthalpie,  $T$  la température et  $S$  l'entropie du système. L'enthalpie est définie comme suit

$$H = U + p \cdot V, \quad (5.2)$$

avec l'énergie interne  $U$ , la pression  $p$  et le volume  $V$  du système. L'énergie de Gibbs avec des variables intensives est,

$$g = \sum n_i \mu_i, \quad (5.3)$$

la somme du nombre de particules  $n_i$  et du potentiel chimique  $\mu_i$ .

Avec  $T$ ,  $p$  et le nombre de particules d'une espèce  $n_i$  comme paramètres de contrôle, la

variation de l'énergie libre de Gibbs peut être exprimée comme suit

$$dG = Vdp - SdT + \sum_i \mu_i dn_i \quad (5.4)$$

où  $\mu_i$  est le potentiel chimique de l'espèce i. La minimisation de l'énergie libre de Gibbs peut être spécifiée comme suit

$$dG = \sum_i \left( \frac{\partial G}{\partial n_i} \right)_{T,p,n_j \neq n_i} = 0 \quad (5.5)$$

où  $i$  est le nombre d'espèces et  $n_i$  le nombre de particules d'une espèce i. L'avancement d'une réaction chimique dans le temps est décrit comme suit

$$\frac{d\xi}{dt} = \frac{d(n_i(t) - n_i(t=0))}{\nu_i dt} \quad (5.6)$$

avec le nombre stoechiométrique  $\nu_i$  de l'espèce  $i$  [26, 27] L'équilibre d'une réaction chimique est donc :

$$dG = \left( \frac{\partial G}{\partial \xi} \right)_{T,p,d\xi} = 0 \quad (5.7)$$

La minimisation de l'énergie libre de Gibbs est résolue dans le CEA à l'aide de la méthode itérative de Newton-Raphson [25].

Dans le travail présenté, l'implémentation web CEARUN du solveur CEA est utilisée pour calculer l'équilibre chimique des modèles utilisés [28].

On utilise le «Assigned Temperature and Pressure Problem» (problème de température et de pression assignées). Il est possible de saisir jusqu'à 24 températures et 24 pressions différentes. Pour plus d'étapes de température ou de pressions, une autre exécution de CEARUN est nécessaire. Les résultats peuvent être affichés en fractions de masse ou en fractions molaires. La sortie du programme est donnée dans un fichier texte, où la composition d'équilibre de la réaction est affichée pour toute pression et température d'entrée donnée.

## Modèle cinétique

Pour comprendre l'évolution temporelle de la dissociation de CO<sub>2</sub> ou de H<sub>2</sub>O, un modèle cinétique 0D dépendant du temps est développé en Python. Ce modèle fournit une approche simplifiée pour examiner les réactions chimiques et les processus de plasma dans les systèmes où les variations spatiales sont négligeables, en se concentrant uniquement sur l'évolution temporelle. Cela conduit à un système homogène sans gradients. Ce modèle a été préféré à des modèles 1D, 2D ou 3D plus complexes en raison de sa simplicité, les fonctions d'état thermodynamiques étant indépendantes de l'espace et du temps. Le

---

calcul temporel est important pour la simulation de la trempe où la température est modifiée dans le temps. Le plasma est supposé être un bain thermalisé idéal avec une température de consigne externe, les autres paramètres de contrôle dans le modèle sont les densités ou les pressions initiales. Le modèle cinétique est calculé pour un laps de temps défini, l'objectif étant d'atteindre un état stable à la fin de ce laps de temps. Un état stable est défini comme un point dans le temps où la concentration des espèces dans le système donné ne change plus. Ce point est d'une importance cruciale pour l'étalonnage par rapport à l'équilibre chimique issu des calculs thermodynamiques. En revanche, pour la simulation de la trempe, il n'est pas nécessaire que la réaction soit en état d'équilibre, car la trempe est un effet de non-équilibre. La trempe est un effet de non-équilibre. Chaque réaction produit une vitesse de réaction propre pour chaque espèce, qui est calculée avec des coefficients de vitesse dépendants de la température  $k_j(T)$ . Ils sont calculés en fonction d'un facteur pré-exponentiel  $A$  et de l'énergie d'activation de la réaction  $E_a$ .

$$k_j(T) = A \cdot \exp\left(-\frac{E_a}{k_B T}\right), \quad (5.8)$$

où  $k_B$  est la constante de Boltzmann et  $T$  la température. Les vitesses de réaction sont ensuite calculées avec les coefficients de vitesse dépendant de la température comme paramètre d'entrée. Un exemple de réactions est donné dans table 2.3. Pour la réaction bimoléculaire 1, la vitesse de réaction de l'espèce C en fonction du temps est la suivante

$$\frac{dn_{C,1}}{dt} = k_1(T) \cdot n_A \cdot n_B \quad (5.9)$$

avec  $k_1(T)$  le coefficient de vitesse de la réaction 1 dépendant de la température,  $n_A$  la densité de l'espèce A et  $n_B$  la densité de l'espèce B. Dans le taux de réaction bimoléculaire considéré pour l'espèce C, les réactifs A et B sont détruits et les produits C, D et E sont produits. Tous les termes de production doivent être considérés avec un signe positif dans le taux de réaction total, tandis que les taux de destruction sont considérés avec un signe négatif. La vitesse de la réaction trimoléculaire 2 pour l'espèce C au cours du temps est donc la suivante

$$\frac{dn_{C,2}}{dt} = -k_2(T) \cdot n_C \cdot n_D \cdot n_E \quad (5.10)$$

avec  $k_2(T)$  le coefficient de vitesse de la réaction 1 dépendant de la température,  $n_C$  la densité de l'espèce C,  $n_D$  la densité de l'espèce D et  $n_E$  la densité de l'espèce E. Pour respecter la conservation de la masse, les réactions en avant et en arrière sont données dans table 2.3, de sorte que les réactions 1 et 2 sont à l'équilibre. Les taux de réaction totaux pour chaque espèce sont calculés comme une somme de tous les termes de production et de destruction [13]. Par conséquent, la vitesse de réaction totale de l'espèce C au cours

du temps est la suivante

$$\frac{dn_C}{dt} = k_1(T) \cdot n_A \cdot n_B - k_2(T) \cdot n_C \cdot n_D \cdot n_E \quad (5.11)$$

Le comportement temporel est alors calculé en intégrant numériquement le système d'équations différentielles sur un temps donné. Après ce laps de temps, le système devrait atteindre un état d'équilibre, qui devrait être égal à l'équilibre chimique.

Pour comparer le solveur CEA et le modèle cinétique 0D, le modèle est résolu pour un ensemble donné de températures. Chaque étape de température nécessite son propre calcul. En couplant les deux approches différentes du calcul de l'équilibre et de l'utilisation de le CEA comme vérification de la composition de l'équilibre, une analyse complète des comportements transitoires et en régime permanent dans les systèmes plasmatiques peut être réalisée.

Cependant, la différence entre ces calculs et une installation réelle est que le temps peut être spécifié comme une période de temps indéfinie. Alors que dans une torche à plasma réelle, le gaz n'est à ces températures élevées que pendant quelques millisecondes avant de se refroidir, ce laps de temps est appelé temps de résidence et varie entre les différentes espèces. C'est pourquoi il est généralement indiqué sous la forme d'une distribution du temps de résidence. En outre, le temps de résidence dépend du flux de masse convectif. Pour simuler le comportement de refroidissement, la trempe est introduite. Cette étape est nécessaire pour calculer la composition chimique après le refroidissement. La composition à haute température peut être maintenue par l'introduction de taux de trempe élevés, ce qui permet d'arrêter les processus de recombinaison.

## Densité

Dans le calcul basé sur la densité, le volume du système change avec la température. Par conséquent, la densité initiale doit être calculée à chaque étape de température. La pression initiale doit être convertie en densité initiale. Pour cela, le point de départ est la loi des gaz idéaux,

$$pV = Nk_B T, \quad (5.12)$$

avec la pression  $p$ , le volume  $V$ , le nombre de particules du gaz  $N$ , la constante de Boltzmann  $k_B$  et la température du gaz  $T$ . Pour calculer le nombre de particules par volume (densité), la loi des gaz idéaux de l'équation 5.12 doit être divisée par le volume, la constante de Boltzmann et la température, comme suit

$$\frac{p}{k_B T} = \frac{N}{V} \quad (5.13)$$

---

D'après équation 5.13, il est clair que pour un nombre constant de particules, le volume ne peut changer que si la pression ou la température changent, car  $k_B$  est une constante. Avec chaque calcul, la température change également. Le nombre de particules divisé par le volume peut alors être exprimé par  $n_i$  pour chaque espèce  $i$ .

$$n_i = \frac{N_i}{V} \quad (5.14)$$

La densité de nombre pour une espèce  $i$  a deux paramètres ajustables : le premier est la pression partielle de chaque espèce  $p_i$  et le second est la température du gaz. En outre, elle dépend également de la constante de Boltzmann.

$$n_i = \frac{p_i}{k_B \cdot T} \quad (5.15)$$

La pression du système est la somme de toutes les pressions partielles des différentes espèces.

$$p = \sum_i p_i \quad (5.16)$$

Ainsi, la densité totale de toutes les espèces peut être calculée comme suit,

$$n = \frac{p}{k_B \cdot T} \quad (5.17)$$

Dans chaque calcul où la température change, la densité numérique change également, car la pression initiale est fixe. Lors du calcul du modèle cinétique, la température, la pression et le nombre de particules sont considérés comme constants, de sorte que le seul paramètre pouvant influencer la densité numérique est le volume. Dans une configuration réaliste, la pression et la température sont constantes, le volume doit donc changer. C'est ce que réalisent les calculs basés sur la pression.

## Pression

Pour maintenir une pression constante dans le système plasma à haute température, le volume doit changer pendant les calculs, c'est pourquoi des calculs basés sur la pression sont introduits. Dans les EDO, les densités sont converties en pressions partielles. Par conséquent, l'équation 5.9 pour le modèle basé sur la pression sans termes de correction est  $\frac{dp_{C,1}}{dt}$  l'évolution de la pression de l'espèce C au cours du temps pour la réaction bimoléculaire 1 du tableau 2.3

$$\frac{dp_{C,1}}{dt} = k_1(T) \cdot \frac{p_A}{p_{system}} \cdot \frac{p_B}{p_{system}} \quad (5.18)$$

avec les pressions partielles des espèces  $p_A$  et  $p_B$  et la pression dans le système à chaque pas de temps discret  $p_{system}$ . Avec tous les termes de correction nécessaires appliqués à

equation 5.18, le terme complet est pour le taux de réaction de la réaction à deux corps 1 du tableau 2.3 est :

$$\frac{dp_{C,1}}{dt} = k_1(T) \cdot \frac{p_A}{p_{system}} \cdot \frac{p_B}{p_{system}} \cdot corr_2 \cdot p_{corr} \quad (5.19)$$

avec un terme de correction unitaire  $corr_2$  pour les réactions bimoléculaires et le terme de correction de pression  $p_{corr}$ . Le terme de correction d'unité est nécessaire car les valeurs de la littérature pour les constantes de vitesse sont généralement exprimées en unités basées sur la densité. Comme les unités changent pour les réactions à deux et trois corps, le terme de pression doit également changer. Ce terme de correction a été introduit par den Harder et al. [13]. Il s'agit d'un facteur de correction unitaire pour le facteur pré-exponentiel basé sur la densité dans le coefficient de vitesse dépendant de la température. Pour les réactions à deux corps, le terme de correction est

$$corr_2 = \frac{p_{init}^2}{k_B \cdot T} \quad (5.20)$$

avec la pression initiale du système  $p_{init}$ , la constante de Boltzmann  $k_B$  et la température  $T$ . Pour les réactions à 3 corps, le terme de correction est le suivant

$$corr_3 = \frac{p_{init}^3}{(k_B \cdot T)^2} \quad (5.21)$$

Le volume du système étant maintenu constant, la pression augmente lors de la division d'une molécule en plusieurs parties. Cette augmentation de pression doit être compensée dans les calculs :

$$p_{corr} = \frac{p_{init}}{p_{system}} \quad (5.22)$$

avec le terme de correction  $p_{corr}$ , la pression initiale dans le système  $p_{init}$  et la pression à chaque pas de temps  $p_{system}$ . La pression du système fermé est calculée à chaque pas de temps comme la somme de toutes les espèces dans la réaction.

$$p_{system} = \sum p_i(t) \quad (5.23)$$

avec la pression  $p_i(t)$  dépendant de chaque espèce  $i$ . Le terme complet pour le taux de réaction 1 avec la pression  $p_i(t)$  dépend de chaque espèce  $i$ . Le terme complet pour le taux de réaction 1 avec les termes de correction appliqués est le suivant

$$\frac{dp_{C,1}}{dt} = k_1(T) \cdot \frac{p_A}{p_{system}} \cdot \frac{p_B}{p_{system}} \cdot \frac{p_{init}^2}{k_B \cdot T} \cdot \frac{p_{init}}{p_{system}} \quad (5.24)$$

---

La vitesse basée sur la pression de la réaction trimoléculaire 2 du tableau 2.3 serait la suivante

$$\frac{dp_{C,2}}{dt} = -k_2(T) \cdot \frac{p_C}{p_{system}} \cdot \frac{p_D}{p_{system}} \cdot \frac{p_E}{p_{system}} \cdot \frac{p_{init}^3}{(k_B \cdot T)^2} \cdot \frac{p_{init}}{p_{system}} \quad (5.25)$$

Pour une meilleure lisibilité et compréhension, les termes de correction sont inclus dans les constantes de taux  $k_j(T)$  dans l'implémentation Python du modèle.

## Validation du code

Le code du modèle Python cinétique 0D nouvellement mis en œuvre pour la dissociation thermique de CO<sub>2</sub> a été validé en comparant sa sortie à la sortie de l'implémentation Python par den Harder et al. [13]. En outre, une première implémentation Mathematica du modèle CO<sub>2</sub> basée sur table B.1 réalisée par le professeur Carbone (INRS) est utilisée pour la validation du modèle.

La validation des modèles CO<sub>2</sub> et H<sub>2</sub>O est également possible grâce aux résultats des expériences de tube à choc. Dans ces expériences, les taux de réaction sont déterminés expérimentalement. Le modèle CO<sub>2</sub> est ensuite validé par les résultats des tubes à chocs de Brabbs et al. [30], réalisés à des pressions de 11 à 20 bars.

## Benchmarking des différents modèles

Afin de sélectionner un modèle approprié pour la combinaison de dissociation CO<sub>2</sub> et H<sub>2</sub>O, il est nécessaire de choisir un modèle complet dans la littérature disponible. Plusieurs modèles différents sont mis en œuvre et leurs résultats sont ensuite comparés aux résultats du solveur CEA de la NASA. Tous les modèles de la littérature sont implémentés en Python et leurs résultats sont ensuite comparés à ceux de CEARUN. On s'attend à un léger écart entre les résultats obtenus et ceux du CEARUN.

Cet écart peut s'expliquer par les différentes méthodologies employées pour le calcul de la composition chimique. Le solveur CEA de la NASA utilise une minimisation de l'énergie libre de Gibbs pour calculer l'équilibre chimique, ce qui est une méthode efficace et précise pour déterminer l'état d'équilibre chimique d'un système. En tout état de cause, le solveur CEA ne permet pas d'étudier l'évolution des réactions dans le temps. Les modèles cinétiques calculent la composition chimique au fil du temps jusqu'à ce que l'état d'équilibre soit atteint, ce qui permet d'étudier la composition chimique à n'importe quel pas de temps discret. Pour effectuer des simulations de trempe, les calculs cinétiques sont nécessaires, car des résultats similaires ne peuvent être obtenus avec le solveur CEA.

L'analyse comparative est effectuée par rapport à la composition chimique la plus correcte à chaque étape de la température.

## Dissociation du CO<sub>2</sub>

Les résultats des calculs de CO<sub>2</sub> seront présentés et discutés. Les résultats du solveur CEA de la NASA seront comparés aux résultats des modèles mis en œuvre. Quelques modèles différents sont pris en compte afin de trouver le meilleur résultat pour les calculs thermodynamiques.

### NASA CEA

CEARUN est utilisé avec le programme de température et de pression assigné pour simuler la dissociation du CO<sub>2</sub> dans une plage de température allant de 1000 K à 6100 K par pas de 100 K. La pression est fixée à 100 mbar. Cette plage de température est choisie pour couvrir tous les modèles comparés [13,31,32]. Le mélange gazeux initial est de 100 % de CO<sub>2</sub>. Le résultat est présenté dans la figure 5.4

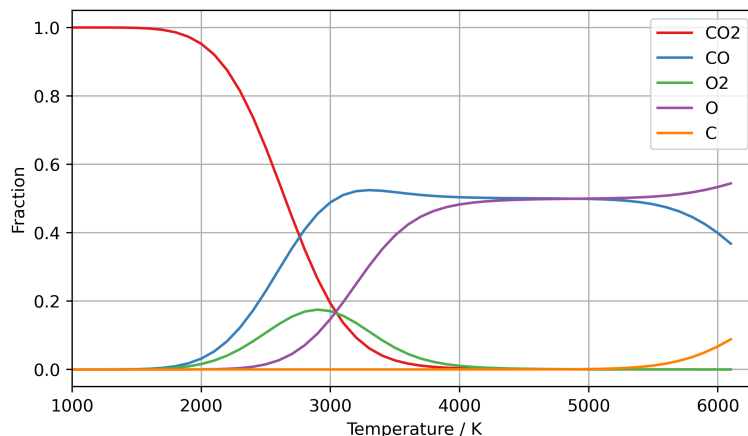


FIGURE 5.4. Résultat du CEARUN pour une plage de température allant de 1000 K à 6100 K. La pression est fixée à 100 mbar.

### Validation du code

Le modèle Python est vérifié avec l'implémentation de den Harder et al [13] et un modèle Mathematica du Prof. Carbone(INRS). Les constantes de vitesse sont calculées à partir de la publication de den Harder et al. [13]. La comparaison est présentée dans la figure 3.2. Les températures considérées sont de 1000 K à 6100 K, avec une composition initiale de 100 % de CO<sub>2</sub> à une pression de 100 mbar. Dans ce calcul, la durée est de 2,5 s. On constate un écart entre le modèle nouvellement mis en œuvre par den Harder et le résultat de la mise en œuvre originale. L'écart a été constaté en examinant le code original et en comparant les constantes de vitesse à la publication. Les constantes de vitesse dans le code original sont calculées à partir des valeurs publiées par Butylkin et al. [32]. Après avoir corrigé les constantes de vitesse dans le modèle nouvellement mis en œuvre, aucun

---

écart visible n'a été constaté. Les constantes de vitesse en question sont présentées dans table 5.1 Pour tous les calculs ultérieurs, l'intervalle de temps est étendu à 10000 s, afin

TABLE 5.1. Comparaison des valeurs publiées dans l'article de den Harder et dans l'article de Butylkin. La mise en œuvre de den Harder utilise directement les valeurs converties de l'article original.

Réaction	den Harder en eV [13]	Butylkin en eV [32]	Butylkin en kcal/mole [32]
9	0.13	0.188 33	4.340
10	0.13	0.188 33	4.340
11	0.13	-0.160 55	-3.700

que l'état d'équilibre puisse également être atteint pour des températures inférieures à 2000 K. La déviation absolue de la mise en œuvre originale de den Harder et du modèle nouvellement mis en œuvre a été comparée. L'écart absolu le plus élevé est un écart de 0,0016 fraction molaire, ce qui se traduit par un écart relatif inférieur à 1 %. Un écart de cet ordre est attendu car les deux implémentations utilisent des solveurs différents pour les équations différentielles ordinaires.

## Benchmarking

Le modèle validé est comparé, en termes de précision, au résultat du solveur CEA. Le modèle validé précédemment est désormais appelé modèle den Harder. Tous les modèles sont considérés dans une plage de température allant de 1000 à 6100 K, le mélange initial est constitué de 100 % de CO<sub>2</sub>, sa densité est calculée à 100 mbar. La durée considérée est de 10000 s. Une déviation distincte du modèle de den Harder par rapport au résultat du CEARUN est constatée dans toute la gamme de températures. L'écart le plus important concerne les températures supérieures à 5 000 K, où le CO se dissocie davantage en C et en O. Ce phénomène n'est pas couvert par le modèle de den Harder. Un autre modèle a été trouvé par Koelman et al. [31]. Ce modèle présente des réactions de carbone atomique et devrait donc mieux correspondre aux résultats de CEARUN. La comparaison entre le modèle de den Harder, les résultats du CEARUN et le modèle de Koelman est présentée dans la figure 5.5. Le modèle de Koelman ne présente aucune amélioration par rapport au modèle de den Harder, quelle que soit la température. Cela s'explique en partie par l'absence de termes de production de carbone atomique dans le modèle de Koelman. Comme le modèle de den Harder correspond globalement bien aux résultats de CEARUN, il est encore amélioré par l'ajout de réactions au carbone atomique. Avant d'être étendu, le modèle est converti en calculs basés sur la densité. Cela rapproche encore le modèle des résultats de CEARUN pour toutes les températures inférieures à 5000 K. Ces résultats renforcent considérablement la confiance dans le modèle.

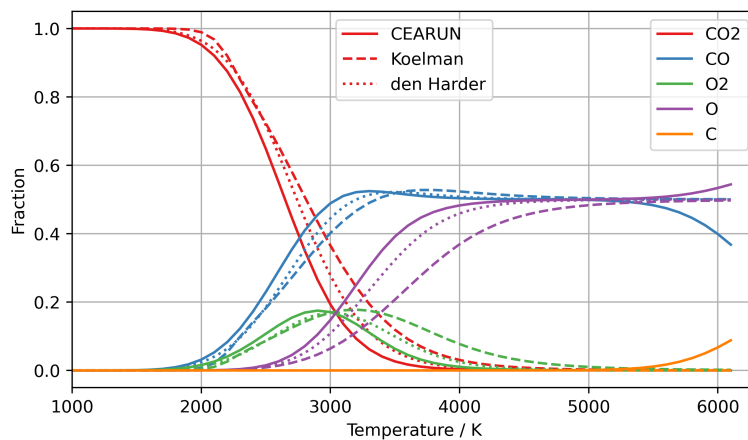


FIGURE 5.5. Comparaison du résultat du CEARUN avec le modèle de den Harder et le modèle de Koelman. Le modèle den Harder s'adapte beaucoup mieux au résultat du CEARUN que le modèle Koelman.

### Ajout de la cinétique des atomes de carbone

La mise en œuvre actuelle du modèle de den Harder ne prend pas en compte la cinétique du carbone atomique, qui est importante pour les températures supérieures à 5000 K. Ici, la pyrolyse du CO le divise en ses composants. Une mise en œuvre appropriée de la dissociation thermique du CO est nécessaire. Un ensemble prometteur de réactions a été publié par Beuthe et al. [35]. Cet ensemble comporte le même terme de production de carbone que celui trouvé dans Butylkin et al. [32], basé sur des expériences de tube à choc pour le CO dilué dans l'argon publiées par Fairbairn [34]. L'ensemble des réactions avec les taux de réaction de Beuthe est donné dans table 3.2. Pour éviter d'introduire de l'argon dans le modèle, car cela ajouterait une complexité inutile, l'argon a été remplacé par le CO<sub>2</sub> dont la masse molaire est similaire. La mise en œuvre de ces réactions a permis d'améliorer le modèle de Den Harders sans la cinétique du carbone atomique. Pour améliorer encore le modèle, différentes vitesses de réaction provenant de la base de données cinétiques du NIST ont été étudiées. Aucun des coefficients de vitesse n'a permis d'améliorer le modèle par rapport à l'ensemble des réactions de Beuthe. Le modèle a été amélioré en remplaçant le CO<sub>2</sub> qui a remplacé l'Ar, par une somme corrigée de la masse de toutes les espèces présentes dans la réaction. Avec cette méthode, l'ensemble du gaz est utilisé comme gaz de bain dans la réaction. Cette correction a permis d'obtenir un résultat nettement meilleur. Aucune déviation n'est visible à des températures supérieures à 5000 K dans la comparaison avec le résultat du CEARUN. Le modèle amélioré est présenté avec le résultat du CEARUN dans la figure 5.6.

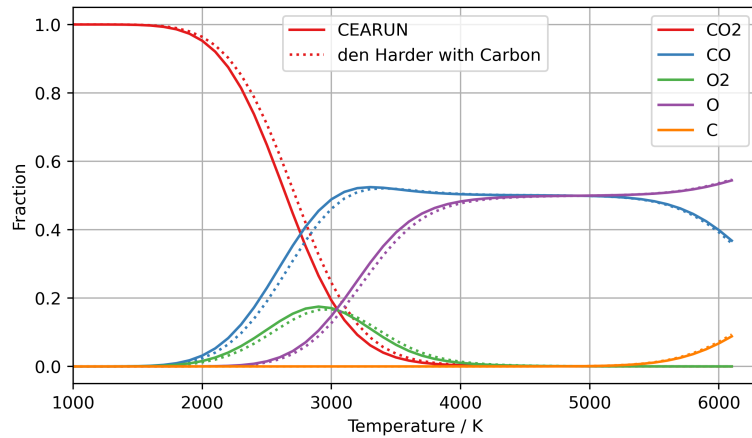


FIGURE 5.6. Le résultat de CEARUN est présenté avec le modèle de den Harder basé sur la pression, auquel est ajouté le carbone du modèle de Beuthe. Dans la plage supérieure à 5000 K, l'écart par rapport au résultat du CEA est minime. La prise en compte supplémentaire du carbone améliore sensiblement le modèle.

## Quenching

Le modèle de Den Harder basé sur la pression améliorée est utilisé pour simuler le processus d'un réacteur à plasma micro-ondes. Le gaz est introduit dans le réacteur à température ambiante, où il est instantanément chauffé à des températures de plasma de plusieurs milliers de kelvins. Le gaz désormais ionisé reste dans ce régime pendant quelques millisecondes où le CO<sub>2</sub> est dissocié. Le plasma est ensuite rapidement refroidi par trempe. Dans un réacteur réel, le flux de gaz peut réguler la durée pendant laquelle le gaz reste à la température du plasma.

Des taux de trempe allant jusqu'à  $1 \times 10^7$  K/s sont couramment utilisés dans les laboratoires et l'industrie. À ces taux de trempe, le cas peut être refroidi à la température ambiante (300 K) à partir de 5000 K en moins de 0,5 ms. Pour des taux de trempe inférieurs, cela peut prendre jusqu'à une demi-seconde. Les pertes de CO sont calculées en tant que perte percentile de la différence entre la fraction CO à l'équilibre et après la trempe.

Les pertes dépendent fortement des températures du plasma pour les taux de trempe les plus faibles. À des taux de trempe plus élevés, les pertes de CO sont saturées à 2 %. L'exception à ce point de saturation est une température de plasma de 6000 K. Ici, le CO est encore dissocié en C et O, avant que le plasma ne soit refroidi. Pendant le refroidissement, le C et l'O se recombinent et forment du CO, ce qui permet d'atteindre une perte de CO négative.

Pour mieux comprendre l'influence des différentes températures du plasma, la production absolue de CO est étudiée. D'immenses différences dans la production de CO sont trou-

vées pour des températures de plasma de 2500 et 3500 K ( $\Delta\text{CO} = 7090 \text{ Pa}$ ), alors que la fraction de perte de CO est la même. D'autre part, aucune amélioration importante de la production de CO n'a été constatée entre les températures de plasma de 3500 K et 6000 K ( $\Delta\text{CO} = 656 \text{ Pa}$ ), où la fraction de perte de CO devient négative entre les deux.

## Dissociation du H<sub>2</sub>O

Les résultats des calculs sur H<sub>2</sub>O sont présentés et discutés. Plusieurs modèles de dissociation cinétique sont mis en œuvre et comparés aux résultats du solveur CEA de la NASA. La température varie de 1000 K à 6300 K par pas de 100 K, les calculs sont présentés pour une pression de 1 bar. La plage de température est choisie pour couvrir tous les modèles considérés et pour s'adapter aux calculs de CO<sub>2</sub> [40–44].

### NASA CEA

CEARUN est utilisé pour calculer l'équilibre chimique de la dissociation thermique de H<sub>2</sub>O. Plusieurs exécutions de CEARUN sont nécessaires pour couvrir toute la gamme de températures. Le mélange initial est constitué de 100 % de H<sub>2</sub>O. Le résultat est présenté en fractions molaires dans la figure 5.7.

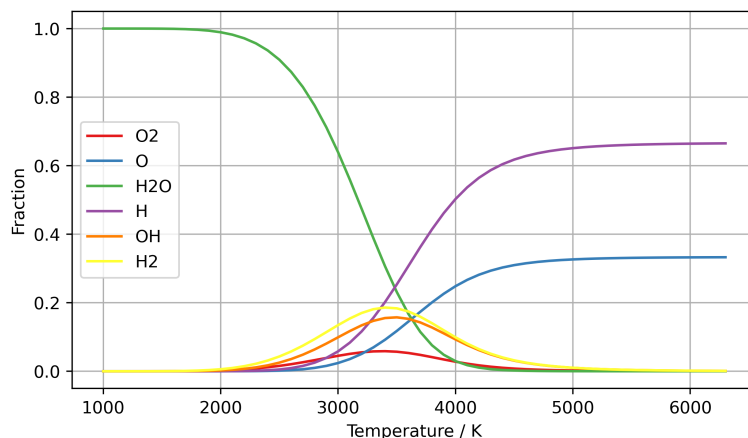


FIGURE 5.7. Résultat du CEARUN pour une plage de température allant de 1000 K à 6300 K. La pression est fixée à 1 bar.

### Modèle cinétique

Les modèles cinétiques sont comparés, en termes de précision, aux résultats du CEARUN présentés dans la figure 5.7

Le premier modèle est publié par Srinivasan et al. [40]. Ce modèle est validé par les résultats du tube à choc qui sont publiés avec le modèle cinétique. Le gradient du profil OH est le même dans la publication et dans l'implémentation Python du modèle de Srinivasan et le modèle est donc validé avec succès. Pour atteindre l'état d'équilibre, le modèle est

---

calculé pendant 10000 s. Le modèle est présenté dans la figure 4.1. Un écart très net entre les calculs cinétiques de l'état d'équilibre et le résultat du CEARUN apparaît. Le H<sub>2</sub>O est dissocié à des températures trop basses. Une amélioration est constatée lorsque l'on modifie le temps de calcul, qui correspond au temps utilisé dans l'expérience. Le résultat est plus proche de l'équilibre chimique, mais la dissociation s'opère à des températures trop basses. De plus, le modèle n'est alors pas considéré comme étant en état d'équilibre. Pour les températures supérieures à 5000 K, le modèle donne une bonne adéquation avec le modèle CEARUN. Il conviendrait donc pour des températures plus élevées, mais n'est pas adapté à la gamme de températures considérée. Les simulations de trempe ne sont pas effectuées car le modèle donnerait des résultats erronés en raison des températures de dissociation trop basses.

Un modèle plus complexe a été publié par Avtaeva et al. [42]. Ce modèle inclut HO<sub>2</sub> et H<sub>2</sub>O<sub>2</sub> qui n'avaient pas été pris en compte auparavant. Un problème possible est identifié d'emblée : la plupart des réactions ne dépendent pas de la température et ne changent donc pas dans la plage de température allant de 1000 K à 6300 K, ce qui est très improbable.

Le modèle d'Avtaeva dissocie H<sub>2</sub>O à des températures trop basses, comme c'est également le cas avec le modèle de Srinivasan. Contrairement au modèle de Srinivasan, ce modèle ne donne pas un résultat proche de celui du CEARUN, quelle que soit la température considérée. Par conséquent, ce modèle n'est pas adapté au cas d'utilisation souhaité.

Medodovic et al. [43] ont publié deux modèles, un modèle pour les températures de 300 K à 2000 K et un modèle pour les températures plus élevées de 2000 K à 5000 K. Le modèle pour les températures élevées est examiné en premier. Il produit une dissociation de H<sub>2</sub>O à des températures excessivement basses. Un problème a été constaté car certaines réactions ne sont pas valables pour l'ensemble de la plage de températures. La composition à l'état stable ne se rapproche jamais des résultats de CEARUN, ce qui constitue un inconvénient majeur. Le modèle est présenté dans la figure 4.6. Les modèles à basse et à haute température ont été combinés pour obtenir un modèle plus complet. Ce modèle combiné dissocie H<sub>2</sub>O à des températures trop élevées, un comportement qui ne se produit généralement qu'à des temps de calcul trop courts avant que le modèle n'atteigne son état d'équilibre. Un intervalle de temps de 10000 s est utilisé avec ce modèle. À 5000 K, l'état d'équilibre est atteint en moins de 1 μs, donc une extension de la durée n'améliorerait pas les résultats. Le modèle est présenté dans la figure 5.8. Le dernier modèle considéré est publié par Liu et al. [44]. Il s'agit du modèle considéré le plus complexe, qui comprend 45 réactions. Ce modèle dissocie également H<sub>2</sub>O à des températures très élevées. Le modèle est étudié à 5000 K, afin d'acquérir des connaissances sur le comportement temporel. Le tracé semi-logarithmique est présenté dans la figure 5.9. L'état d'équilibre est atteint en moins de 20 μs. Ce modèle ne peut être amélioré qu'en remplaçant les constantes

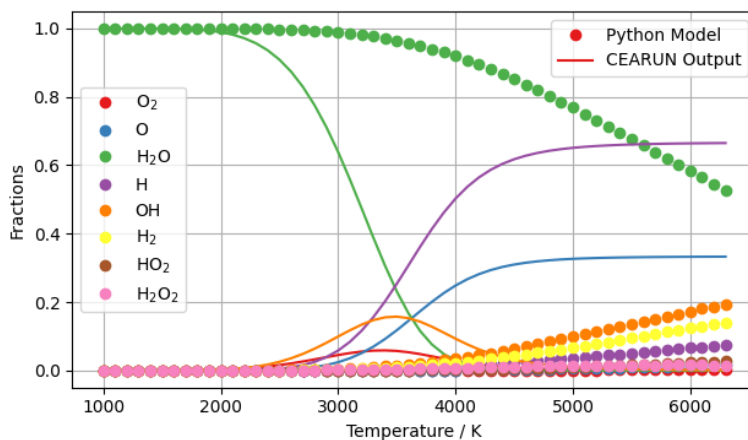


FIGURE 5.8. Comparaison du modèle combiné de Medodovic avec le résultat du CEA-RUN. Le temps de calcul est de 10 000 s, la pression est maintenue à 1 bar.

de vitesse. Les seuls modèles qui conviennent de loin aux simulations de trempe sont le modèle de Liu et le modèle combiné de Medodovic, car tous les autres modèles dissocient H<sub>2</sub>O à des températures trop basses. Il est important d'avoir un modèle qui atteint l'état d'équilibre très rapidement pour la simulation de la trempe.

Aucun modèle approprié n'a été trouvé pour être combiné avec le modèle de dissociation de CO<sub>2</sub> de den Harder/Beuthe.

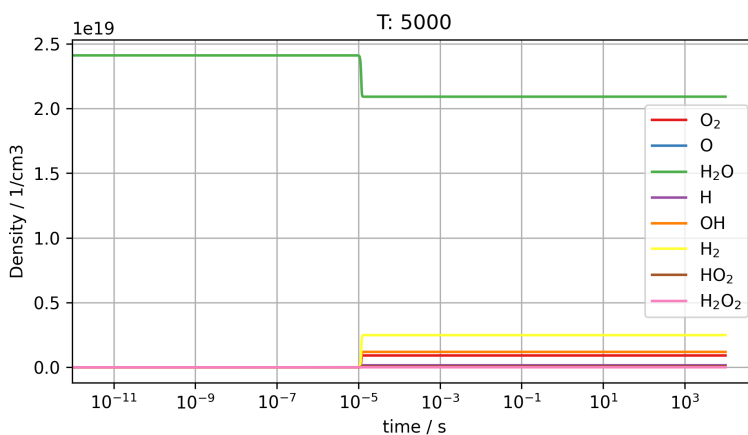


FIGURE 5.9. Résultat de l'évolution temporelle du modèle de Liu à 5000 K. Il en ressort que l'état d'équilibre a été atteint en moins de 20 µs.

## Résumé et perspectives

L'objectif de ce travail était de trouver des modèles de dissociation de CO<sub>2</sub> et de H<sub>2</sub>O appropriés pour une combinaison permettant d'étudier l'effet des impuretés de l'eau sur le rendement de la conversion de CO<sub>2</sub> en CO. Les modèles de dissociation de CO<sub>2</sub> et de

---

$\text{H}_2\text{O}$  sont présentés et comparés quant à leur précision en régime permanent avec l'équilibre chimique. L'équilibre chimique est calculé à l'aide de l'implémentation en ligne du solveur CEA de la NASA.

Pour la dissociation  $\text{CO}_2$ , un modèle approprié a été trouvé avec succès. Le modèle validé avec succès est le modèle de dissociation  $\text{CO}_2$  basé sur la pression publié par den Harder. Ce modèle a également pu être validé par des expériences de tubes à chocs réalisées indépendamment dans la littérature. Il est étendu aux réactions du carbone atomique dans le cadre de ce travail. Un autre modèle envisagé pour la dissociation de  $\text{CO}_2$ , publié par Koelman, inclut déjà les réactions du carbone atomique. Le modèle de Koelman n'est pas examiné plus avant, car le modèle de den Harder s'écarte moins des résultats du CEA. L'écart est ensuite réduit par une conversion des calculs basés sur la densité en calculs basés sur la pression. Avec cette étape, le volume de réaction du modèle ne change pas pendant les calculs, de sorte que la pression dans le système peut augmenter, ce qui est l'approche de simulation la plus réaliste. L'écart est encore réduit avec succès par l'introduction de réactions au carbone atomique. Les réactions du carbone atomique ont été tirées d'un modèle de dissociation Ar- $\text{CO}_2$  publié par Beuthe. D'autres constantes de vitesse ont été prises en compte pour ces réactions à partir de la base de données cinétiques du NIST. Les résultats les mieux adaptés sont ceux publiés par Beuthe. Avec cette extension du modèle en incluant la cinétique du carbone atomique, il n'y a pas de déviation visible par rapport au modèle CEA dans la gamme de température de 5000 K à 6100 K.

Ce modèle den Harder étendu est également utilisé pour simuler des expériences de trempe, où le gaz est à la température du plasma pendant plusieurs millisecondes avant d'être refroidi à la température ambiante. Ces expériences sont importantes car il y a recombinaison pendant le refroidissement du gaz de traitement. Cette expérience permet de déterminer la quantité de CO produite. Les expériences de trempe sont simulées à 2500, 3000, 3500 et 6000 K. La production de CO la plus élevée est archivée avec 6000 K et des taux de refroidissement supérieurs à  $1 \times 10^6$  K/s. La fraction de perte relative de CO est saturée pour les vitesses de refroidissement supérieures à  $1 \times 10^7$  K/s, pour toutes les températures à 2 %, sauf pour 6000 K où la fraction de perte relative devient négative à un taux de refroidissement de  $4 \times 10^5$  K/s. Ce phénomène n'est possible qu'en raison de la pyrolyse thermique de CO en C et O. Par conséquent, la concentration de CO est plus élevée après le processus de refroidissement qu'elle ne l'était pendant l'état d'équilibre aux températures du plasma.

Ce modèle combiné den Harder/Beuthe basé sur la pression devrait être utilisé pour la combinaison avec un modèle de dissociation  $\text{H}_2\text{O}$ . Ce modèle devrait ensuite être étendu

aux réactions directes de H<sub>2</sub>O avec C, CO et CO<sub>2</sub>.

Il reste à trouver un modèle de dissociation de H<sub>2</sub>O approprié, car tous les modèles comparés sont très éloignés de l'équilibre chimique lorsqu'ils sont considérés en régime permanent. Le modèle de Srinivasan est un modèle assez simple qui est vérifié par l'expérience publiée du tube de choc. Il présente une très bonne adéquation à l'état d'équilibre pour les températures supérieures à 5000 K. Pour les températures comprises entre 1000 K et 5000 K, la composition à l'état stable est très éloignée de l'équilibre chimique. H<sub>2</sub>O est dissocié à des températures beaucoup trop basses. Une amélioration peut être trouvée si le modèle est considéré après seulement quelques millisecondes, bien que H<sub>2</sub>O soit toujours dissocié à des températures trop basses. Les expériences de trempe ne sont pas possibles avec ce modèle en raison de la température de dissociation excessivement basse de H<sub>2</sub>O, ce qui fausserait les résultats. Un autre modèle simple a été trouvé par Lede, mais les calculs conduisent toujours à des problèmes de convergence, ce qui fait que le modèle ne donne pas de résultats significatifs.

Le modèle d'Avtaeva introduit un ensemble de réactions légèrement plus complexe. Il inclut également HO<sub>2</sub> et H<sub>2</sub>O<sub>2</sub>, qui n'avaient pas été pris en compte auparavant. La plupart des constantes de vitesse de ce modèle sont données à une température fixe de 300 K et n'ont pas de paramètre dépendant de la température. Cela conduit, comme dans le modèle de Srinivasans, à une dissociation de H<sub>2</sub>O à des températures trop basses. Par conséquent, ce modèle n'est pas non plus adapté au cas d'utilisation souhaité. Une autre publication de Medodovic fournit deux modèles, un modèle pour les basses températures de 300 K à 2000 K et un modèle pour les hautes températures entre 2000 K et 5000 K. Le modèle pour les températures élevées dissocie H<sub>2</sub>O à des températures trop basses dans son état stable. Dans ce modèle, H<sub>2</sub>O est à nouveau produit à des températures supérieures à 4000 K, ce qui n'est pas le cas dans les résultats du CEA. Pour améliorer le modèle à haute température et l'étendre à des températures plus basses, les deux modèles disponibles sont combinés. Avec ce modèle combiné, le H<sub>2</sub>O est dissocié à des températures plus élevées que celles prévues par le CEA. L'état d'équilibre est atteint à 5000 K en moins de 1 μs, de sorte qu'une extension des temps de calcul n'améliorera pas la précision.

Le dernier modèle étudié a été publié par Liu. Ce modèle est le plus complexe des modèles étudiés. H<sub>2</sub>O est dissocié à des températures trop élevées dans ce modèle. L'état d'équilibre à 5000 K est atteint en moins de 20 μs, donc une extension des temps de calcul n'améliorera pas le résultat.

La combinaison des deux modèles n'est pas possible dans le cadre de ce travail. D'autres travaux doivent être réalisés avec les modèles de dissociation de H<sub>2</sub>O. Il faut trouver un modèle qui corresponde mieux à l'équilibre chimique à l'état stable. Il sera alors possible

---

de combiner les modèles de dissociation de CO<sub>2</sub> et de dissociation de H<sub>2</sub>O, afin d'étudier l'influence des impuretés de l'eau sur le rendement de conversion de CO<sub>2</sub>.



# List of Figures

2.1. The phase diagram shows the states of matter in dependence of temperature (x axis) and pressure (y axis). On the intersections between the different phases, the name of the respective phase transition is given. The critical point is at a substance specific critical temperature and critical pressure, where all three phases coexist. Above this point it is not possible to distinguish between a liquid and a gas. The arrangement of the molecules is displayed in each state as a schematic. From this diagram it is clear that plasma only occurs at high temperatures, even at low pressures. (Cf. [8, Figure 2]). . . . . .	4
2.2. A schematic overview of a typical microwave plasma torch setup. The microwaves are generated and then coupled into the waveguide, which guides the microwaves to the dielectric tube where the gas absorbs the microwaves and the energy is high enough to ionize the gas. To sustain the plasma, a gas is continuously fed into the dielectric tube. The waveguide is designed in such a way that a maximum of the EM wave is at the intersection of the dielectric tube and the waveguide. . . . .	5
2.3. Overview of quenching methods. The ionized gas from the plasma is always described as hot gas in the figure. In these processes, the cooling fluid is typically the process gas, which prevents further contamination of the reaction. The only exception is the cold wall method, where any fluid can be used as it should not come in contact with the ionized gas. With these methods, quenching rates of up to $10^6 \text{ K s}^{-1}$ are commonly realized. (Cf. [21, Figure 4]) . . . . .	7
3.1. Output from CEARUN for a temperature range from 1000 K to 6100 K. The pressure is fixed at 100 mbar. . . . .	15
3.2. Comparison of the newly implemented Python model with den Harder's implementation and the Mathematica model. The Mathematica implementation clearly deviates in the range from 2000 K to 2300 K. The deviation of the other models is noticeable in the range of 2300 K to 4000 K. .	16

---

*LIST OF FIGURES*

---

3.3. Comparison of the Python implementation with <code>odeint</code> from den Harder and the new Python implementation with <code>solve_ivp</code> . It is not possible to see a difference on this scale. . . . .	17
3.4. Relative and absolute deviation for den Harder's model with <code>odeint</code> and the new Python implementation with <code>solve_ivp</code> . The given deviation is always the between den Harder's original implementation and the new Python implementation. . . . .	18
3.5. Comparison of the CEARUN result and den Harder's model. There is a deviation in the range from 2000 K to 4500 K. Above 5000 K there is again a deviation which is a result of thermal CO dissociation into C and O which is not covered by this model. . . . .	19
3.6. Comparison of the CEARUN result, with the den Harder model and the Koelman model. The den Harder model fits far better to the result from CEARUN than the Koelman model. . . . .	20
3.7. In this plot, the result from the CEARUN program is compared to the result from the density based and the pressure based den Harder model. . . . .	21
3.8. The absolute deviation of the density and pressure model against the CEA result is presented. . . . .	21
3.9. The CEARUN result is presented with the pressure based den Harder model with carbon from Beuthe's Model added to it. CO <sub>2</sub> is used as bath gas instead of argon. The the deviation from the CEA result for temperatures above 5000 K is smaller. The additional consideration of carbon enhances the model. . . . .	23
3.10. The CEARUN result is presented with the improved pressure based den Harder model with carbon from Beuthe's Model added to it. In the range above 5000 K, the deviation from the CEA result is minimal. The additional mass correction noticeably enhances the model. . . . .	24
3.11. The development of CO at 2665 K is shown. The initial CO <sub>2</sub> concentration is 7.02 % of 20.95 bar. . . . .	25
3.12. Validation of the pressure based model extended with carbon at a pressure of 1 Pa. CEARUN result and density based model are given as references. . . . .	25
3.13. Validation of the pressure based model extended with carbon at a pressure of 1 MPa. CEARUN result and density based model are given as references. . . . .	26

---

*LIST OF FIGURES*

---

3.14. The temporal development of the mixture composition is presented. The gas is at room temperature for 100 ms, afterwards it is instantaneously heated to 3000 K where it stays for 500 ms. During this time the CO <sub>2</sub> is dissociated and the other species are produced. After this constant heating period, the gas is quenched and rapidly cooled. In the plot, the cooling rate is $1 \times 10^4$ K/s, hence the room temperature is reached after 270 ms. This cooling rate is chosen to better visualize the quenching. . . . .	27
3.15. The evolution of the CO loss fraction is presented in dependence of the cooling rate. The lowest losses are reached for lower temperatures or at cooling rates above $1 \times 10^7$ K/s. A commonly used temperature for quenching is 3000 K as the energy efficiency for the conversion from CO <sub>2</sub> into CO is excellent at this temperature. The temperatures in the legend are the temperatures in the plasma region. . . . .	28
3.16. Double logarithmic plot of the evolution of the absolute CO production in dependence from the cooling rate. The temperatures in the legend are the temperatures in the plasma region. . . . .	29
4.1. Output from CEARUN for a temperature range from 1000 K to 6300 K. The pressure is fixed at 1 bar. . . . .	31
4.2. Comparison of the OH profile from Srinivasan et al. [40] and the implemented model based on their publication. Both figures yield the same gradient for the OH profile. . . . .	33
4.3. Comparison of the Python implementation from Srinivasan et al. [40] with the CEARUN result. The initial H <sub>2</sub> O density is calculated at 1 bar. The datapoints for this plot are taken after 10 000 s. . . . .	34
4.4. Comparison of the Python implementation from Srinivasan et al. [40] with the CEARUN result. The calculation time is 1.3 ms, the pressure is kept at 1 bar. . . . .	34
4.5. Comparison of the Python implementation from Avtaeva et al. [42] with the CEARUN result. The calculation time is 10 000 s; the pressure is kept at 1 bar. . . . .	35
4.6. Comparison of the high temperature model from Medodovic et al. [43] with the CEARUN result. The calculation time is 10 000 s, the pressure is kept at 1 bar. . . . .	37
4.7. Comparison of the combined Medodovic model with the CEARUN result. The calculation time is 10 000 s, the pressure is kept at 1 bar. . . . .	37
4.8. Result of the temporal calculations of the combined model at 5000 K. From this plot it is very obvious that the steady state was reached in under 1 $\mu$ s. . . . .	38
4.9. Comparison of Liu's model with the CEARUN result. The calculation time is 10 000 s, the pressure is kept at 1 bar. . . . .	39

## *LIST OF FIGURES*

# List of Tables

2.1. Phase transants . . . . .	3
2.2. CEARUN problem types . . . . .	9
2.3. Exemplary list of reactions . . . . .	10
3.1. Comparison of the values published in den Harder's paper and in Butylkin's paper. The implementation of den Harder directly used the converted values from the original paper. . . . .	17
3.2. Reactions from Beuthe et al. [35] involving C. These reactions are implemented into the pressure based model. With argon as M (see text for more details). The unit of the reaction rate constants is $\frac{\text{cm}^3}{\text{s}}$ for two-body reactions and in $\frac{\text{cm}^6}{\text{s}}$ for three-body reactions. $T_g$ is the temperature of the gas . . . . .	22
4.1. Reactions of Avtaeva model. According to the NIST kinetic reactions database, these reactions should be 3-body reactions [36]. . . . .	36
B.1. Reactions of den Harder . . . . .	99
B.2. Reactions of Koelman . . . . .	100
B.3. Reactions from Beuthe et al. [35] involving C . . . . .	101
B.4. Reactions of den Harder/Beuthe . . . . .	102
D.1. Reactions of Srinivasan . . . . .	119
D.2. Reactions of Lede . . . . .	120
D.3. Reactions of Lede with Rate constants . . . . .	120
D.4. Reactions of Avtaeva . . . . .	121
D.5. Reactions of Mededovic, high temperature model . . . . .	122
D.6. Reactions of Mededovic, combined model . . . . .	123
D.7. Reactions of Liu . . . . .	125



## Bibliography

- [1] N. Noorani, S. Pourebrahimi, and A. Mehrdad, “Enhancing CO<sub>2</sub> adsorption performance of cold oxygen plasma-treated almond shell-derived activated carbons through ionic liquid incorporation,” *Journal of CO<sub>2</sub> Utilization*, vol. 88, p. 102927, 9 2024. [Online]. Available: <https://doi.org/10.1016/j.jcou.2024.102927>
- [2] M. F. Bashir, M. Shahbaz, B. Ma, and K. Alam, “Evaluating the roles of energy innovation, fossil fuel costs and environmental compliance towards energy transition in advanced industrial economies,” *Journal of Environmental Management*, vol. 351, p. 119709, 12 2023. [Online]. Available: <https://doi.org/10.1016/j.jenvman.2023.119709>
- [3] S. Pourebrahimi, M. Pirooz, S. Ahmadi, M. Kazemeini, and L. Vafajoo, “Nanoengineering of metal-based electrocatalysts for carbon dioxide (CO<sub>2</sub>) reduction: A critical review,” *Materials Today Physics*, vol. 38, p. 101250, 10 2023. [Online]. Available: <https://doi.org/10.1016/j.mtphys.2023.101250>
- [4] S. Fawzy, A. I. Osman, J. Doran, and D. W. Rooney, “Strategies for mitigation of climate change: a review,” *Environmental Chemistry Letters*, vol. 18, no. 6, pp. 2069–2094, 7 2020.
- [5] H. Zhu, Y. Huang, S. Yin, and W. Zhang, “Microwave plasma setups for co<sub>2</sub> conversion: A mini-review,” *Green Energy and Resources*, vol. 2, no. 1, p. 100061, 2024. [Online]. Available: <https://www.sciencedirect.com/science/article/pii/S2949720524000158>
- [6] F. A. D’Isa, E. A. D. Carbone, A. Hecimovic, and U. Fantz, “Performance analysis of a 2.45 GHz microwave plasma torch for CO<sub>2</sub> decomposition in gas swirl configuration,” *Plasma sources science & technology*, vol. 29, no. 10, p. 105009, 10 2020. [Online]. Available: <https://doi.org/10.1088/1361-6595/abaa84>
- [7] C. K. Kiefer, R. Antunes, A. Hecimovic, A. Meindl, and U. Fantz, “CO<sub>2</sub> dissociation using a lab-scale microwave plasma torch: An experimental study in view of industrial application,” *Chemical engineering journal*, vol. 481, p. 148326, 2 2024. [Online]. Available: <https://doi.org/10.1016/j.cej.2023.148326>

---

## BIBLIOGRAPHY

---

- [8] M. Ong, S. Nomanbhay, F. Kusumo, and P. Show, “Application of microwave plasma technology to convert carbon dioxide (co<sub>2</sub>) into high value products: A review,” *Journal of Cleaner Production*, vol. 336, p. 130447, 2022. [Online]. Available: <https://www.sciencedirect.com/science/article/pii/S0959652622000920>
- [9] D. A. Frank-Kamenetskii, *Plasma: the fourth state of matter*, 1 1972. [Online]. Available: <https://doi.org/10.1007/978-1-4684-1896-5>
- [10] A. Fridman, *Plasma chemistry*. Cambridge University Press, 5 2008.
- [11] J. A. Bittencourt, *Fundamentals of Plasma Physics*, 1 2004. [Online]. Available: <https://doi.org/10.1007/978-1-4757-4030-1>
- [12] M. Füner, C. Wild, and P. Koidl, “Simulation and development of optimized microwave plasma reactors for diamond deposition,” *Surface and Coatings Technology*, vol. 116-119, pp. 853–862, 9 1999. [Online]. Available: [https://doi.org/10.1016/s0257-8972\(99\)00233-9](https://doi.org/10.1016/s0257-8972(99)00233-9)
- [13] N. den Harder, D. C. M. Van Den Bekerom, R. S. Al, M. F. Graswinckel, J. M. Palomares, F. J. J. Peeters, S. Ponduri, T. Minea, W. A. Bongers, M. C. M. Van De Sanden, and G. J. Van Rooij, “Homogeneous CO<sub>2</sub> conversion by microwave plasma: Wave propagation and diagnostics,” *Plasma processes and polymers*, vol. 14, no. 6, 11 2016. [Online]. Available: <https://doi.org/10.1002/ppap.201600120>
- [14] B. Hrycak, D. Czylkowski, M. Jasiński, M. Dors, and J. Mizeraczyk, “Hydrogen production via synthetic biogas reforming in Atmospheric-Pressure microwave (915 MHz) plasma at high Gas-Flow output,” *Plasma Chemistry and Plasma Processing*, vol. 39, no. 3, pp. 695–711, 2 2019. [Online]. Available: <https://doi.org/10.1007/s11090-019-09962-z>
- [15] V. Orsat, G. Raghavan, and K. Krishnaswamy, *Microwave technology for food processing*, 1 2017. [Online]. Available: <https://www.sciencedirect.com/science/article/pii/B978008100528600005X>
- [16] J. Musil, “Deposition of thin films using microwave plasmas: present status and trends,” *Vacuum*, vol. 47, no. 2, pp. 145–155, 2 1996. [Online]. Available: [https://doi.org/10.1016/0042-207x\(95\)00213-8](https://doi.org/10.1016/0042-207x(95)00213-8)
- [17] K. Suzuki, K. Ninomiya, and S. Mishimatsu, “Microwave plasma etching,” *Vacuum*, vol. 34, no. 10-11, pp. 953–957, 10 1984. [Online]. Available: [https://doi.org/10.1016/0042-207x\(84\)90177-5](https://doi.org/10.1016/0042-207x(84)90177-5)
- [18] A. A. Zamri, M. Y. Ong, S. Nomanbhay, and P. L. Show, “Microwave plasma technology for sustainable energy production and the electromagnetic interaction

---

## BIBLIOGRAPHY

---

- within the plasma system: A review,” *Environmental Research*, vol. 197, p. 111204, 6 2021. [Online]. Available: <https://doi.org/10.1016/j.envres.2021.111204>
- [19] V. Vermeiren and A. Bogaerts, “Plasma-Based CO<sub>2</sub> conversion: to quench or not to quench?” *The Journal of Physical Chemistry C*, vol. 124, no. 34, pp. 18 401–18 415, 8 2020. [Online]. Available: <https://doi.org/10.1021/acs.jpcc.0c04257>
- [20] P. Fauchais and J. Rakowitz, “Physics on plasma chemistry,” *Le Journal de Physique Colloques*, vol. 40, no. C7, pp. C7–312, 7 1979. [Online]. Available: <https://doi.org/10.1051/jphyscol:19797444>
- [21] T. Yang, J. Shen, T. Ran, J. Li, P. Chen, and Y. Yin, “Understanding CO<sub>2</sub> decomposition by thermal plasma with supersonic expansion quench,” *Plasma Science and Technology*, vol. 20, no. 6, p. 065502, 4 2018. [Online]. Available: <https://doi.org/10.1088/2058-6272/aaa969>
- [22] E. Mercer, S. Van Alphen, C. Van Deursen, T. Righart, W. Bongers, R. Snyders, A. Bogaerts, M. Van De Sanden, and F. Peeters, “Post-plasma quenching to improve conversion and energy efficiency in a CO<sub>2</sub> microwave plasma,” *Fuel*, vol. 334, p. 126734, 2 2023. [Online]. Available: <https://doi.org/10.1016/j.fuel.2022.126734>
- [23] J. Lede, F. Lapicque, J. Villermaux, B. Cales, A. Ounalli, J. Baumard, and A. Anthony, “Production of hydrogen by direct thermal decomposition of water: Preliminary investigations,” *International Journal of Hydrogen Energy*, vol. 7, no. 12, pp. 939–950, 1 1982. [Online]. Available: [https://doi.org/10.1016/0360-3199\(82\)90162-8](https://doi.org/10.1016/0360-3199(82)90162-8)
- [24] NASA Glenn Research Center, “Chemical Equilibrium with Applications | Glenn Research Center | NASA,” 4 2023. [Online]. Available: <https://www1.grc.nasa.gov/research-and-engineering/ceaweb>
- [25] S. Gordon and B. J. McBride, “Computer program for calculation of complex chemical equilibrium compositions and applications. Part 1: Analysis,” 10 1994. [Online]. Available: <https://ntrs.nasa.gov/citations/19950013764>
- [26] “stoichiometric number,” 2019. [Online]. Available: <https://doi.org/10.1351/goldbook.S06025>
- [27] “extent of reaction,” 2019. [Online]. Available: <https://doi.org/10.1351/goldbook.E02283>
- [28] M. Leader and NASA Glenn Research Center, “CEARUN rev4.” [Online]. Available: <https://cearun.grc.nasa.gov/>

## BIBLIOGRAPHY

---

- [29] B. J. McBride and S. Gordon, “Computer Program for calculation of complex chemical equilibrium compositions and applications II. Users Manual and program description,” 6 1996. [Online]. Available: <https://ntrs.nasa.gov/citations/19960044559>
- [30] T. A. Brabbs, F. E. Belles, and S. A. Zlatarich, “Shock-Tube study of carbon dioxide dissociation rate,” *The Journal of Chemical Physics*, vol. 38, no. 8, pp. 1939–1944, 4 1963. [Online]. Available: <https://doi.org/10.1063/1.1733900>
- [31] P. Koelman, S. Heijkers, S. T. Mousavi, W. Graef, D. Mihailova, T. Kozak, A. Bogaerts, and J. Van Dijk, “A comprehensive chemical model for the splitting of CO<sub>2</sub> in Non-Equilibrium plasmas,” *Plasma processes and polymers*, vol. 14, no. 4-5, 10 2016. [Online]. Available: <https://doi.org/10.1002/ppap.201600155>
- [32] Y. P. Butylkin, A. A. Grinenko, A. A. Levitskii, L. Polak, N. Rytova, and D. I. Slovetskii, “Mathematical modeling of the kinetics of the thermal decomposition of carbon dioxide in an electric arc discharge and quenching of the products,” *High Energy Chemistry*, vol. 13, no. 456, 1979.
- [33] D. Müller-Komorowska, “Differential equations with scipy – odeint or solve\_ivp,” 2 2021. [Online]. Available: [https://simulationbased.com/2021/02/16/differential-equations-with-scipy-odeint-or-solve\\_ivp/comment-page-1/](https://simulationbased.com/2021/02/16/differential-equations-with-scipy-odeint-or-solve_ivp/comment-page-1/)
- [34] A. R. Fairbairn, “The dissociation of carbon monoxide,” *Proceedings of the Royal Society of London A Mathematical and Physical Sciences*, vol. 312, no. 1509, pp. 207–227, 9 1969. [Online]. Available: <https://doi.org/10.1098/rspa.1969.0149>
- [35] T. G. B. Beuthe and J.-S. C. Chang, “Chemical kinetic modelling of Non-Equilibrium AR-CO<sub>2</sub> thermal plasmas,” *Japanese Journal of Applied Physics*, vol. 36, no. 7S, p. 4997, 7 1997. [Online]. Available: <https://doi.org/10.1143/jjap.36.4997>
- [36] “NIST Chemical Kinetics Database, Standard Reference Database 17, Version 7.1 (Web Version), Release 1.6.8,” 2024.
- [37] H.-J. Mick, M. Burmeister, and P. Roth, “Atomic resonance absorption spectroscopy measurements on high-temperature CO dissociation kinetics,” *AIAA Journal*, vol. 31, no. 4, pp. 671–676, 4 1993. [Online]. Available: <https://doi.org/10.2514/3.11602>
- [38] R. K. Hanson, “Shock-tube study of carbon monoxide dissociation kinetics,” *The Journal of Chemical Physics*, vol. 60, no. 12, pp. 4970–4976, 6 1974. [Online]. Available: <https://doi.org/10.1063/1.1681010>

---

## BIBLIOGRAPHY

---

- [39] J. P. Appleton, M. Steinberg, and D. J. Liquornik, “Shock-Tube study of carbon monoxide dissociation using Vacuum-Ultraviolet absorption,” *The Journal of Chemical Physics*, vol. 52, no. 5, pp. 2205–2221, 3 1970. [Online]. Available: <https://doi.org/10.1063/1.1673286>
- [40] N. K. Srinivasan and J. V. Michael, “The thermal decomposition of water,” *International Journal of Chemical Kinetics*, vol. 38, no. 3, pp. 211–219, 1 2006. [Online]. Available: <https://doi.org/10.1002/kin.20172>
- [41] J. Lede, F. Lapicque, and J. Villermaux, “Production of hydrogen by direct thermal decomposition of water,” *International Journal of Hydrogen Energy*, vol. 8, no. 9, pp. 675–679, 1 1983. [Online]. Available: [https://doi.org/10.1016/0360-3199\(83\)90175-1](https://doi.org/10.1016/0360-3199(83)90175-1)
- [42] S. V. Avtaeva, A. A. General, and V. A. Kel'man, “Kinetic model for low-density non-stationary gas discharge in water vapour,” *Journal of Physics D Applied Physics*, vol. 43, no. 31, p. 315201, 7 2010. [Online]. Available: <https://doi.org/10.1088/0022-3727/43/31/315201>
- [43] S. Medodovic and B. R. Locke, “Primary chemical reactions in pulsed electrical discharge channels in water,” *Journal of Physics D Applied Physics*, vol. 42, no. 4, p. 049801, 1 2009. [Online]. Available: <https://doi.org/10.1088/0022-3727/42/4/049801>
- [44] D. X. Liu, P. Bruggeman, F. Iza, M. Z. Rong, and M. G. Kong, “Global model of low-temperature atmospheric-pressure He + H<sub>2</sub>O plasmas,” *Plasma Sources Science and Technology*, vol. 19, no. 2, p. 025018, 3 2010. [Online]. Available: <https://doi.org/10.1088/0963-0252/19/2/025018>



## A. CEARUN files for CO<sub>2</sub>

In the following the output files from CEARUN are shown. An issue with the current implementation of CEARUN leads to the fact that only 21 input temperatures can be used. This bug is reported to NASA already.

### A.1. 1000 - 3000 K

```
1
*****
2
3      NASA-GLENN CHEMICAL EQUILIBRIUM PROGRAM CEA2, FEBRUARY 5, 2004
4          BY BONNIE MCBRIDE AND SANFORD GORDON
5      REFS: NASA RP-1311, PART I, 1994 AND NASA RP-1311, PART II, 1996
6
7
*****
8
9
10
11
12  ### CEA analysis performed on Sun 15-Sep-2024 11:50:06
13
14  # Problem Type: "Assigned Temperature and Pressure"
15
16  prob case=-----8923 tp
17
18  # Pressure (1 value):
19  p,bar= 0.1
20  # Temperature (21 values):
21  t,k= 1000, 1100, 1200, 1300, 1400, 1500, 1600, 1700, 1800, 1900, 2000,
22  2100, 220
23  0, 2300, 2400, 2500, 2600, 2700, 2800, 2900, 3000
24
25  # You selected the following fuels and oxidizers:
26  reac
27  fuel CO2           wt%=100.0000
28  oxid CO2           wt%=100.0000
29  # You selected these options for output:
```

---

## APPENDIX A. CEARUN FILES FOR CO<sub>2</sub>

---

```
30 # long version of output
31 # Proportions of any products will be expressed as Mole Fractions.
32 # Heat will be expressed as siunits
33 output siunits
34
35 # Input prepared by this script:/var/www/sites/cearun.grc.nasa.gov/cgi-
   bin/CEARU
36 N/prepareInputFile.cgi
37
38 ##### IMPORTANT: The following line is the end of your CEA input file!
39 end
40
41 OPTIONS: TP=T HP=F SP=F TV=F UV=F SV=F DETN=F SHOCK=F REFL=F
   INCD=F
42 RKT=F FROZ=F EQL=F IONS=F SIUNIT=T DEBUGF=F SHKDBG=F DETDBG=F
   TRNSPT=F
43
44 T,K = 1000.0000 1100.0000 1200.0000 1300.0000 1400.0000 1500.0000
   1600.0000
45
46 T,K = 1700.0000 1800.0000 1900.0000 2000.0000 2100.0000 2200.0000
   2300.0000
47
48 T,K = 2400.0000 2500.0000 2600.0000 2700.0000 2800.0000 2900.0000
   3000.0000
49
50 TRACE= 0.00E+00 S/R= 0.000000E+00 H/R= 0.000000E+00 U/R= 0.000000E+00
51
52 P,BAR = 0.100000
53
54      REACTANT          WT.FRAC    (ENERGY/R),K    TEMP ,K    DENSITY
55      EXPLODED FORMULA
56 F: CO2           1.000000  0.000000E+00        0.00  0.0000
57     C  1.000000  0  2.000000
58 O: CO2           1.000000  0.000000E+00        0.00  0.0000
59     C  1.000000  0  2.000000
60
61 SPECIES BEING CONSIDERED IN THIS SYSTEM
62 (CONDENSED PHASE MAY HAVE NAME LISTED SEVERAL TIMES)
63 LAST thermo.inp UPDATE: 9/09/04
64
65 g 7/97 *C          tpis79 *CO          g 9/99 *C02
66 tpis91 *C2          g 8/00 C20         tpis79 *C3
67 g 7/88 C302         g tpis *C4          g 8/00 *C5
68 g 5/97 *O          tpis89 *O2          g 8/01 03
69 n 4/83 C(gr)       n 4/83 C(gr)       n 4/83 C(gr)
70
71 O/F = 1.000000
```

### A.1. 1000 - 3000 K

---

```

72
73          EFFECTIVE FUEL      EFFECTIVE OXIDANT      MIXTURE
74  ENTHALPY           h(2)/R          h(1)/R          h0/R
75  (KG-MOL)(K)/KG    0.00000000E+00  0.00000000E+00  0.00000000E
    +00
76
77  KG-FORM.WT./KG      bi(2)          bi(1)          b0i
78  *C                  0.22722367E-01  0.22722367E-01  0.22722367E
    -01
79  *0                  0.45444734E-01  0.45444734E-01  0.45444734E
    -01
80
81  POINT ITN          T              C              0
82
83
84
85
86          THERMODYNAMIC EQUILIBRIUM PROPERTIES AT ASSIGNED
87
88          TEMPERATURE AND PRESSURE
89
90  CASE = -----
91
92          REACTANT          WT FRACTION      ENERGY        TEMP
93                           (SEE NOTE)      KJ/KG-MOL      K
94  FUEL               CO2            1.0000000      0.000
    0.000
95  OXIDANT             CO2            1.0000000      0.000
    0.000
96
97  O/F=    1.00000  %FUEL= 50.000000  R,EQ.RATIO= 1.000000  PHI,EQ.RATIO=
    0.000000
98
99  THERMODYNAMIC PROPERTIES
100
101 P, BAR           0.10000  0.10000  0.10000  0.10000  0.10000  0.10000
    0.10000  0.10000
102 T, K            1000.00  1100.00  1200.00  1300.00  1400.00  1500.00
    1600.00  1700.00
103 RHO, KG/CU M   5.2931-2  4.8119-2  4.4109-2  4.0715-2  3.7803-2  3.5274-2
    3.3049-2  3.1065-2
104 H, KJ/KG         -8182.56  -8057.85  -7930.72  -7801.40  -7669.59  -7534.32
    -7393.40  -7242.94
105 U, KJ/KG         -8371.48  -8265.67  -8157.44  -8047.01  -7934.12  -7817.82
    -7695.98  -7564.84
106 G, KJ/KG         -14736.6  -15398.1  -16070.9  -16754.5  -17448.2  -18151.3
    -18863.7  -19585.1

```

---

## APPENDIX A. CEARUN FILES FOR CO<sub>2</sub>

---

107 S, KJ/(KG)(K) 6.5541 6.6729 6.7835 6.8870 6.9847 7.0780  
108 7.1689 7.2601

109 M, (1/n) 44.009 44.010 44.009 44.008 44.004 43.992  
110 43.966 43.910  
110 (dLV/dLP)t -1.00000 -1.00000 -1.00000 -1.00001 -1.00004 -1.00013  
-1.00033 -1.00076

111 (dLV/dLT)p 1.0000 1.0000 1.0002 1.0007 1.0022 1.0059  
1.0140 1.0299

112 Cp, KJ/(KG)(K) 1.2341 1.2594 1.2822 1.3047 1.3329 1.3761  
1.4487 1.5707

113 GAMMAS 1.1808 1.1765 1.1729 1.1696 1.1659 1.1612  
1.1546 1.1456

114 SON VEL ,M/SEC 472.3 494.5 515.7 536.0 555.4 573.8  
591.1 607.3

115

116 MOLE FRACTIONS

117

118 \*CO 0.00000 0.00000 0.00002 0.00008 0.00027 0.00078  
0.00199 0.00453

119 \*CO2 1.00000 1.00000 0.99997 0.99988 0.99960 0.99883  
0.99701 0.99320

120 \*O 0.00000 0.00000 0.00000 0.00000 0.00000 0.00000  
0.00000 0.00001

121 \*O2 0.00000 0.00000 0.00001 0.00004 0.00013 0.00039  
0.00099 0.00226

122

123 \* THERMODYNAMIC PROPERTIES FITTED TO 20000.K

124

125 PRODUCTS WHICH WERE CONSIDERED BUT WHOSE MOLE FRACTIONS  
126 WERE LESS THAN 5.000000E-06 FOR ALL ASSIGNED CONDITIONS

127

128 \*C \*C2 C20 \*C3 C302  
129 \*C4 \*C5 O3 C(gr)

130

131 NOTE. WEIGHT FRACTION OF FUEL IN TOTAL FUELS AND OF OXIDANT IN TOTAL  
OXIDANTS

132

133

134

135

136

137

138 POINT ITN T C O

139

140

141

142

```

143          THERMODYNAMIC EQUILIBRIUM PROPERTIES AT ASSIGNED
144
145          TEMPERATURE AND PRESSURE
146
147  CASE = -----
148
149          REACTANT           WT FRACTION      ENERGY      TEMP
150                           (SEE NOTE)      KJ/KG-MOL      K
151  FUEL       CO2            1.0000000      0.000
152          0.000
152  OXIDANT    CO2            1.0000000      0.000
153          0.000
154  O/F=      1.00000 %FUEL= 50.000000 R,EQ.RATIO= 1.000000 PHI,EQ.RATIO=
155          0.000000
156  THERMODYNAMIC PROPERTIES
157
158  P, BAR        0.10000   0.10000   0.10000   0.10000   0.10000   0.10000
159          0.10000   0.10000
159  T, K         1800.00   1900.00   2000.00   2100.00   2200.00   2300.00
160          2400.00   2500.00
160  RHO, KG/CU M 2.9268-2 2.7608-2 2.6042-2 2.4532-2 2.3044-2 2.1559-2
161          2.0068-2 1.8580-2
161  H, KJ/KG     -7076.77 -6886.01 -6658.81 -6380.63 -6034.89 -5604.53
162          -5074.27 -4433.55
162  U, KJ/KG     -7418.44 -7248.22 -7042.80 -6788.27 -6468.84 -6068.37
163          -5572.57 -4971.76
163  G, KJ/KG     -20315.8 -21056.4 -21807.9 -22571.9 -23350.8 -24147.1
164          -24964.3 -25805.8
164  S, KJ/(KG)(K) 7.3550   7.4581   7.5745   7.7101   7.8708   8.0620
165          8.2875   8.5489
166  M, (1/n)     43.803   43.614   43.306   42.833   42.152   41.228
167          40.046   38.621
167  (dLV/dLP)t  -1.00156 -1.00298 -1.00530 -1.00882 -1.01381 -1.02042
168          -1.02855 -1.03781
168  (dLV/dLT)p  1.0583   1.1051   1.1769   1.2795   1.4167   1.5874
169          1.7842   1.9925
169  Cp, KJ/(KG)(K) 1.7674   2.0677   2.5006   3.0910   3.8527   4.7805
170          5.8427   6.9770
170  GAMMAS      1.1347   1.1231   1.1124   1.1037   1.0976   1.0939
171          1.0924   1.0925
171  SON VEL ,M/SEC 622.7    637.8    653.6    670.8    690.2    712.3
172          737.8    766.8
173  MOLE FRACTIONS
174

```

---

## APPENDIX A. CEARUN FILES FOR CO<sub>2</sub>

---

175 \*CO 0.00937 0.01786 0.03170 0.05275 0.08269 0.12259  
0.17227 0.22987

176 \*CO2 0.98593 0.97316 0.95231 0.92053 0.87510 0.81420  
0.73767 0.64769

177 \*O 0.00003 0.00009 0.00027 0.00071 0.00172 0.00382  
0.00786 0.01501

178 \*O2 0.00467 0.00889 0.01572 0.02602 0.04049 0.05938  
0.08220 0.10743

179

180 \* THERMODYNAMIC PROPERTIES FITTED TO 20000.K

181

182 PRODUCTS WHICH WERE CONSIDERED BUT WHOSE MOLE FRACTIONS

183 WERE LESS THAN 5.000000E-06 FOR ALL ASSIGNED CONDITIONS

184

185 \*C \*C2 C20 \*C3 C302  
186 \*C4 \*C5 03 C(gr)

187

188 NOTE. WEIGHT FRACTION OF FUEL IN TOTAL FUELS AND OF OXIDANT IN TOTAL  
OXIDANTS

189

190

191

192

193

194

195 POINT ITN T C 0

196

197

198

199

200 THERMODYNAMIC EQUILIBRIUM PROPERTIES AT ASSIGNED

201

202 TEMPERATURE AND PRESSURE

203

204 CASE = -----

205

	REACTANT	WT FRACTION (SEE NOTE)	ENERGY KJ/KG-MOL	TEMP K
206				
207				
208	FUEL CO2	1.0000000	0.000	
	0.000			
209	OXIDANT CO2	1.0000000	0.000	
	0.000			

210

211 O/F= 1.00000 %FUEL= 50.000000 R,EQ.RATIO= 1.000000 PHI,EQ.RATIO=

0.000000

212

213 THERMODYNAMIC PROPERTIES

214

---

## A.2. 3100 - 5100 K

---

```
215 P, BAR          0.10000  0.10000  0.10000  0.10000  0.10000
216 T, K            2600.00   2700.00   2800.00   2900.00   3000.00
217 RHO, KG/CU M   1.7115-2  1.5703-2  1.4371-2  1.3142-2  1.2027-2
218 H, KJ/KG        -3679.36  -2817.88  -1863.72  -836.93   240.04
219 U, KJ/KG        -4263.63  -3454.70  -2559.56  -1597.86  -591.41
220 G, KJ/KG        -26675.2   -27575.7   -28509.9   -29479.5   -30485.4
221 S, KJ/(KG)(K)  8.8446   9.1696   9.5165   9.8767   10.2418
222
223 M, (1/n)       36.999   35.252   33.457   31.688   30.000
224 (dLV/dLP)t    -1.04751  -1.05684  -1.06513  -1.07194  -1.07699
225 (dLV/dLT)p    2.1931   2.3667   2.5003   2.5891   2.6330
226 Cp, KJ/(KG)(K) 8.0964   9.1083   9.9408   10.5575  10.9413
227 GAMMAS        1.0941   1.0967   1.1003   1.1046   1.1094
228 SON VEL ,M/SEC 799.5    835.7    875.0    916.8    960.4
229
230 MOLE FRACTIONS
231
232 *C0             0.29179  0.35319  0.40896  0.45497  0.48889
233 *C02            0.54893  0.44781  0.35126  0.26505  0.19278
234 *O              0.02678  0.04481  0.07059  0.10498  0.14778
235 *O2             0.13251  0.15419  0.16919  0.17500  0.17056
236
237 * THERMODYNAMIC PROPERTIES FITTED TO 20000.K
238
239 PRODUCTS WHICH WERE CONSIDERED BUT WHOSE MOLE FRACTIONS
240 WERE LESS THAN 5.000000E-06 FOR ALL ASSIGNED CONDITIONS
241
242 *C               *C2           C20          *C3           C302
243 *C4              *C5           03           C(gr)
244
245 NOTE. WEIGHT FRACTION OF FUEL IN TOTAL FUELS AND OF OXIDANT IN TOTAL
OXIDANTS
```

## A.2. 3100 - 5100 K

```
1
*****
2
3      NASA-GLENN CHEMICAL EQUILIBRIUM PROGRAM CEA2, FEBRUARY 5, 2004
4      BY BONNIE MCBRIDE AND SANFORD GORDON
5      REFS: NASA RP-1311, PART I, 1994 AND NASA RP-1311, PART II, 1996
6
7
*****
8
9
```

---

## APPENDIX A. CEARUN FILES FOR CO<sub>2</sub>

---

```
10
11
12 ##### CEA analysis performed on Sun 15-Sep-2024 11:52:19
13
14 # Problem Type: "Assigned Temperature and Pressure"
15
16 prob case=-----8923 tp
17
18 # Pressure (1 value):
19 p,bar= 0.1
20 # Temperature (21 values):
21 t,k= 3100, 3200, 3300, 3400, 3500, 3600, 3700, 3800, 3900, 4000, 4100,
   4200, 430
22 0, 4400, 4500, 4600, 4700, 4800, 4900, 5000, 5100
23
24 # You selected the following fuels and oxidizers:
25 reac
26 fuel CO2           wt%=100.0000
27 oxid CO2           wt%=100.0000
28
29 # You selected these options for output:
30 # long version of output
31 # Proportions of any products will be expressed as Mole Fractions.
32 # Heat will be expressed as siunits
33 output siunits
34
35 # Input prepared by this script:/var/www/sites/cearun.grc.nasa.gov/cgi-
   bin/CEARU
36 N/prepareInputFile.cgi
37
38 ##### IMPORTANT: The following line is the end of your CEA input file!
39 end
40
41 OPTIONS: TP=T  HP=F  SP=F  TV=F  UV=F  SV=F  DETN=F  SHOCK=F  REFL=F
   INCD=F
42 RKT=F  FROZ=F  EQL=F  IONS=F  SIUNIT=T  DEBUGF=F  SHKDBG=F  DETDBG=F
   TRNSPT=F
43
44 T,K = 3100.0000 3200.0000 3300.0000 3400.0000 3500.0000 3600.0000
   3700.0000
45
46 T,K = 3800.0000 3900.0000 4000.0000 4100.0000 4200.0000 4300.0000
   4400.0000
47
48 T,K = 4500.0000 4600.0000 4700.0000 4800.0000 4900.0000 5000.0000
   5100.0000
49
50 TRACE= 0.00E+00  S/R= 0.000000E+00  H/R= 0.000000E+00  U/R= 0.000000E+00
```

A.2. 3100 - 5100 K

---

```

51
52 P , BAR = 0.100000
53
54      REACTANT          WT . FRAC   (ENERGY/R) , K    TEMP , K   DENSITY
55      EXPLODED FORMULA
56 F: C02           1.000000  0.000000E+00      0.00  0.0000
57             C 1.000000  0 2.00000
58 O: C02           1.000000  0.000000E+00      0.00  0.0000
59             C 1.000000  0 2.00000
60
61 SPECIES BEING CONSIDERED IN THIS SYSTEM
62 (CONDENSED PHASE MAY HAVE NAME LISTED SEVERAL TIMES)
63 LAST thermo.inp UPDATE: 9/09/04
64
65 g 7/97 *C          tpis79 *CO          g 9/99 *C02
66 tpis91 *C2          g 8/00 C20          tpis79 *C3
67 g 7/88 C3O2          g tpis *C4          g 8/00 *C5
68 g 5/97 *O          tpis89 *O2          g 8/01 O3
69 n 4/83 C(gr)          n 4/83 C(gr)          n 4/83 C(gr)
70
71 O/F = 1.000000
72
73          EFFECTIVE FUEL          EFFECTIVE OXIDANT          MIXTURE
74 ENTHALPY          h(2)/R          h(1)/R          h0/R
75 (KG-MOL)(K)/KG          0.00000000E+00          0.00000000E+00          0.00000000E
76 +00
77 KG-FORM.WT./KG          bi(2)          bi(1)          b0i
78 *C          0.22722367E-01          0.22722367E-01          0.22722367E
79 -01
80 *O          0.45444734E-01          0.45444734E-01          0.45444734E
81 -01
82 POINT ITN          T          C          O
83
84
85
86 THERMODYNAMIC EQUILIBRIUM PROPERTIES AT ASSIGNED
87
88 TEMPERATURE AND PRESSURE
89
90 CASE = -----
91
92      REACTANT          WT FRACTION          ENERGY          TEMP
93          (SEE NOTE)          KJ/KG-MOL          K
94 FUEL          C02          1.0000000          0.000
          0.000

```

---

## APPENDIX A. CEARUN FILES FOR CO<sub>2</sub>

---

95 OXIDANT CO2 1.0000000 0.000  
0.000

96

97 O/F= 1.00000 %FUEL= 50.000000 R,EQ.RATIO= 1.000000 PHI,EQ.RATIO= 0.000000

98

99 THERMODYNAMIC PROPERTIES

100

101 P, BAR 0.10000 0.10000 0.10000 0.10000 0.10000 0.10000 0.10000  
0.10000 0.10000

102 T, K 3100.00 3200.00 3300.00 3400.00 3500.00 3600.00  
3700.00 3800.00

103 RHO, KG/CU M 1.1032-2 1.0156-2 9.4016-3 8.7649-3 8.2388-3 7.8093-3  
7.4585-3 7.1680-3

104 H, KJ/KG 1342.39 2439.41 3491.55 4454.02 5288.82 5977.80  
6526.47 6956.91

105 U, KJ/KG 435.89 1454.81 2427.90 3313.11 4075.05 4697.28  
5185.72 5561.82

106 G, KJ/KG -31527.7 -32605.6 -33717.2 -34859.5 -36028.2 -37218.8  
-38426.6 -39647.5

107 S, KJ/(KG)(K) 10.6033 10.9516 11.2754 11.5628 11.8049 11.9991  
12.1495 12.2643

108

109 M, (1/n) 28.434 27.022 25.796 24.778 23.975 23.375  
22.945 22.647

110 (dLV/dLP)t -1.07984 -1.07970 -1.07577 -1.06789 -1.05709 -1.04526  
-1.03423 -1.02505

111 (dLV/dLT)p 2.6288 2.5674 2.4394 2.2484 2.0180 1.7838  
1.5762 1.4104

112 Cp, KJ/(KG)(K) 11.0551 10.8189 10.1470 9.0365 7.6286 6.1616  
4.8506 3.8059

113 GAMMAS 1.1148 1.1208 1.1277 1.1362 1.1468 1.1607  
1.1784 1.2003

114 SON VEL,M/SEC 1005.3 1050.5 1095.2 1138.5 1179.8 1219.1  
1256.9 1294.0

115

116 MOLE FRACTIONS

117

118 \*CO 0.51049 0.52140 0.52438 0.52252 0.51849 0.51410  
0.51028 0.50732

119 \*CO2 0.13559 0.09261 0.06176 0.04049 0.02629 0.01703  
0.01109 0.00728

120 \*O 0.19734 0.25057 0.30332 0.35146 0.39195 0.42362  
0.44698 0.46348

121 \*O2 0.15657 0.13542 0.11053 0.08553 0.06327 0.04524  
0.03165 0.02192

122

123 \* THERMODYNAMIC PROPERTIES FITTED TO 20000.K

---

```

124
125      PRODUCTS WHICH WERE CONSIDERED BUT WHOSE MOLE FRACTIONS
126      WERE LESS THAN 5.000000E-06 FOR ALL ASSIGNED CONDITIONS
127
128 *C          *C2          C20          *C3          C302
129 *C4          *C5          03           C(gr)
130
131 NOTE. WEIGHT FRACTION OF FUEL IN TOTAL FUELS AND OF OXIDANT IN TOTAL
132      OXIDANTS
133
134
135
136
137
138 POINT ITN      T          C          O
139
140
141
142
143      THERMODYNAMIC EQUILIBRIUM PROPERTIES AT ASSIGNED
144
145      TEMPERATURE AND PRESSURE
146
147 CASE = -----
148
149      REACTANT          WT FRACTION        ENERGY        TEMP
150                      (SEE NOTE)        KJ/KG-MOL      K
151 FUEL      CO2          1.0000000        0.000
152
153      0.000
154 OXIDANT    CO2          1.0000000        0.000
155
156      0.000
157
158 P, BAR      0.10000    0.10000    0.10000    0.10000    0.10000    0.10000
159      0.10000    0.10000
160 T, K       3900.00     4000.00     4100.00     4200.00     4300.00     4400.00
161      4500.00     4600.00
162 RHO, KG/CU M   6.9218-3  6.7077-3  6.5171-3  6.3440-3  6.1845-3  6.0359-3
163      5.8961-3  5.7638-3
164 H, KJ/KG     7296.88    7571.92    7802.17    8002.21    8182.11    8348.76
165      8506.92    8660.04
166 U, KJ/KG     5852.16    6081.09    6267.74    6425.93    6565.18    6692.00
167      6810.87    6925.07

```

---

## APPENDIX A. CEARUN FILES FOR CO<sub>2</sub>

---

163 G, KJ/KG -40878.6 -42117.5 -43362.6 -44613.0 -45867.9 -47126.8  
-48389.4 -49655.5

164 S, KJ/(KG)(K) 12.3527 12.4223 12.4792 12.5274 12.5698 12.6081  
12.6436 12.6773

165

166 M, (1/n) 22.445 22.308 22.216 22.154 22.111 22.081  
22.060 22.045

167 (dLV/dLP)t -1.01799 -1.01282 -1.00914 -1.00655 -1.00474 -1.00348  
-1.00260 -1.00200

168 (dLV/dLT)p 1.2871 1.1995 1.1388 1.0972 1.0688 1.0496  
1.0367 1.0286

169 Cp, KJ/(KG)(K) 3.0365 2.4978 2.1313 1.8860 1.7234 1.6174  
1.5513 1.5157

170 GAMMAS 1.2257 1.2529 1.2797 1.3038 1.3236 1.3387  
1.3487 1.3537

171 SON VEL ,M/SEC 1330.7 1366.7 1401.3 1433.6 1463.0 1489.2  
1512.4 1532.5

172

173 MOLE FRACTIONS

174

175 \*C 0.00000 0.00000 0.00000 0.00001 0.00001 0.00003  
0.00005 0.00010

176 \*CO 0.50515 0.50362 0.50256 0.50182 0.50130 0.50092  
0.50062 0.50037

177 \*CO2 0.00485 0.00328 0.00225 0.00157 0.00111 0.00080  
0.00058 0.00043

178 \*O 0.47485 0.48258 0.48782 0.49139 0.49384 0.49554  
0.49674 0.49761

179 \*O2 0.01515 0.01052 0.00737 0.00522 0.00374 0.00272  
0.00200 0.00149

180

181 \* THERMODYNAMIC PROPERTIES FITTED TO 20000.K

182

183 PRODUCTS WHICH WERE CONSIDERED BUT WHOSE MOLE FRACTIONS

184 WERE LESS THAN 5.000000E-06 FOR ALL ASSIGNED CONDITIONS

185

186 \*C2 C20 \*C3 C302 \*C4

187 \*C5 O3 C(gr)

188

189 NOTE. WEIGHT FRACTION OF FUEL IN TOTAL FUELS AND OF OXIDANT IN TOTAL  
OXIDANTS

190

191

192

193

194

195

196 POINT ITN T C O

---

197  
 198  
 199  
 200  
 201                    THERMODYNAMIC EQUILIBRIUM PROPERTIES AT ASSIGNED  
 202  
 203                    TEMPERATURE AND PRESSURE  
 204  
 205 CASE = -----  
 206  
 207                    REACTANT                    WT FRACTION            ENERGY            TEMP  
 208    (SEE NOTE)            KJ/KG-MOL            K  
 209 FUEL            CO2                            1.0000000            0.000  
       0.000  
 210 OXIDANT        CO2                            1.0000000            0.000  
       0.000  
 211  
 212 O/F=        1.00000    %FUEL= 50.000000    R,EQ.RATIO= 1.000000    PHI,EQ.RATIO=  
       0.000000  
 213  
 214                    THERMODYNAMIC PROPERTIES  
 215  
 216 P, BAR            0.10000    0.10000    0.10000    0.10000    0.10000  
 217 T, K              4700.00    4800.00    4900.00    5000.00    5100.00  
 218 RHO, KG/CU M    5.6380-3   5.5178-3   5.4024-3   5.2910-3   5.1828-3  
 219 H, KJ/KG          8810.94    8962.30    9117.19    9279.61    9455.08  
 220 U, KJ/KG          7037.25    7149.97    7266.15    7389.61    7525.64  
 221 G, KJ/KG          -50924.9   -52197.4   -53473.2   -54752.2   -56034.5  
 222 S, KJ/(KG)(K)    12.7097    12.7416    12.7735    12.8064    12.8411  
 223  
 224 M, (1/n)        22.032    22.021    22.010    21.996    21.977  
 225 (dLV/dLP)t     -1.00162   -1.00143   -1.00144   -1.00169   -1.00226  
 226 (dLV/dLT)p     1.0243    1.0237    1.0271    1.0359    1.0520  
 227 Cp, KJ/(KG)(K) 1.5067    1.5256    1.5788    1.6786    1.8440  
 228 GAMMAS           1.3535    1.3475    1.3351    1.3157    1.2900  
 229 SON VEL,M/SEC   1549.4    1562.7    1572.0    1576.9    1577.6  
 230  
 231 MOLE FRACTIONS  
 232  
 233 \*C                0.00019    0.00035    0.00061    0.00105    0.00176  
 234 \*CO              0.50011    0.49978    0.49932    0.49861    0.49750  
 235 \*CO2             0.00032    0.00024    0.00019    0.00014    0.00011  
 236 \*O               0.49826    0.49877    0.49923    0.49969    0.50022  
 237 \*O2              0.00112    0.00085    0.00066    0.00051    0.00040  
 238  
 239 \* THERMODYNAMIC PROPERTIES FITTED TO 20000.K  
 240  
 241 PRODUCTS WHICH WERE CONSIDERED BUT WHOSE MOLE FRACTIONS

---

## APPENDIX A. CEARUN FILES FOR CO<sub>2</sub>

---

```
242      WERE LESS THAN 5.000000E-06 FOR ALL ASSIGNED CONDITIONS
243
244 *C2          C20          *C3          C302          *C4
245 *C5          03           C(gr)
246
247 NOTE. WEIGHT FRACTION OF FUEL IN TOTAL FUELS AND OF OXIDANT IN TOTAL
       OXIDANTS
```

### A.3. 5200 - 6100 K

```
1 ****
2
3      NASA-GLENN CHEMICAL EQUILIBRIUM PROGRAM CEA2 , FEBRUARY 5, 2004
4          BY BONNIE MCBRIDE AND SANFORD GORDON
5      REFS: NASA RP-1311, PART I, 1994 AND NASA RP-1311, PART II, 1996
6
7 ****
8
9
10
11
12 ### CEA analysis performed on Sun 15-Sep-2024 11:53:02
13
14 # Problem Type: "Assigned Temperature and Pressure"
15
16 prob case=_8923 tp
17
18 # Pressure (1 value):
19 p,bar= 0.1
20 # Temperature (10 values):
21 t,k= 5200, 5300, 5400, 5500, 5600, 5700, 5800, 5900, 6000, 6100
22
23 # You selected the following fuels and oxidizers:
24 reac
25 fuel CO2          wt% =100.0000
26 oxid CO2          wt% =100.0000
27
28 # You selected these options for output:
29 # long version of output
30 # Proportions of any products will be expressed as Mole Fractions.
31 # Heat will be expressed as siunits
32 output siunits
33
34 # Input prepared by this script:/var/www/sites/cearun.grc.nasa.gov/cgi-
   bin/CEARU
```

```

35 N/prepareInputFile.cgi
36
37 ##### IMPORTANT: The following line is the end of your CEA input file!
38 end
39
40 OPTIONS: TP=T HP=F SP=F TV=F UV=F SV=F DETN=F SHOCK=F REFL=F
41 INCD=F
42 RKT=F FROZ=F EQL=F IONS=F SIUNIT=T DEBUGF=F SHKDBG=F DETDBG=F
43 TRNSPT=F
44
45 T,K = 5200.0000 5300.0000 5400.0000 5500.0000 5600.0000 5700.0000
46 5800.0000
47
48 T,K = 5900.0000 6000.0000 6100.0000
49
50
51      REACTANT          WT.FRAC   (ENERGY/R),K    TEMP,K  DENSITY
52      EXPLODED FORMULA
53 F: CO2           1.000000  0.000000E+00     0.00  0.0000
54             C 1.000000  0  2.00000
55 O: CO2           1.000000  0.000000E+00     0.00  0.0000
56             C 1.000000  0  2.00000
57
58      SPECIES BEING CONSIDERED IN THIS SYSTEM
59 (CONDENSED PHASE MAY HAVE NAME LISTED SEVERAL TIMES)
60 LAST thermo.inp UPDATE: 9/09/04
61
62 g 7/97 *C          tpis79 *CO          g 9/99 *CO2
63 tpis91 *C2          g 8/00 C2O        tpis79 *C3
64 g 7/88 C3O2         g tpis *C4        g 8/00 *C5
65 g 5/97 *O           tpis89 *O2        g 8/01 O3
66 n 4/83 C(gr)       n 4/83 C(gr)      n 4/83 C(gr)
67
68 O/F = 1.000000
69
70          EFFECTIVE FUEL      EFFECTIVE OXIDANT      MIXTURE
71 ENTHALPY          h(2)/R        h(1)/R        h0/R
72 (KG-MOL)(K)/KG  0.00000000E+00  0.00000000E+00  0.00000000E
73 +00
74 KG-FORM.WT./KG    bi(2)        bi(1)        b0i
75 *C               0.22722367E-01  0.22722367E-01  0.22722367E
76 -01
77 *O               0.45444734E-01  0.45444734E-01  0.45444734E
78 -01

```

---

## APPENDIX A. CEARUN FILES FOR CO<sub>2</sub>

---

77  
78 POINT ITN T C O  
79  
80  
81  
82  
83                   THERMODYNAMIC EQUILIBRIUM PROPERTIES AT ASSIGNED  
84  
85                   TEMPERATURE AND PRESSURE  
86  
87 CASE = -----  
88  
89                   REACTANT                   WT FRACTION           ENERGY           TEMP  
90   (SEE NOTE)           KJ/KG-MOL           K  
91 FUEL           CO2                           1.0000000           0.000  
0.000  
92 OXIDANT       CO2                           1.0000000           0.000  
0.000  
93  
94 O/F=       1.00000   %FUEL= 50.000000   R,EQ.RATIO= 1.000000   PHI,EQ.RATIO=  
0.000000  
95  
96 THERMODYNAMIC PROPERTIES  
97  
98 P, BAR           0.10000   0.10000   0.10000   0.10000   0.10000   0.10000  
0.10000   0.10000  
99 T, K           5200.00   5300.00   5400.00   5500.00   5600.00   5700.00  
5800.00   5900.00  
100 RHO, KG/CU M   5.0768-3 4.9718-3 4.8662-3 4.7583-3 4.6459-3 4.5269-3  
4.3992-3 4.2615-3  
101 H, KJ/KG       9651.50   9879.99   10155.9   10499.8   10937.7   11501.1  
12224.4   13141.1  
102 U, KJ/KG       7681.78   7868.65   8100.92   8398.17   8785.30   9292.10  
9951.26   10794.5  
103 G, KJ/KG       -57320.5 -58610.5 -59905.3 -61205.8 -62513.3 -63829.7  
-65157.4 -66499.1  
104 S, KJ/(KG)(K)   12.8792   12.9227   12.9743   13.0374   13.1163   13.2159  
13.3417   13.4983  
105  
106 M, (1/n)       21.950   21.909   21.849   21.760   21.632   21.454  
21.215   20.905  
107 (dLV/dLP)t     -1.00327 -1.00492 -1.00745 -1.01118 -1.01642 -1.02347  
-1.03243 -1.04313  
108 (dLV/dLT)p     1.0785   1.1196   1.1810   1.2690   1.3901   1.5493  
1.7474   1.9786  
109 Cp, KJ/(KG)(K)   2.1028   2.4923   3.0600   3.8609   4.9510   6.3749  
8.1475   10.2326  
110 GAMMAS        1.2598   1.2284   1.1990   1.1740   1.1542   1.1395

---

1.1292 1.1224  
111 SON VEL , M/SEC 1575.3 1571.9 1569.7 1570.7 1576.2 1586.6  
1602.2 1622.9  
112  
113 MOLE FRACTIONS  
114  
115 \*C 0.00290 0.00467 0.00736 0.01135 0.01711 0.02516  
0.03600 0.05006  
116 \*CO 0.49577 0.49309 0.48903 0.48303 0.47437 0.46229  
0.44600 0.42490  
117 \*CO2 0.00009 0.00007 0.00006 0.00005 0.00004 0.00003  
0.00002 0.00002  
118 \*C2 0.00000 0.00000 0.00000 0.00000 0.00000 0.00001  
0.00001 0.00002  
119 \*O 0.50093 0.50192 0.50334 0.50540 0.50833 0.51240  
0.51786 0.52492  
120 \*O2 0.00032 0.00025 0.00021 0.00017 0.00014 0.00012  
0.00010 0.00008  
121  
122 \* THERMODYNAMIC PROPERTIES FITTED TO 20000.K  
123  
124 PRODUCTS WHICH WERE CONSIDERED BUT WHOSE MOLE FRACTIONS  
125 WERE LESS THAN 5.000000E-06 FOR ALL ASSIGNED CONDITIONS  
126  
127 C20 \*C3 C302 \*C4 \*C5  
128 O3 C(gr)  
129  
130 NOTE. WEIGHT FRACTION OF FUEL IN TOTAL FUELS AND OF OXIDANT IN TOTAL  
OXIDANTS  
131  
132  
133  
134  
135  
136  
137 POINT ITN T C O  
138  
139  
140  
141  
142 THERMODYNAMIC EQUILIBRIUM PROPERTIES AT ASSIGNED  
143 TEMPERATURE AND PRESSURE  
144  
145  
146 CASE = -----  
147  
148 REACTANT WT FRACTION ENERGY TEMP  
149 (SEE NOTE) KJ/KG-MOL K

---

## APPENDIX A. CEARUN FILES FOR CO<sub>2</sub>

---

150 FUEL CO2 1.0000000 0.000  
0.000

151 OXIDANT CO2 1.0000000 0.000  
0.000

152

153 O/F= 1.00000 %FUEL= 50.000000 R,EQ.RATIO= 1.000000 PHI,EQ.RATIO= 0.000000

154

155 THERMODYNAMIC PROPERTIES

156

157 P, BAR 0.10000 0.10000

158 T, K 6000.00 6100.00

159 RHO, KG/CU M 4.1136-3 3.9566-3

160 H, KJ/KG 14278.0 15648.3

161 U, KJ/KG 11847.0 13120.9

162 G, KJ/KG -67858.2 -69238.1

163 S, KJ/(KG)(K) 13.6894 13.9158

164

165 M, (1/n) 20.521 20.067

166 (dLV/dLP)t -1.05502 -1.06714

167 (dLV/dLT)p 2.2288 2.4761

168 Cp, KJ/(KG)(K) 12.5286 14.8662

169 GAMMAS 1.1181 1.1157

170 SON VEL,M/SEC 1648.7 1679.3

171

172 MOLE FRACTIONS

173

174 \*C 0.06747 0.08808

175 \*CO 0.39875 0.36781

176 \*CO2 0.00002 0.00001

177 \*C2 0.00003 0.00004

178 \*O 0.53366 0.54399

179 \*O2 0.00007 0.00006

180

181 \* THERMODYNAMIC PROPERTIES FITTED TO 20000.K

182

183 PRODUCTS WHICH WERE CONSIDERED BUT WHOSE MOLE FRACTIONS

184 WERE LESS THAN 5.000000E-06 FOR ALL ASSIGNED CONDITIONS

185

186 C20 \*C3 C302 \*C4 \*C5

187 O3 C(gr)

188

189 NOTE. WEIGHT FRACTION OF FUEL IN TOTAL FUELS AND OF OXIDANT IN TOTAL OXIDANTS

## B. CO<sub>2</sub> Dissociation Models

### B.1. den Harder Model

Neutral reactions, published in den Harder et al. [13], original model from Butylkin et al. [32]. Reactions 9, 10, 11 deviate from den Harder et al. [13] as explained in section 3.2. A table with the published values for reactions 9, 10 and 11 is given in table 3.1.

Table B.1. Reactions of CO<sub>2</sub>, CO, O<sub>2</sub> and O. With the pre-exponential factor and activation energies from [13, 32]. The pre-exponential factors are given in  $\frac{m^3}{s}$  for two-body reactions and in  $\frac{m^6}{s}$  for three-body reactions.

Index	Reaction	$k_0$	$E_a$ (eV)
1	CO <sub>2</sub> + CO <sub>2</sub> → CO + O + CO <sub>2</sub>	$4.38 \times 10^{-13}$	5.58
2	CO <sub>2</sub> + CO → CO + O + CO	$4.38 \times 10^{-13}$	5.58
3	CO <sub>2</sub> + O <sub>2</sub> → CO + O + O <sub>2</sub>	$3.72 \times 10^{-16}$	5.19
4	CO <sub>2</sub> + O → CO + O <sub>2</sub>	$7.77 \times 10^{-18}$	1.57
5	O <sub>2</sub> + O <sub>2</sub> → O + O + O <sub>2</sub>	$8.14 \times 10^{-15}$	5.14
6	O <sub>2</sub> + O → O + O + O	$1.99 \times 10^{-14}$	4.99
7	O <sub>2</sub> + CO → O + O + CO	$2.41 \times 10^{-15}$	5.12
8	O <sub>2</sub> + CO <sub>2</sub> → O + O + CO <sub>2</sub>	$2.57 \times 10^{-15}$	5.14
9	CO + O + CO <sub>2</sub> → CO <sub>2</sub> + CO <sub>2</sub>	$6.54 \times 10^{-45}$	0.19
10	CO + O + CO → CO <sub>2</sub> + CO	$6.54 \times 10^{-45}$	0.19
11	CO + O + O <sub>2</sub> → CO <sub>2</sub> + O <sub>2</sub>	$6.51 \times 10^{-48}$	-0.16
12	CO + O <sub>2</sub> → CO <sub>2</sub> + O	$1.23 \times 10^{-18}$	1.32
13	O + O + O <sub>2</sub> → O <sub>2</sub> + O <sub>2</sub>	$6.81 \times 10^{-46}$	0.00
14	O + O + O → O <sub>2</sub> + O	$2.19 \times 10^{-45}$	-0.20
15	O + O + CO → O <sub>2</sub> + CO	$2.76 \times 10^{-46}$	0.00
16	O + O + CO <sub>2</sub> → O <sub>2</sub> + CO <sub>2</sub>	$2.76 \times 10^{-46}$	0.00

## B.2. Koelman Model

Neutral reactions, published in Koelman et al. [31]. The reaction 4 was split into 3 reactions in the python implementation, in the following table the reactions are given as implemented.

Table B.2. Neutral neutral reactions with rate coefficients. The unit of the rate coefficients is  $\frac{m^3}{s}$  for two-body reactions and in  $\frac{m^6}{s}$  for three-body reactions.

No.	Reaction	Rate Coefficient
N1	$CO_2 + M \rightarrow CO + O + M$	$1.81 \times 10^{-16} \exp(-49000/T_g)$
N2	$CO_2 + O \rightarrow CO + O_2$	$2.8 \times 10^{-17} \exp(-26500/T_g)$
N3	$CO_2 + C \rightarrow CO + CO$	$\leq 1.0 \times 10^{-21}$
N4 <sub>CO<sub>2</sub></sub>	$O + CO + CO_2 \rightarrow CO_2 + CO_2$	$8.2 \times 10^{-46} \exp(-1510/T_g) \cdot 2$
N4 <sub>O<sub>2</sub></sub>	$O + CO + O_2 \rightarrow CO_2 + O_2$	$8.2 \times 10^{-46} \exp(-1510/T_g) \cdot 1$
N4 <sub>CO</sub>	$O + CO + CO \rightarrow CO_2 + CO$	$8.2 \times 10^{-46} \exp(-1510/T_g) \cdot 1$
N5	$O_2 + CO \rightarrow CO_2 + O$	$4.2 \times 10^{-18} \exp(-24000/T_g)$
N6	$O_3 + CO \rightarrow CO_2 + O_2$	$\leq 4.0 \times 10^{-31}$
N7	$C + CO + M \rightarrow C_2O + M$	$6.31 \times 10^{-44}$
N8	$O_2 + C \rightarrow CO + O$	$3.0 \times 10^{-17}$
N9	$O + C + M \rightarrow CO + M$	$2.14 \times 10^{-41} (T_g/300)^{-3.08} \exp(-2114/T_g)$
N10	$O + C_2O \rightarrow CO + CO$	$9.51 \times 10^{-17}$
N11	$O_2 + C_2O \rightarrow CO_2 + CO$	$3.3 \times 10^{-19}$
N12	$O + O_3 \rightarrow O_2 + O_2$	$8.0 \times 10^{-18} \exp(-2056/T_g)$
N13	$O_3 + M \rightarrow O_2 + O + M$	$4.12 \times 10^{-16} \exp(-11430/T_g)$
N14	$O + O_2 + M \rightarrow O_3 + M$	$5.51 \times 10^{-46} (T_g/298)^{-2.6}$
N15	$O + O + M \rightarrow O_2 + M$	$5.2 \times 10^{-47} \exp(900/T_g)$

### B.3. Combined den Harder/Beuthe Model

table B.4 contains the combined model from den Harder et al. [13] with the carbon reactions from Beuthe et al. [35] which are also given in table B.3.

Table B.3. Reactions from Beuthe et al. [35] involving C. These reactions are implemented into the pressure based model. With argon as M (see section 3.4 for more details). The unit of the reaction rate constants is  $\frac{\text{cm}^3}{\text{s}}$  for two-body reactions and in  $\frac{\text{cm}^6}{\text{s}}$  for three-body reactions.  $T_g$  is the gas temperature.

Index	Reaction	Reaction rate constants
C1	$\text{CO} + \text{M} \rightarrow \text{C} + \text{O} + \text{M}$	$1.46 \times 10^6 \cdot T_g^{-3.52} \exp(-128700/T_g)$
C2	$\text{CO}_2 + \text{C} \rightarrow \text{CO} + \text{CO}$	$1.0 \times 10^{-15}$
C3	$\text{C} + \text{O} + \text{M} \rightarrow \text{CO} + \text{M}$	$9.1 \times 10^{-22} \cdot T_g^{-3.08} \exp(2114/T_g)$

The reaction rate constants were split into the pre-exponential factor and the activation energy. The activation energy was calculated from the temperature in the exponent as

$$E = k_B \cdot T \quad (\text{B.1})$$

Calculations were performed with the full accuracy of the energy. The pre-exponential factor was converted from  $\text{cm}^3/\text{s}$  to  $\text{m}^3/\text{s}$ , and respectively from  $\text{cm}^6/\text{s}$  to  $\text{m}^6/\text{s}$ .

Table B.4. Combined den Harder/Beuthe model. The pre-exponential factors are given in  $\frac{\text{m}^3}{\text{s}}$  for two-body reactions and in  $\frac{\text{m}^6}{\text{s}}$  for three-body reactions. With the gas temperature  $T_g$ .

Index	Reaction	$k_0$	$E_a(\text{eV})$
1	$\text{CO}_2 + \text{CO}_2 \rightarrow \text{CO} + \text{O} + \text{CO}_2$	$4.38 \times 10^{-13}$	5.58
2	$\text{CO}_2 + \text{CO} \rightarrow \text{CO} + \text{O} + \text{CO}$	$4.38 \times 10^{-13}$	5.58
3	$\text{CO}_2 + \text{O}_2 \rightarrow \text{CO} + \text{O} + \text{O}_2$	$3.72 \times 10^{-16}$	5.19
4	$\text{CO}_2 + \text{O} \rightarrow \text{CO} + \text{O}_2$	$7.77 \times 10^{-18}$	1.57
5	$\text{O}_2 + \text{O}_2 \rightarrow \text{O} + \text{O} + \text{O}_2$	$8.14 \times 10^{-15}$	5.14
6	$\text{O}_2 + \text{O} \rightarrow \text{O} + \text{O} + \text{O}$	$1.99 \times 10^{-14}$	4.99
7	$\text{O}_2 + \text{CO} \rightarrow \text{O} + \text{O} + \text{CO}$	$2.41 \times 10^{-15}$	5.12
8	$\text{O}_2 + \text{CO}_2 \rightarrow \text{O} + \text{O} + \text{CO}_2$	$2.57 \times 10^{-15}$	5.14
9	$\text{CO} + \text{O} + \text{CO}_2 \rightarrow \text{CO}_2 + \text{CO}_2$	$6.54 \times 10^{-45}$	0.19
10	$\text{CO} + \text{O} + \text{CO} \rightarrow \text{CO}_2 + \text{CO}$	$6.54 \times 10^{-45}$	0.19
11	$\text{CO} + \text{O} + \text{O}_2 \rightarrow \text{CO}_2 + \text{O}_2$	$6.51 \times 10^{-48}$	-0.16
12	$\text{CO} + \text{O}_2 \rightarrow \text{CO}_2 + \text{O}$	$1.23 \times 10^{-18}$	1.32
13	$\text{O} + \text{O} + \text{O}_2 \rightarrow \text{O}_2 + \text{O}_2$	$6.81 \times 10^{-46}$	0.00
14	$\text{O} + \text{O} + \text{O} \rightarrow \text{O}_2 + \text{O}$	$2.19 \times 10^{-45}$	-0.20
15	$\text{O} + \text{O} + \text{CO} \rightarrow \text{O}_2 + \text{CO}$	$2.76 \times 10^{-46}$	0.00
16	$\text{O} + \text{O} + \text{CO}_2 \rightarrow \text{O}_2 + \text{CO}_2$	$2.76 \times 10^{-46}$	0.00
C1	$\text{CO} + \text{M} \rightarrow \text{C} + \text{O} + \text{M}$	$1.46 \cdot T_g^{-3.52}$	-11.09
C2	$\text{CO}_2 + \text{C} \rightarrow \text{CO} + \text{CO}$	$1.0 \times 10^{-21}$	n/a
C3	$\text{C} + \text{O} + \text{M} \rightarrow \text{CO} + \text{M}$	$9.1 \times 10^{-28} \cdot T_g^{-3.08}$	0.18

## C. CEARUN files for H<sub>2</sub>O

In the following the output files from CEARUN are shown. An issue with the current implementation of CEARUN leads to the fact that only 21 input temperatures can be used. This bug is reported to NASA already.

### C.1. 1000 - 3000 K

```
1 ****
2
3      NASA-GLENN CHEMICAL EQUILIBRIUM PROGRAM CEA2, FEBRUARY 5, 2004
4          BY BONNIE MCBRIDE AND SANFORD GORDON
5      REFS: NASA RP-1311, PART I, 1994 AND NASA RP-1311, PART II, 1996
6
7 ****
8
9
10
11
12 ### CEA analysis performed on Thu 19-Sep-2024 14:59:56
13
14 # Problem Type: "Assigned Temperature and Pressure"
15
16 prob case=-----3194 tp
17
18 # Pressure (1 value):
19 p,bar= 1
20 # Temperature (21 values):
21 t,k= 1000, 1100, 1200, 1300, 1400, 1500, 1600, 1700, 1800, 1900, 2000,
22   2100, 220
23 0, 2300, 2400, 2500, 2600, 2700, 2800, 2900, 3000
24
25 # You selected the following fuels and oxidizers:
26 reac
27 fuel H2O           wt% = 100.0000
28 oxid H2O           wt% = 100.0000
29
30 # You selected these options for output:
31 # short version of output
32 output short
```

---

## APPENDIX C. CEARUN FILES FOR $H_2O$

---

```
32 # Proportions of any products will be expressed as Mole Fractions.
33 # Heat will be expressed as siunits
34 output siunits
35
36 # Input prepared by this script:/var/www/sites/cearun.grc.nasa.gov/cgi-
37 bin/CEARU
38 N/prepareInputFile.cgi
39
40 ##### IMPORTANT: The following line is the end of your CEA input file!
41 end
42
43
44
45             THERMODYNAMIC EQUILIBRIUM PROPERTIES AT ASSIGNED
46
47             TEMPERATURE AND PRESSURE
48
49 CASE = -----
50
51             REACTANT          WT FRACTION      ENERGY        TEMP
52                               (SEE NOTE)      KJ/KG-MOL      K
53 FUEL       H2O           1.0000000      0.000
54
55             0.000
56 OXIDANT    H2O           1.0000000      0.000
57
58             0.000
59
60 O/F=      1.00000 %FUEL= 50.000000 R,EQ.RATIO= 1.000000 PHI,EQ.RATIO=
61             0.000000
62
63             THERMODYNAMIC PROPERTIES
64
65             P, BAR          1.0000   1.0000   1.0000   1.0000   1.0000   1.0000
66             1.0000   1.0000
67             T, K           1000.00  1100.00  1200.00  1300.00  1400.00  1500.00
68             1600.00  1700.00
69             RHO, KG/CU M   2.1667-1  1.9698-1  1.8056-1  1.6667-1  1.5476-1  1.4443-1
70             1.3539-1  1.2738-1
71             H, KJ/KG       -11980.0 -11747.2 -11507.3 -11260.2 -11006.0 -10744.4
72             -10474.5 -10194.8
73             U, KJ/KG       -12441.5 -12254.9 -12061.1 -11860.2 -11652.2 -11436.7
74             -11213.1 -10979.8
75             G, KJ/KG       -24898.8 -26201.9 -27526.5 -28871.4 -30235.6 -31618.3
76             -33018.6 -34436.1
77             S, KJ/(KG)(K)  12.9189  13.1407  13.3494  13.5471  13.7355  13.9159
78             14.0901  14.2596
79
```

C.1. 1000 - 3000 K

---

68 M, (1/n) 18.015 18.015 18.015 18.015 18.015 18.015 18.013  
18.011 18.005

69 (dLV/dLP)t -1.00000 -1.00000 -1.00000 -1.00000 -1.00001 -1.00004  
-1.00009 -1.00019

70 (dLV/dLT)p 1.0000 1.0000 1.0001 1.0002 1.0006 1.0015  
1.0034 1.0069

71 Cp, KJ/(KG)(K) 2.2921 2.3634 2.4351 2.5061 2.5783 2.6557  
2.7446 2.8544

72 GAMMAS 1.2521 1.2427 1.2339 1.2258 1.2183 1.2111  
1.2037 1.1959

73 SON VEL ,M/SEC 760.2 794.3 826.7 857.6 887.3 915.7  
942.9 968.9

74

75 MOLE FRACTIONS

76

77 \*H2 0.00000 0.00000 0.00001 0.00003 0.00008 0.00020  
0.00046 0.00098

78 H2O 1.00000 1.00000 0.99999 0.99996 0.99988 0.99967  
0.99922 0.99832

79 \*OH 0.00000 0.00000 0.00000 0.00000 0.00001 0.00004  
0.00012 0.00028

80 \*O2 0.00000 0.00000 0.00000 0.00001 0.00003 0.00009  
0.00020 0.00042

81

82 \* THERMODYNAMIC PROPERTIES FITTED TO 20000.K

83

84 NOTE. WEIGHT FRACTION OF FUEL IN TOTAL FUELS AND OF OXIDANT IN TOTAL  
OXIDANTS

85

86

87

88

89

90

91

92

93

94 THERMODYNAMIC EQUILIBRIUM PROPERTIES AT ASSIGNED

95

96 TEMPERATURE AND PRESSURE

97

98 CASE = -----

99

100 REACTANT WT FRACTION ENERGY TEMP

101 (SEE NOTE) KJ/KG-MOL K

102 FUEL H2O 1.0000000 0.000

0.000

---

APPENDIX C. CEARUN FILES FOR  $H_2O$

---

```

103 OXIDANT      H2O                      1.0000000      0.000
104          0.000
104
105 O/F=      1.00000  %FUEL= 50.000000  R,EQ.RATIO= 1.000000  PHI,EQ.RATIO=
106          0.000000
106
107 THERMODYNAMIC PROPERTIES
108
109 P, BAR        1.0000    1.0000    1.0000    1.0000    1.0000    1.0000
110          1.0000
110 T, K          1800.00   1900.00   2000.00   2100.00   2200.00   2300.00
111          2400.00   2500.00
111 RHO, KG/CU M 1.2024-1  1.1380-1  1.0794-1  1.0255-1  9.7529-2  9.2790-2
112          8.8251-2  8.3837-2
112 H, KJ/KG     -9902.51 -9593.68 -9262.51 -8901.16 -8499.31 -8043.71
113          -7517.63 -6900.27
113 U, KJ/KG     -10734.2 -10472.4 -10188.9 -9876.29 -9524.64 -9121.41
114          -8650.77 -8093.07
114 G, KJ/KG     -35870.5 -37321.4 -38789.3 -40274.3 -41777.5 -43300.1
115          -44844.0 -46411.6
115 S, KJ/(KG)(K) 14.4266  14.5936  14.7634  14.9396  15.1265  15.3289
116          15.5527  15.8045
116
117 M, (1/n)     17.995   17.978   17.950   17.906   17.840   17.745
118          17.610   17.427
118 (dLV/dLP)t  -1.00038 -1.00070 -1.00124 -1.00210 -1.00341 -1.00536
119          -1.00818 -1.01217
119 (dLV/dLT)p  1.0131   1.0232   1.0391   1.0630   1.0977   1.1467
120          1.2141   1.3047
120 Cp, KJ/(KG)(K) 2.9973   3.1887   3.4476   3.7965   4.2625   4.8773
121          5.6788   6.7109
121 GAMMAS      1.1874   1.1781   1.1680   1.1575   1.1472   1.1376
122          1.1291   1.1221
122 SON VEL,M/SEC 993.8    1017.4   1040.2   1062.4   1084.6   1107.2
123          1131.1   1156.9
123
124 MOLE FRACTIONS
125
126 *H           0.00002  0.00005  0.00012  0.00030  0.00068  0.00143
127          0.00282  0.00523
127 H02          0.00000  0.00000  0.00000  0.00000  0.00000  0.00000
128          0.00000  0.00001
128 *H2          0.00190  0.00344  0.00587  0.00951  0.01471  0.02184
129          0.03122  0.04312
129 H2O          0.99666  0.99383  0.98924  0.98216  0.97170  0.95680
130          0.93631  0.90900
130 *O           0.00000  0.00001  0.00003  0.00008  0.00020  0.00045
131          0.00093  0.00181

```

---

C.1. 1000 - 3000 K

---

131 \*OH 0.00062 0.00126 0.00237 0.00420 0.00704 0.01124  
0.01716 0.02516  
132 \*O2 0.00080 0.00141 0.00236 0.00374 0.00566 0.00824  
0.01156 0.01567  
133  
134 \* THERMODYNAMIC PROPERTIES FITTED TO 20000.K  
135  
136 NOTE. WEIGHT FRACTION OF FUEL IN TOTAL FUELS AND OF OXIDANT IN TOTAL  
OXIDANTS  
137  
138  
139  
140  
141  
142  
143  
144  
145  
146 THERMODYNAMIC EQUILIBRIUM PROPERTIES AT ASSIGNED  
147  
148 TEMPERATURE AND PRESSURE  
149  
150 CASE = -----  
151  
152 REACTANT WT FRACTION ENERGY TEMP  
153 (SEE NOTE) KJ/KG-MOL K  
154 FUEL H2O 1.0000000 0.000  
0.000  
155 OXIDANT H2O 1.0000000 0.000  
0.000  
156  
157 O/F= 1.00000 %FUEL= 50.000000 R,EQ.RATIO= 1.000000 PHI,EQ.RATIO= 0.000000  
158  
159 THERMODYNAMIC PROPERTIES  
160  
161 P, BAR 1.0000 1.0000 1.0000 1.0000 1.0000  
162 T, K 2600.00 2700.00 2800.00 2900.00 3000.00  
163 RHO, KG/CU M 7.9478-2 7.5114-2 7.0692-2 6.6179-2 6.1560-2  
164 H, KJ/KG -6166.09 -5284.13 -4217.42 -2922.63 -1350.22  
165 U, KJ/KG -7424.29 -6615.44 -5632.01 -4433.69 -2974.65  
166 G, KJ/KG -48006.1 -49631.6 -51293.0 -52996.3 -54748.9  
167 S, KJ/(KG)(K) 16.0923 16.4250 16.8127 17.2668 17.7996  
168  
169 M, (1/n) 17.181 16.862 16.458 15.957 15.355  
170 (dLV/dLP)t -1.01768 -1.02510 -1.03486 -1.04734 -1.06283  
171 (dLV/dLT)p 1.4237 1.5765 1.7678 2.0008 2.2757  
172 Cp, KJ/(KG)(K) 8.0243 9.6765 11.7299 14.2487 17.2907

---

APPENDIX C. CEARUN FILES FOR  $H_2O$

---

```
173 GAMMAS          1.1168   1.1130   1.1108   1.1099   1.1103
174 SON VEL ,M/SEC  1185.4    1217.3   1253.5   1295.1    1343.0
175
176 MOLE FRACTIONS
177
178 *H              0.00923   0.01555   0.02509   0.03890   0.05805
179 H02             0.00001   0.00001   0.00002   0.00003   0.00003
180 *H2             0.05764   0.07466   0.09375   0.11416   0.13471
181 H20             0.87369   0.82939   0.77543   0.71175   0.63906
182 *O              0.00334   0.00584   0.00976   0.01563   0.02402
183 *OH             0.03551   0.04835   0.06358   0.08075   0.09907
184 *O2             0.02057   0.02619   0.03236   0.03878   0.04506
185
186 * THERMODYNAMIC PROPERTIES FITTED TO 20000.K
187
188 NOTE. WEIGHT FRACTION OF FUEL IN TOTAL FUELS AND OF OXIDANT IN TOTAL
       OXIDANTS
189
```

## C.2. 3100 - 5100 K

```
1 ****
2
3 NASA-GLENN CHEMICAL EQUILIBRIUM PROGRAM CEA2, FEBRUARY 5, 2004
4 BY BONNIE MCBRIDE AND SANFORD GORDON
5 REFS: NASA RP-1311, PART I, 1994 AND NASA RP-1311, PART II, 1996
6
7 ****
8
9
10
11
12 ### CEA analysis performed on Thu 19-Sep-2024 15:02:28
13
14 # Problem Type: "Assigned Temperature and Pressure"
15
16 prob case=-----3194 tp
17
18 # Pressure (1 value):
19 p,bar= 1
20 # Temperature (21 values):
21 t,k= 3100, 3200, 3300, 3400, 3500, 3600, 3700, 3800, 3900, 4000, 4100,
      4200, 430
22 0, 4400, 4500, 4600, 4700, 4800, 4900, 5000, 5100
```

```

23
24 # You selected the following fuels and oxidizers:
25 reac
26 fuel H2O          wt% = 100.0000
27 oxid H2O          wt% = 100.0000
28
29 # You selected these options for output:
30 # short version of output
31 output short
32 # Proportions of any products will be expressed as Mole Fractions.
33 # Heat will be expressed as siunits
34 output siunits
35
36 # Input prepared by this script:/var/www/sites/cearun.grc.nasa.gov/cgi-
   bin/CEARU
37 N/prepareInputFile.cgi
38
39 ##### IMPORTANT: The following line is the end of your CEA input file!
40 end
41
42
43
44
45          THERMODYNAMIC EQUILIBRIUM PROPERTIES AT ASSIGNED
46
47          TEMPERATURE AND PRESSURE
48
49 CASE = -----
50
51          REACTANT          WT FRACTION      ENERGY      TEMP
52                               (SEE NOTE)      KJ/KG-MOL      K
53 FUEL        H2O           1.00000000      0.000
54
55          0.000
56 OXIDANT     H2O           1.00000000      0.000
57
58          0.000
59
60 O/F=      1.00000 %FUEL= 50.000000 R,EQ.RATIO= 1.000000 PHI,EQ.RATIO=
   0.000000
61
62          THERMODYNAMIC PROPERTIES
63
64          P, BAR          1.0000    1.0000    1.0000    1.0000    1.0000    1.0000
65          1.0000    1.0000
66          T, K           3100.00  3200.00  3300.00  3400.00  3500.00  3600.00
67          3700.00  3800.00
68          RHO, KG/CU M   5.6848-2 5.2088-2 4.7355-2 4.2749-2 3.8387-2 3.4383-2
69          3.0824-2 2.7760-2
70          H, KJ/KG       554.18   2846.25   5575.84   8774.96   12440.6   16516.0

```

---

APPENDIX C. CEARUN FILES FOR  $H_2O$

---

20878.6 25346.8  
64 U, KJ/KG -1204.88 926.43 3464.11 6435.73 9835.61 13607.6  
17634.3 21744.4  
65 G, KJ/KG -56559.3 -58437.1 -60393.2 -62439.1 -64585.9 -66843.5  
-69218.6 -71713.5  
66 S, KJ/(KG)(K) 18.4237 19.1511 19.9906 20.9453 22.0076 23.1554  
24.3506 25.5422  
67  
68 M, (1/n) 14.653 13.859 12.993 12.085 11.171 10.291  
9.482 8.771  
69 (dLV/dLP)t -1.08136 -1.10254 -1.12538 -1.14815 -1.16833 -1.18308  
-1.18987 -1.18747  
70 (dLV/dLT)p 2.5879 2.9254 3.2671 3.5817 3.8300 3.9724  
3.9803 3.8485  
71 Cp, KJ/(KG)(K) 20.8913 25.0351 29.6130 34.3679 38.8530 42.4493  
44.4940 44.5130  
72 GAMMAS 1.1118 1.1143 1.1177 1.1219 1.1270 1.1328  
1.1394 1.1467  
73 SON VEL,M/SEC 1398.5 1462.6 1536.3 1620.0 1713.4 1815.1  
1922.6 2032.5  
74  
75 MOLE FRACTIONS  
76  
77 \*H 0.08352 0.11601 0.15568 0.20194 0.25337 0.30772  
0.36228 0.41428  
78 H02 0.00004 0.00005 0.00005 0.00006 0.00005 0.00005  
0.00004 0.00004  
79 \*H2 0.15388 0.16992 0.18107 0.18588 0.18356 0.17425  
0.15913 0.14011  
80 H20 0.55903 0.47438 0.38874 0.30629 0.23116 0.16671  
0.11484 0.07573  
81 \*O 0.03551 0.05057 0.06944 0.09197 0.11759 0.14525  
0.17354 0.20094  
82 \*OH 0.11730 0.13389 0.14710 0.15529 0.15731 0.15283  
0.14246 0.12771  
83 \*O2 0.05071 0.05517 0.05792 0.05857 0.05695 0.05319  
0.04772 0.04120  
84  
85 \* THERMODYNAMIC PROPERTIES FITTED TO 20000.K  
86  
87 NOTE. WEIGHT FRACTION OF FUEL IN TOTAL FUELS AND OF OXIDANT IN TOTAL  
OXIDANTS  
88  
89  
90  
91  
92  
93

```

94
95
96
97          THERMODYNAMIC EQUILIBRIUM PROPERTIES AT ASSIGNED
98
99          TEMPERATURE AND PRESSURE
100
101 CASE = -----
102
103          REACTANT          WT FRACTION      ENERGY      TEMP
104                               (SEE NOTE)      KJ/KG-MOL      K
105 FUEL        H2O           1.0000000      0.000
106          0.000
107
108 OXIDANT      H2O           1.0000000      0.000
109          0.000
110
111          THERMODYNAMIC PROPERTIES
112
113          P, BAR           1.0000      1.0000      1.0000      1.0000      1.0000
114          1.0000      1.0000
115          T, K             3900.00    4000.00    4100.00    4200.00    4300.00    4400.00
116          4500.00    4600.00
117          RHO, KG/CU M     2.5195-2   2.3092-2   2.1391-2   2.0020-2   1.8911-2   1.8003-2
118          1.7250-2   1.6614-2
119
120          H, KJ/KG         29711.0    33778.8    37414.6    40555.1    43201.4    45397.5
121          47208.2    48702.5
122          U, KJ/KG         25741.9    29448.4    32739.8    35560.1    37913.4    39843.0
123          41411.1    42683.4
124          G, KJ/KG         -74325.1   -77045.2   -79861.9   -82761.3   -85729.6   -88754.1
125          -91824.1   -94930.7
126
127          S, KJ/(KG)(K)    26.6759    27.7060    28.6040    29.3610    29.9840    30.4890
128          30.8961    31.2246
129
130          M, (1/n)        8.170      7.680      7.292      6.991      6.761      6.586
131          6.454      6.354
132          (dLV/dLP)t     -1.17647   -1.15909   -1.13827   -1.11678   -1.09657   -1.07873
133          -1.06363   -1.05120
134
135          (dLV/dLT)p     3.5991     3.2742     2.9212     2.5792     2.2725     2.0120
136          1.7986     1.6280
137
138          Cp, KJ/(KG)(K)  42.4435    38.6846    33.9272    28.8885    24.1147    19.9180
139          16.4122    13.5822
140
141          GAMMAS        1.1549     1.1640     1.1744     1.1863     1.2002     1.2163
142          1.2350     1.2565
143
144          SON VEL,M/SEC   2141.0     2245.2     2343.1     2434.3     2519.2     2599.2
145          2675.7     2750.1

```

---

APPENDIX C. CEARUN FILES FOR  $H_2O$

---

126  
127 MOLE FRACTIONS  
128  
129 \*H 0.46147 0.50246 0.53676 0.56464 0.58681 0.60418  
0.61768 0.62812  
130 H02 0.00003 0.00002 0.00001 0.00001 0.00001 0.00000  
0.00000 0.00000  
131 \*H2 0.11943 0.09909 0.08052 0.06446 0.05113 0.04036  
0.03182 0.02513  
132 H20 0.04804 0.02953 0.01774 0.01051 0.00618 0.00364  
0.00215 0.00129  
133 \*O 0.22613 0.24818 0.26668 0.28167 0.29351 0.30268  
0.30970 0.31504  
134 \*OH 0.11054 0.09289 0.07626 0.06156 0.04915 0.03900  
0.03088 0.02447  
135 \*O2 0.03436 0.02783 0.02203 0.01716 0.01322 0.01013  
0.00776 0.00595  
136  
137 \* THERMODYNAMIC PROPERTIES FITTED TO 20000.K  
138  
139 NOTE. WEIGHT FRACTION OF FUEL IN TOTAL FUELS AND OF OXIDANT IN TOTAL  
OXIDANTS  
140  
141  
142  
143  
144  
145  
146  
147  
148  
149 THERMODYNAMIC EQUILIBRIUM PROPERTIES AT ASSIGNED  
150  
151 TEMPERATURE AND PRESSURE  
152  
153 CASE = -----  
154  
155 REACTANT WT FRACTION ENERGY TEMP  
156 (SEE NOTE) KJ/KG-MOL K  
157 FUEL H20 1.0000000 0.000  
0.000  
158 OXIDANT H20 1.0000000 0.000  
0.000  
159  
160 O/F= 1.00000 %FUEL= 50.000000 R,EQ.RATIO= 1.000000 PHI,EQ.RATIO=  
0.000000  
161  
162 THERMODYNAMIC PROPERTIES

---

163  
164 P, BAR 1.0000 1.0000 1.0000 1.0000 1.0000  
165 T, K 4700.00 4800.00 4900.00 5000.00 5100.00  
166 RHO, KG/CU M 1.6066-2 1.5587-2 1.5160-2 1.4774-2 1.4422-2  
167 H, KJ/KG 49944.5 50988.8 51879.8 52652.8 53335.0  
168 U, KJ/KG 43720.2 44573.0 45283.4 45884.3 46401.2  
169 G, KJ/KG -98067.0-101227.5-104408.1-107605.7-110817.8  
170 S, KJ/(KG)(K) 31.4918 31.7117 31.8955 32.0517 32.1868  
171  
172 M, (1/n) 6.278 6.221 6.176 6.142 6.116  
173 (dLV/dLP)t -1.04116 -1.03312 -1.02673 -1.02167 -1.01764  
174 (dLV/dLT)p 1.4937 1.3888 1.3073 1.2440 1.1948  
175 Cp, KJ/(KG)(K) 11.3488 9.6105 8.2685 7.2361 6.4424  
176 GAMMAS 1.2807 1.3074 1.3361 1.3658 1.3959  
177 SON VEL ,M/SEC 2823.4 2896.2 2968.7 3040.5 3111.1  
178  
179 MOLE FRACTIONS  
180  
181 \*H 0.63618 0.64241 0.64725 0.65102 0.65397  
182 \*H2 0.01991 0.01585 0.01269 0.01022 0.00828  
183 H2O 0.00078 0.00048 0.00030 0.00019 0.00012  
184 \*O 0.31910 0.32219 0.32455 0.32635 0.32775  
185 \*OH 0.01945 0.01552 0.01245 0.01005 0.00816  
186 \*O2 0.00459 0.00355 0.00277 0.00217 0.00172  
187  
188 \* THERMODYNAMIC PROPERTIES FITTED TO 20000.K  
189  
190 NOTE. WEIGHT FRACTION OF FUEL IN TOTAL FUELS AND OF OXIDANT IN TOTAL  
OXIDANTS

## C.3. 5200 - 6100 K

1 \*\*\*\*=  
2  
3 NASA-GLENN CHEMICAL EQUILIBRIUM PROGRAM CEA2, FEBRUARY 5, 2004  
4 BY BONNIE MCBRIDE AND SANFORD GORDON  
5 REFS: NASA RP-1311, PART I, 1994 AND NASA RP-1311, PART II, 1996  
6  
7 \*\*\*\*=  
8  
9  
10  
11  
12 ### CEA analysis performed on Thu 19-Sep-2024 15:03:06  
13

---

## APPENDIX C. CEARUN FILES FOR $H_2O$

---

```
14 # Problem Type: "Assigned Temperature and Pressure"
15
16 prob case=-----3194 tp
17
18 # Pressure (1 value):
19 p,bar= 1
20 # Temperature (12 values):
21 t,k= 5200, 5300, 5400, 5500, 5600, 5700, 5800, 5900, 6000, 6100, 6200,
   6300
22
23 # You selected the following fuels and oxidizers:
24 reac
25 fuel H2O           wt% = 100.0000
26 oxid H2O           wt% = 100.0000
27
28 # You selected these options for output:
29 # short version of output
30 output short
31 # Proportions of any products will be expressed as Mole Fractions.
32 # Heat will be expressed as siunits
33 output siunits
34
35 # Input prepared by this script:/var/www/sites/cearun.grc.nasa.gov/cgi-
   bin/CEARU
36 N/prepareInputFile.cgi
37
38 ##### IMPORTANT: The following line is the end of your CEA input file!
39 end
40
41
42
43
44          THERMODYNAMIC EQUILIBRIUM PROPERTIES AT ASSIGNED
45
46          TEMPERATURE AND PRESSURE
47
48 CASE = -----
49
50          REACTANT          WT FRACTION      ENERGY      TEMP
51                      (SEE NOTE)      KJ/KG-MOL      K
52 FUEL        H2O            1.0000000      0.000
53 OXIDANT     H2O            1.0000000      0.000
54
55 O/F=      1.00000  %FUEL= 50.000000  R,EQ.RATIO= 1.000000  PHI,EQ.RATIO=
   0.000000
56
```

C.3. 5200 - 6100 K

---

57 THERMODYNAMIC PROPERTIES  
 58  
 59 P, BAR 1.0000 1.0000 1.0000 1.0000 1.0000 1.0000 1.0000  
     1.0000 1.0000  
 60 T, K 5200.00 5300.00 5400.00 5500.00 5600.00 5700.00  
     5800.00 5900.00  
 61 RHO, KG/CU M 1.4097-2 1.3794-2 1.3510-2 1.3241-2 1.2987-2 1.2745-2  
     1.2514-2 1.2293-2  
 62 H, KJ/KG 53947.4 54505.9 55022.8 55507.4 55966.7 56406.2  
     56830.2 57241.8  
 63 U, KJ/KG 46853.6 47256.3 47620.7 47955.3 48266.8 48560.1  
     48839.1 49106.9  
 64 G, KJ/KG -114042.5-117278.5-120524.6-123780.0-127044.0-130316.0-133595.5-136882.2  
  
 65 S, KJ/(KG)(K) 32.3057 32.4122 32.5088 32.5977 32.6805 32.7583  
     32.8320 32.9024  
 66  
 67 M, (1/n) 6.095 6.079 6.066 6.055 6.047 6.040  
     6.035 6.030  
 68 (dLV/dLP)t -1.01444 -1.01189 -1.00984 -1.00819 -1.00686 -1.00577  
     -1.00489 -1.00416  
 69 (dLV/dLT)p 1.1564 1.1263 1.1026 1.0839 1.0689 1.0570  
     1.0474 1.0397  
 70 Cp, KJ/(KG)(K) 5.8314 5.3596 4.9939 4.7092 4.4864 4.3113  
     4.1729 4.0629  
 71 GAMMAS 1.4253 1.4532 1.4790 1.5023 1.5228 1.5407  
     1.5560 1.5690  
 72 SON VEL ,M/SEC 3179.7 3245.8 3308.7 3368.3 3424.3 3476.9  
     3526.2 3572.6  
 73  
 74 MOLE FRACTIONS  
 75  
 76 \*H 0.65630 0.65814 0.65961 0.66080 0.66175 0.66252  
     0.66316 0.66368  
 77 \*H2 0.00676 0.00555 0.00458 0.00381 0.00319 0.00268  
     0.00227 0.00193  
 78 H2O 0.00008 0.00005 0.00003 0.00002 0.00002 0.00001  
     0.00001 0.00001  
 79 \*O 0.32883 0.32968 0.33034 0.33087 0.33129 0.33163  
     0.33191 0.33213  
 80 \*OH 0.00667 0.00548 0.00454 0.00378 0.00316 0.00266  
     0.00225 0.00192  
 81 \*O2 0.00137 0.00110 0.00089 0.00072 0.00059 0.00049  
     0.00041 0.00034  
 82  
 83 \* THERMODYNAMIC PROPERTIES FITTED TO 20000.K  
 84

---

## APPENDIX C. CEARUN FILES FOR H<sub>2</sub>O

---

85 NOTE. WEIGHT FRACTION OF FUEL IN TOTAL FUELS AND OF OXIDANT IN TOTAL  
OXIDANTS

86

87

88

89

90

91

92

93

94

95 THERMODYNAMIC EQUILIBRIUM PROPERTIES AT ASSIGNED

96

97 TEMPERATURE AND PRESSURE

98

99 CASE = -----

100

	REACTANT	WT FRACTION	ENERGY	TEMP
		(SEE NOTE)	KJ/KG-MOL	K
101	FUEL	H2O	1.0000000	0.000
102		0.000		
103	OXIDANT	H2O	1.0000000	0.000
104		0.000		

105

106 O/F= 1.00000 %FUEL= 50.000000 R,EQ.RATIO= 1.000000 PHI,EQ.RATIO=

0.000000

107

108 THERMODYNAMIC PROPERTIES

109

110	P, BAR	1.0000	1.0000	1.0000	1.0000
111	T, K	6000.00	6100.00	6200.00	6300.00
112	RHO, KG/CU M	1.2081-2	1.1876-2	1.1680-2	1.1490-2
113	H, KJ/KG	57643.5	58037.3	58424.8	58807.1
114	U, KJ/KG	49365.7	49617.3	49863.1	50104.2
115	G, KJ/KG	-140175.9	-143476.1	-146782.8	-150095.7
116	S, KJ/(KG)(K)	32.9699	33.0350	33.0980	33.1592
117	M, (1/n)	6.027	6.024	6.021	6.019
118	(dLV/dLP)t	-1.00355	-1.00305	-1.00263	-1.00228
119	(dLV/dLT)p	1.0333	1.0282	1.0239	1.0204
120	Cp, KJ/(KG)(K)	3.9752	3.9039	3.8468	3.8008
121	GAMMAS	1.5799	1.5891	1.5968	1.6030
122	SON VEL,M/SEC	3616.3	3657.9	3697.4	3735.0

123

124 MOLE FRACTIONS

125

126	*H	0.66411	0.66446	0.66476	0.66501
127	*H2	0.00165	0.00142	0.00122	0.00106

C.3. 5200 - 6100 K

---

```
129 *0          0.33231  0.33246  0.33259  0.33269
130 *OH         0.00164  0.00141  0.00122  0.00106
131 *O2         0.00029  0.00024  0.00020  0.00017
132
133 * THERMODYNAMIC PROPERTIES FITTED TO 20000.K
134
135 NOTE. WEIGHT FRACTION OF FUEL IN TOTAL FUELS AND OF OXIDANT IN TOTAL
       OXIDANTS
```



## D. H<sub>2</sub>O Dissociation Models

### D.1. Srinivasan Model

Neutral reactions, published in Srinivasan et al. [40]. The considered species are H<sub>2</sub>O, H, H<sub>2</sub>, O, O<sub>2</sub> and OH.

Table D.1. Reactions of the Srinivasan Model. The species are H<sub>2</sub>O, H, H<sub>2</sub>, O, O<sub>2</sub> and OH.

Index	Reaction	Rate constant in $\frac{\text{cm}^3}{\text{s}}$
1 <sub>Kr</sub>	H <sub>2</sub> O + Kr → H + OH + Kr	$k_{1,\text{Kr}} = (2.43 \pm 0.57) \times 10^{-10} \exp(-47117 \pm 633/T)$
1 <sub>Ar</sub>	H <sub>2</sub> O + Ar → H + OH + Ar	$k_{1,\text{Ar}} = 1.007 \times 10^4 T^{-3.312} \exp(-60782/T)$
1 <sub>H<sub>2</sub>O</sub>	H <sub>2</sub> O + H <sub>2</sub> O → H + OH + H <sub>2</sub> O	$k_{1,\text{H}_2\text{O}} = 1.671 \times 10^2 T^{-2.440} \exp(-60475/T)$
2	H + H <sub>2</sub> O → OH + H <sub>2</sub>	$k_2 = 1.56 \times 10^{-15} T^{1.52} \exp(-9083/T)$
3	OH + OH → O + H <sub>2</sub> O	$k_3 = 7.19 \times 10^{-21} T^{2.7} \exp(917/T)$
4	O + H <sub>2</sub> O → OH + OH	$k_4 = 7.48 \times 10^{-20} T^{2.7} \exp(-7323/T)$
5	H + O <sub>2</sub> → OH + O	$k_5 = 1.62 \times 10^{-10} \exp(-7474/T)$
6	OH + O → O <sub>2</sub> + H	$k_6 = 5.42 \times 10^{-13} T^{0.375} \exp(950/T)$
7	O + H <sub>2</sub> → OH + H	$k_7 = 8.44 \times 10^{-20} T^{2.67} \exp(-3167/T)$
8	OH + H → H <sub>2</sub> + O	$k_8 = 3.78 \times 10^{-20} T^{2.67} \exp(-2393/T)$
9	OH + H <sub>2</sub> → H <sub>2</sub> O + H	$k_9 = 3.56 \times 10^{-16} T^{1.52} \exp(-1736/T)$

## D.2. Lede Model

Neutral reactions, published in Lede et al. [41]. The considered species are  $H_2O$ ,  $H$ ,  $H_2$ ,  $O$ ,  $O_2$  and  $OH$ .

Table D.2. Reactions of Lede et al. [41] with  $H_2O$ ,  $H$ ,  $H_2$ ,  $O$ ,  $O_2$  and  $OH$ .

Index	Reaction
1	$H_2O + H_2O \rightleftharpoons H + OH + H_2O$
2	$H_2O + H \rightleftharpoons H_2 + OH$
3	$OH + H \rightleftharpoons H_2 + O$
4	$OH + O \rightleftharpoons O_2 + H$

The reactions with the kinetic rate constants and divided into 8 reactions is presented in table D.3.

Table D.3. Reactions of Lede. With rate constants in  $\frac{m^3}{s}$  for two-body reactions and in  $\frac{m^6}{s}$  for three-body reactions.

Index	Reaction	Rate constant
1	$H_2O + H_2O \rightarrow H + OH + H_2O$	$k_1 = 2.2 \times 10^{10} \exp(-52900/T)$
-1	$H + OH + H_2O \rightarrow H_2O + H_2O$	$k_{-1} = 1.4 \times 10^{11} T^{-2}$
2	$H_2O + H \rightarrow H_2 + OH$	$k_2 = 9 \times 10^7 \exp(-10250/T)$
-2	$H_2 + OH \rightarrow H_2O + H$	$k_{-2} = 2.2 \times 10^7 \exp(-2590/T)$
3	$OH + H \rightarrow H_2 + O$	$k_3 = 8.3 \times 10^3 T \exp(-3500/T)$
-3	$H_2 + O \rightarrow OH + H$	$k_{-3} = 1.8 \times 10^4 T \exp(-4480/T)$
4	$OH + O \rightarrow O_2 + H$	$k_4 = 2 \times 10^7$
-4	$O_2 + H \rightarrow OH + O$	$k_{-4} = 2.2 \times 10^8 \exp(-8420/T)$

### D.3. Avtaeva Model

Neutral reactions, published in Avtaeva et al. [42]. The rate constants are mostly calculated at 300 K. The considered species are O<sub>2</sub>, O, H<sub>2</sub>O, H, OH, H<sub>2</sub>, HO<sub>2</sub> and H<sub>2</sub>O<sub>2</sub>

Table D.4. Reactions of Avtaeva. With rate constants in  $\frac{m^3}{s}$  for two-body reactions and in  $\frac{m^6}{s}$  for three-body reactions.

No.	Reaction	Rate constant
1	$2\text{OH} \rightarrow \text{O} + \text{H}_2\text{O}$	$1.8 \times 10^{-18}$
2	$\text{OH} + \text{H}_2 \rightarrow \text{H}_2\text{O} + \text{H}$	$7.7 \times 10^{-18} \exp(-2100 \times 8.6 \times 10^{-5}/T)$
3	$\text{OH} + \text{O} \rightarrow \text{H} + \text{O}_2$	$2.3 \times 10^{-17} \exp(-110 \times 8.6 \times 10^{-5}/T)$
4	$\text{OH} + \text{O} \rightarrow \text{HO}_2$	$2.1 \times 10^{-16}$
5	$\text{OH} + \text{H} \rightarrow \text{O} + \text{H}_2$	$1.03 \times 10^{-22}$
6	$\text{OH} + \text{H}_2\text{O} \rightarrow \text{HO}_2 + \text{H}_2\text{O}$	$1.7 \times 10^{-18}$
7	$\text{OH} + \text{OH} \rightarrow \text{H}_2\text{O}_2$	$1.51 \times 10^{-17}$
8	$\text{H} + \text{HO}_2 \rightarrow 2\text{OH}$	$8 \times 10^{-17}$
9	$\text{H} + \text{HO}_2 \rightarrow \text{H}_2\text{O} + \text{O}$	$2 \times 10^{-18}$
10	$\text{OH} + \text{HO}_2 \rightarrow \text{H}_2\text{O} + \text{O}_2$	$4.8 \times 10^{-17} \exp(-250 \times 8.6 \times 10^{-5}/T)$
11	$\text{O} + \text{HO}_2 \rightarrow \text{OH} + \text{O}_2$	$3 \times 10^{-17} \exp(-200 \times 8.6 \times 10^{-5}/T)$
12	$\text{HO}_2 + \text{H} \rightarrow \text{H}_2 + \text{O}_2$	$3.08 \times 10^{-18}$
13	$2\text{HO}_2 \rightarrow \text{H}_2\text{O}_2 + \text{O}_2$	$3.01 \times 10^{-18}$
14	$\text{H}_2\text{O}_2 + \text{O} \rightarrow \text{HO}_2 + \text{OH}$	$1.8 \times 10^{-21}$
15	$\text{H}_2\text{O}_2 + \text{H} \rightarrow \text{H}_2\text{O} + \text{OH}$	$5.09 \times 10^{-20}$
16	$\text{H}_2\text{O}_2 + \text{H} \rightarrow \text{HO}_2 + \text{H}_2$	$1.22 \times 10^{-22}$
17	$\text{O} + \text{H}_2 \rightarrow \text{OH} + \text{H}$	$9.1 \times 10^{-24}$
18	$\text{H} + \text{O}_2 + \text{H}_2\text{O} \rightarrow \text{HO}_2 + \text{H}_2\text{O}$	$6.4 \times 10^{-43}$
19	$\text{H} + \text{O}_2 \rightarrow \text{HO}_2$	$1.8 \times 10^{-18}$

## D.4. Mededovic Model

Neutral reactions, published in Mededovic et al. [43]. The model of Mededovic consists of two reaction sets. One Set for temperatures from 2000 K up to 5000K and another set for lower temperatures from 300 K up to 2000 K. The high temperature set is presented in table D.5. The considered species are  $O_2$ , O,  $H_2O$ , H, OH and  $H_2$

The low temperature set was combined with the high temperature set to fit a wider temperature range, this set of reactions is presented in table D.6. Additionally here  $HO_2$  and  $H_2O_2$  are considered. The combined set of reactions features 32 reactions.

Table D.5. Reactions of Reactions of Mededovic, high temperature model. With rate constants in  $\frac{cm^3}{s}$  for two-body reactions and in  $\frac{cm^6}{s}$  for three-body reactions.

No.	Reactions	Rate constant
T2.1	$H_2O + H_2O \rightarrow H + OH + H_2O$	$5.8 \times 10^{-9} \exp(-440 \text{ kJ } /RT)$
T2.2	$OH + H_2O \rightarrow H + O + H_2O$	$4.09 \times 10^{-9} \exp(-416 \text{ kJ } /RT)$
T2.3	$O + H + H_2O \rightarrow OH + H_2O$	$2 \times 10^{-32}$
T2.4	$H + H + H_2O \rightarrow H_2 + H_2O$	$1.68 \times 10^{-32}$
T2.5	$H_2 + H_2O \rightarrow H + H + H_2O$	$1.5 \times 10^{-9} \exp(-402 \text{ kJ } /RT)$
T2.6	$O + O + H_2O \rightarrow O_2 + H_2O$	$9.26 \times 10^{-34} (T/298)^{-1}$
T2.7	$O_2 + H_2O \rightarrow O + O + H_2O$	$1.99 \times 10^{-10} \exp(-9.5 \text{ kJ } /RT)$
T2.8	$OH + O \rightarrow O_2 + H$	$4.55 \times 10^{-12} (T/298)^{0.40} \exp(49.64 \text{ kJ } /RT)$
T2.9	$OH + OH \rightarrow H_2O + O$	$1.02 \times 10^{-12} (T/298)^{1.40} \exp(1.66 \text{ kJ } /RT)$
T2.10	$H + O_2 \rightarrow O + OH$	$2.56 \times 10^{-11} (T/298)^{0.55} \exp(49.64 \text{ kJ } /RT)$

Table D.6. Reactions of Reactions of Mededovic, combined model. With rate constants in  $\frac{\text{cm}^3}{\text{s}}$  for two-body reactions and in  $\frac{\text{cm}^6}{\text{s}}$  for three-body reactions.

No.	Reaction	Rate expression
1	$\text{H}_2\text{O} + \text{H}_2\text{O} \rightarrow \text{H} + \text{OH} + \text{H}_2\text{O}$	$5.8 \times 10^{-9} \exp(-440 \text{ kJ } /RT)$
2	$\text{OH} + \text{H}_2\text{O} \rightarrow \text{H} + \text{O} + \text{H}_2\text{O}$	$4.09 \times 10^{-9} \exp(-416 \text{ kJ } /RT)$
3	$\text{O} + \text{H} + \text{H}_2\text{O} \rightarrow \text{OH} + \text{H}_2\text{O}$	$2 \times 10^{-32}$
4	$\text{H} + \text{H} + \text{H}_2\text{O} \rightarrow \text{H}_2 + \text{H}_2\text{O}$	$1.68 \times 10^{-32}$
5	$\text{H}_2 + \text{H}_2\text{O} \rightarrow \text{H} + \text{H} + \text{H}_2\text{O}$	$1.5 \times 10^{-9} \exp(-402 \text{ kJ } /RT)$
6	$\text{O} + \text{O} + \text{H}_2\text{O} \rightarrow \text{O}_2 + \text{H}_2\text{O}$	$9.26 \times 10^{-34} (T/298)^{-1}$
7	$\text{O}_2 + \text{H}_2\text{O} \rightarrow \text{O} + \text{O} + \text{H}_2\text{O}$	$1.99 \times 10^{-10} \exp(-9.5 \text{ kJ } /RT)$
8	$\text{OH} + \text{O} \rightarrow \text{O}_2 + \text{H}$	$4.55 \times 10^{-12} (T/298)^{0.40} \exp(49.64 \text{ kJ } /RT)$
9	$\text{OH} + \text{OH} \rightarrow \text{H}_2\text{O} + \text{O}$	$1.02 \times 10^{-12} (T/298)^{1.40} \exp(1.66 \text{ kJ } /RT)$
10	$\text{H} + \text{O}_2 \rightarrow \text{O} + \text{OH}$	$2.56 \times 10^{-11} (T/298)^{0.55} \exp(49.64 \text{ kJ } /RT)$
11	$\text{O} + \text{OH} \rightarrow \text{H}_2\Theta + \text{HO}_2$	$2.69 \times 10^{-10} \exp(-0.62 \text{ kJ } /RT)$
12	$\text{H} + \text{OH} \rightarrow \text{O} + \text{H}_2$	$6.86 \times 10^{-14} (T/298)^{2.80} \exp(-16.21 \text{ kJ } /RT)$
13	$\text{H}_2\text{O}_2 + \text{OH} \rightarrow \text{HO}_2 + \text{H}_2\text{O}$	$2.91 \times 10^{-12} \exp(-1.33 \text{ kJ } /RT)$
14	$\text{O}_2 + \text{OH} \rightarrow \text{HO}_2 + \text{O}$	$3.7 \times 10^{-11} \exp(-220 \text{ kJ } /RT)$
15	$\text{OH} + \text{OH} \rightarrow \text{H}_2\text{O}_2$	$1.51 \times 10^{-11} (T/298)^{-0.37}$
16	$\text{OH} + \text{OH} \rightarrow 2\text{O} + 2\text{H}$	$4.09 \times 10^{-9} \exp(-416 \text{ kJ } /RT)$
17	$\text{H}_2\text{O}_2 + \text{O} \rightarrow \text{HO}_2 + \text{OH}$	$1.42 \times 10^{-12} (T/298)^2 \exp(-16.631 \text{ kJ } /RT)$
18	$\text{H}_2\text{O}_2 + \text{H} \rightarrow \text{OH} + \text{H}_2\text{O}$	$4.01 \times 10^{-11} \exp(-16.63 \text{ kJ } /RT)$
19	$\text{H}_2\text{O}_2 + \text{H} \rightarrow \text{HO}_2 + \text{H}_2$	$8 \times 10^{-11} \exp(-33.26 \text{ kJ } /RT)$
20	$\text{H}_2\text{O}_2 + \text{O}_2 \rightarrow 2\text{HO}_2$	$9 \times 10^{-11} \exp(-166 \text{ kJ } /RT)$
21	$\text{HO}_2 + \text{OH} \rightarrow \text{H}_2\text{O} + \text{O}_2$	$4.81 \times 10^{-11} \exp(2.08 \text{ kJ } /RT)$
22	$\text{HO}_2 + \text{O} \rightarrow \text{OH} + \text{O}_2$	$2.91 \times 10^{-11} \exp(-1.66 \text{ kJ } /RT)$
23	$\text{HO}_2 + \text{H} \rightarrow 2\text{OH}$	$2.81 \times 10^{-10} \exp(-3.66 \text{ kJ } /RT)$
24	$\text{HO}_2 + \text{H} \rightarrow \text{H}_2 + \text{O}_2$	$1.1 \times 10^{-10} \exp(-8.90 \text{ kJ } /RT)$
25	$\text{HO}_2 + \text{HO}_2 \rightarrow \text{H}_2\text{O}_2 + \text{O}_2$	$3.01 \times 10^{-12}$
26	$\text{HO}_2 + \text{H}_2 \rightarrow \text{H}_2\text{O}_2 + \text{H}$	$5 \times 10^{-11} \exp(-109 \text{ kJ } /RT)$
27	$\text{HO}_2 + \text{H}_2\text{O} \rightarrow \text{O}_2 + \text{H} + \text{H}_2\text{O}$	$2.41 \times 10^{-8} (T/298)^{-1.18} \exp(-2031 \text{ kJ } /RT)$
28	$\text{O}_2 + \text{H} \rightarrow \text{OH} + \text{O}$	$2.94 \times 10^{-10} \exp(-69.68 \text{ kJ } /RT)$
29	$\text{O}_2 + \text{H} + \text{H}_2\text{O} \rightarrow \text{HO}_2 + \text{H}_2\text{O}$	$1.94 \times 10^{-32} (T/298)^{-1}$
30	$\text{OH} + \text{H}_2 \rightarrow \text{H}_2\text{O} + \text{H}$	$2.97 \times 10^{-12} (T/298)^{1.21} \exp(-19.71 \text{ kJ } /RT)$
31	$\text{O} + \text{H}_2 \rightarrow \text{OH} + \text{H}$	$3.44 \times 10^{-13} (T/298)^{2.67} \exp(-26.27 \text{ kJ } /RT)$
32	$\text{O} + \text{H}_2\text{O} \rightarrow \text{OH} + \text{OH}$	$6.68 \times 10^{-13} (T/298)^{2.60} \exp(-63.52 \text{ kJ } /RT)$

## D.5. Liu Model

Neutral reactions, published in Liu et al. [44]. This is the most complex considered model with 46 species. The considered species are O<sub>2</sub>, O, H<sub>2</sub>O, H, OH, H<sub>2</sub>, HO<sub>2</sub> and H<sub>2</sub>O<sub>2</sub>. The reaction set is presented in table D.7.

Table D.7. Reactions of Liu model. With rate constants in  $\frac{\text{cm}^3}{\text{s}}$  for two-body reactions and in  $\frac{\text{cm}^6}{\text{s}}$  for three-body reactions.

No.	Reaction	Rate expression
1	$\text{H} + \text{H} \rightarrow \text{H}_2$	$6.04 \times 10^{-33} \cdot (T/298)^{-1}$
2	$\text{H} + \text{O} \rightarrow \text{OH}$	$4.36 \times 10^{-32} \cdot (T/298)^{-1}$
3	$\text{H} + \text{O}_2 \rightarrow \text{OH} + \text{O}$	$1.62 \times 10^{-10} \cdot \exp(-7470/T)$
4	$\text{H} + \text{O}_2 \rightarrow \text{HO}_2$	$5.4 \times 10^{-32} \cdot (T/298)^{-1.8}$
5	$\text{H} + \text{OH} \rightarrow \text{H}_2 + \text{O}$	$8 \times 10^{-21} \cdot T^{2.8} \cdot \exp(-1950/T)$
6	$\text{H} + \text{OH} \rightarrow \text{H}_2\text{O}$	$6.87 \times 10^{-31} \cdot (T/298)^{-2}$
7	$\text{H} + \text{HO}_2 \rightarrow \text{H}_2\text{O} + \text{O}$	$9.18 \times 10^{-11} \cdot \exp(-971.9/T)$
8	$\text{H} + \text{HO}_2 \rightarrow \text{O}_2 + \text{H}_2$	$1.1 \times 10^{-12} \cdot T^{0.56} \cdot \exp(-346/T)$
9	$\text{H} + \text{HO}_2 \rightarrow 2 \text{OH}$	$2.35 \times 10^{-10} \cdot \exp(-373.7/T)$
10	$\text{H} + \text{H}_2\text{O}_2 \rightarrow \text{H}_2 + \text{HO}_2$	$8.0 \times 10^{-11} \cdot \exp(-4000/T)$
11	$\text{H} + \text{H}_2\text{O}_2 \rightarrow \text{H}_2\text{O} + \text{OH}$	$4.0 \times 10^{-11} \cdot \exp(-2000/T)$
12	$\text{H} + \text{H}_2\text{O} \rightarrow \text{H}_2 + \text{OH}$	$7.4 \times 10^{-16} \cdot T^{1.6} \cdot \exp(-9720/T)$
13	$3 \text{H} \rightarrow \text{H} + \text{H}_2$	$6 \times 10^{-31} \cdot (T/300)^{-1}$
14	$2 \text{H} + \text{H}_2 \rightarrow 2 \text{H}_2$	$8.1 \times 10^{-33} \cdot (T/300)^{-0.6}$
15	$2 \text{H} + \text{H}_2\text{O} \rightarrow \text{H}_2 + \text{H}_2\text{O}$	$1.32 \times 10^{-31} \cdot (T/300)^{-1.25}$
16	$\text{H} + \text{O} + \text{H}_2 \rightarrow \text{OH} + \text{H}_2$	$9.19 \times 10^{-33} \cdot (T/300)^{-1}$
17	$\text{H} + \text{O} + \text{H}_2\text{O} \rightarrow \text{OH} + \text{H}_2\text{O}$	$2.76 \times 10^{-32} \cdot (T/300)^{-1}$
18	$\text{H} + \text{O}_2 + \text{H}_2 \rightarrow \text{HO}_2 + \text{H}_2$	$5.72 \times 10^{-32} \cdot (T/300)^{-0.86}$
19	$\text{H} + \text{O}_2 + \text{O}_2 \rightarrow \text{HO}_2 + \text{O}_2$	$4.86 \times 10^{-32} \cdot (T/300)^{-1.24}$
20	$\text{H} + \text{O}_2 + \text{H}_2\text{O} \rightarrow \text{HO}_2 + \text{H}_2\text{O}$	$4.08 \times 10^{-31} \cdot (T/300)^{-0.76}$
21	$\text{H} + \text{OH} + \text{H}_2 \rightarrow \text{H}_2\text{O} + \text{H}_2$	$4.92 \times 10^{-31} \cdot (T/300)^{-2}$
22	$\text{H} + \text{OH} + \text{O}_2 \rightarrow \text{H}_2\text{O} + \text{O}_2$	$6.74 \times 10^{-31} \cdot (T/300)^{-2}$
23	$\text{H} + \text{OH} + \text{H}_2\text{O} \rightarrow 2 \text{H}_2\text{O}$	$2.46 \times 10^{-30} \cdot (T/300)^{-2}$
24	$2 \text{O} \rightarrow \text{O}_2$	$9.26 \times 10^{-34} \cdot (T/298)^{-1}$
25	$\text{O} + \text{H}_2 \rightarrow \text{OH} + \text{H}$	$3 \times 10^{-14} \cdot T \cdot \exp(-4480/T)$
26	$\text{O} + \text{OH} \rightarrow \text{H} + \text{O}_2$	$6 \times 10^{-11} \cdot T^{-0.186} \cdot \exp(-154/T)$
27	$\text{O} + \text{HO}_2 \rightarrow \text{OH} + \text{O}_2$	$2.9 \times 10^{-11} \cdot \exp(200/T)$
28	$\text{O} + \text{H}_2\text{O}_2 \rightarrow \text{OH} + \text{HO}_2$	$3 \times 10^{-18} \cdot T^{2.92} \cdot \exp(-1294/T)$
29	$\text{O} + \text{H}_2\text{O} \rightarrow 2 \text{OH}$	$2.5 \times 10^{-14} \cdot T^{1.14} \cdot \exp(-8624/T)$
30	$3 \text{O} \rightarrow \text{O} + \text{O}_2$	$9.21 \times 10^{-34} \cdot (T/300)^{-0.63}$
31	$2 \text{O} + \text{H}_2$	$2.65 \times 10^{-33} \cdot (T/300)^{-1}$
32	$2 \text{O} + \text{O}_2 \rightarrow 2 \text{O}_2$	$2.56 \times 10^{-34} \cdot (T/300)^{-0.63}$
33	$2 \text{O} + \text{H}_2\text{O} \rightarrow \text{O}_2 + \text{H}_2\text{O}$	$1.7 \times 10^{-32} \cdot (T/300)^{-1}$
34	$\text{H}_2 + \text{OH} \rightarrow \text{H} + \text{H}_2\text{O}$	$5.3 \times 10^{-16} \cdot T^{1.47} \cdot \exp(-1761/T)$
35	$\text{H}_2 + \text{HO}_2 \rightarrow \text{H}_2\text{O}_2 + \text{H}$	$5 \times 10^{-11} \cdot \exp(-13110/T)$
36	$\text{H}_2 + \text{H}_2\text{O} \rightarrow \text{OH} + \text{H} + \text{H}_2$	$5.8 \times 10^{-9} \cdot \exp(-52900/T)$
37	$\text{O}_2 + \text{H}_2\text{O}_2 \rightarrow 2 \text{HO}_2$	$9 \times 10^{-11} \cdot \exp(-19965/T)$
38	$\text{O}_2 + \text{H}_2\text{O} \rightarrow \text{HO}_2 + \text{OH}$	$7.72 \times 10^{-12} \cdot \exp(-37284/T)$
39	$2 \text{OH} \rightarrow \text{H}_2\text{O} + \text{O}$	$2.5 \times 10^{-15} \cdot T^{1.14} \cdot \exp(-50/T)$
40	$2 \text{OH} \rightarrow \text{H}_2\text{O}_2$	$1.5 \times 10^{-11} \cdot (T/300)^{-0.37}$
41	$\text{OH} + \text{HO}_2 \rightarrow \text{O}_2 + \text{H}_2\text{O}$	$4.38 \times 10^{-11} \cdot \exp(110.9/T)$
42	$\text{OH} + \text{H}_2\text{O}_2 \rightarrow \text{H}_2\text{O} + \text{HO}_2$	$4.53 \times 10^{-12} \cdot \exp(-288.9/T)$
43	$2 \text{HO}_2 \rightarrow \text{H}_2\text{O}_2 + \text{O}_2$	$8.05 \times 10^{-11} \cdot (T/300)^{-1}$
44	$\text{HO}_2 \rightarrow \text{H} + \text{O}_2$	$2 \times 10^{-5} \cdot T^{-1.18} \cdot \exp(-24415/T)$
45	$\text{HO}_2 + \text{H}_2\text{O} \rightarrow \text{H}_2\text{O}_2 + \text{OH}$	$4.65 \times 10^{-11} \cdot \exp(-16477/T)$
46	$\text{H}_2\text{O}_2 \rightarrow 2 \text{OH}$	$2 \times 10^9 \cdot T^{-4.86} \cdot \exp(-26821/T)$